

Coarsening Kinetics of Chemically-Active Emulsions

Dissertation
zur Erlangung des akademischen Grades
Doctor rerum naturalium

vorgelegt

der Fakultät Physik
Bereich Mathematik und Naturwissenschaften
der Technischen Universität Dresden

von

Jacqueline Anna Janssen
geboren am 31.03.1994 in Poznań, Polen

erstellt am

Max-Planck-Institut für Physik komplexer Systeme
Dresden, 2023



Gutachter:

Prof. Dr. Christoph A. Weber

Prof. Dr. Frank Jülicher, co-signed by Prof. Dr. Benjamin Friedrich

Acknowledgments

My very special thanks go to Christoph Weber for mentoring me during my Ph.D. and for many helpful discussions and valuable lessons. Thank you for your constant support and trust during my Ph.D. time and for letting me grow and develop my scientific independence. I thank Frank Jülicher for his interest in my work, his constant willingness to discuss my open questions, for his mentoring and support.

Special thanks go to the Weber group, to Sudarshana and Giacomo. Sudarshana, who can always make me laugh, thank you for your support and great sense of humor. I also thank Thomas, who I had the pleasure of supervising during my PhD. Thank you for your interesting ideas and your time to discuss the project.

I thank all the former and current members of the Biological Physics division at the Max Planck Institute for the Physics of Complex Systems. I have a lot of beautiful memories; thank you for creating such an open and friendly environment. Thank you for your attention and time during our PhD meetings, droplet meetings, and internal seminars. Thank you for your constant willingness to discuss both science and life questions with me. Christian, Ali, Omar, Talía, Abuthaleb, Ryota, Charlie, Joanthan, Lars, Martin, Adolfo, Felix, Kathrin, Ahandeep, Mariona, Riccard, Amit (Ksenia and Wanja), Aida, Boyi, Jack, Daniel, Tarun, Suganthan, Ivan, Fabrizio, Nicolò. With each of you I have a memory of supportive and inspiring interactions. I want to thank Charu, for his open ear to my stories, our interesting chats his wisdom and genuine support. Stefano, thank you for being always open to talk, sharing with me your knowledge, opinions and culinary skills. Matteo, you were the best office mate I can imagine. Thank you for the time together, for the scent of freshly ground coffee, original snacks, for the warm and friendly atmosphere each day at work. I would like to thank Efe. Thank you for helpful discussions, your valuable insights, our friendship and your support. Big thanks go to the administration of our institute, to Ulrike and Anna who take care of all formalities around our work.

I am very grateful for the time at the institute and that I could cross paths with so many wonderful people. I wish everybody all the best for their future. I hope to see you all again, during conferences, alumni meetings or privately wherever we will be in the world. Thank you.

Abstract

Droplets form via phase separation and coexist with a dilute phase. After nucleation and growth of droplets, the resulting emulsion of many droplets undergoes coarsening kinetics to reach its thermal equilibrium state. Ostwald ripening describes the coarsening kinetics of emulsions for which the total droplet material is conserved. During Ostwald ripening, the droplet number density decreases, the average radius increases, and the droplet size distribution function broadens in a universal manner.

Phase separation and kinetics of emulsions are relevant for the spatial organization of cells and synthetic chemical systems. In these systems, droplet material is often not conserved due to the active production of droplet building blocks by fuel-driven chemical reaction cycles. In this thesis, we derive the theoretical framework for coarsening in emulsions with matter supply.

The first part of this thesis is dedicated to droplet growth in binary mixtures, where we consider deviations from local equilibrium at the phase boundary. The resulting droplet growth law allows for multiple scenarios and asymptotically comprises two regimes: diffusion limited and interface-kinetics limited growth law. We derive the growth of an emulsion and learn how the competition between the droplets and their growth are influenced by matter supply. Compared to emulsions without supply, we find an acceleration in coarsening kinetics for constant matter supply. The scaling of the average radius differs through a fixed shift in the prefactor, which in some cases can be supply-independent. The droplet size distribution can narrow but only in the diffusion limited regime for increasing supply rates. For matter supply that maintains the supersaturation constant, we find different scaling laws than in emulsion without matter supply. The droplet size distribution always narrows, even if the emulsion was initially in the interface-kinetics limited regime. In the last part, we discuss emulsions in which matter is supplied and removed from the system through a chemical reaction cycle. We discuss the effect of the chemical reaction cycle on emulsions' transient and longtime kinetics and the difference to passive emulsions. We discuss experimental results, which show accelerated ripening in chemically-fuelled emulsions. We study how the different fuel supply methods influence the chemical reaction cycle and droplet kinetics.

The importance of this work is in understanding how matter supply can lead to size control in chemically-active emulsions. Our work paves the way to decipher regulatory mechanisms mediated by biomolecular condensates in living cells and protocells at the origin of life.

Contents

1	Introduction to coarsening kinetics of emulsions	1
1.1	Kinetic pathways of coarsening: Fusion and Ostwald ripening	2
1.2	Emulsions in biology and at the molecular origin of life	4
1.2.1	Phase separation and its kinetics in cell biology	4
1.2.2	Model systems for membraneless organelles	7
1.2.3	Emulsions in the study of protocells	8
1.3	Physics of liquid-liquid phase separation	9
1.3.1	Thermodynamics of phase separation	9
1.3.2	Interface effects on phase equilibrium	12
1.4	Classification of emulsions by matter supply	14
1.5	Coarsening kinetics of passive emulsions	15
1.5.1	Diffusion limited and interface-kinetics limited coarsening	16
1.5.2	Universal coarsening kinetics of passive emulsions	21
1.6	Scope of this thesis	24
2	Theory of droplet growth in emulsions with broken conservation law	27
2.1	Effective droplet model	28
2.1.1	Interface kinetics with local departure from equilibrium	30
2.1.2	Cases of departure from the local equilibrium at the droplet interface	32
2.1.3	Constant conditions inside the droplet	34
2.1.4	Quasi-static approximation and the concentration profile	34
2.1.5	Asymptotic relaxation at the interface	35
2.2	Statistics of growth in emulsions	36
2.2.1	Derivation of emulsion growth kinetics for each droplet	37
2.2.2	Continuum theory for emulsion kinetics	42
2.2.3	Separation ansatz for the droplet size distribution function	45

2.3	Analytical solution of the droplet size distribution function for emulsions with matter supply	47
2.4	Prediction of a broadening and narrowing zone of the droplet size distribution function	51
2.5	Summary	53
3	Coarsening kinetics of emulsions with matter supply	54
3.1	Emulsions with constant matter supply	55
3.1.1	Supply-independent acceleration of coarsening in emulsions with constant matter supply	57
3.1.2	Switch between a broadening and narrowing distribution function for increasing supply	63
3.1.3	Universal coarsening kinetics of emulsions with constant matter supply	67
3.2	Emulsions with time-dependent matter supply maintaining constant supersaturation	70
3.2.1	Moments of droplet size distribution function in emulsions with constant supersaturation	71
3.2.2	Universal coarsening kinetics of emulsions with constant supersaturation	75
3.3	Summary	76
4	Coarsening kinetics of chemically-active emulsions	78
4.1	Model for emulsions with fuel-driven chemical reactions in dilute phase	79
4.1.1	Experimental realization of emulsions with fuel-driven chemical reactions in the dilute phase	83
4.2	Experimentally observed acceleration of coarsening in chemically-active emulsions	85
4.2.1	Estimation of the average volume	86
4.2.2	Collapse of the acceleration of coarsening	91
4.3	Transient acceleration of coarsening in chemically-active emulsions	93
4.4	Summary	97
5	Summary and future outlook	99
	Bibliography	106

Chapter 1

Introduction to coarsening kinetics of emulsions

A homogeneous mixture can undergo phase separation and separate into phases of distinct compositions. A common type of phase separation is liquid-liquid phase separation resulting in liquid condensed phases. The phase-separated system can be organized into droplets forming an emulsion. We study here binary mixtures, and droplets we consider are small condensed phases coexisting with a large dilute phase. The evolution of an emulsion toward its thermal equilibrium state is a process with nearly three separate stages [1], Fig. 1.1: The first stage is nucleation of droplets, where the two distinct phases are formed from a homogeneous mixture. In the second stage, droplets grow at the expense of the dilute phase, depleting the excess droplet material in the dilute phase for overall growth. The measure of the excess droplet material in the dilute phase is referred to as supersaturation. During the growth stage, there is an increase in the total droplet phase volume. Upon completion of this stage, the system has lowered its free energy, but the effect of the surface area at the interface of the two phases is still high enough, such that thermodynamic equilibrium is not reached yet. Since the energy associated with the total surface area is usually small [2] compared to the energetic contributions of the bulk phases, the effects of surface energy become apparent at the last stage of a first-order phase separation kinetics. The total energy of the two-phase system can be decreased further, via an increase of the dense phase and thus a decrease in the total area of the interface between the two phases [2]. The increase of the dense phase is manifested through the increase in the average droplet radius. This happens through growth of larger droplets and shrinkage followed by dissolution of smaller ones. Coarsening is this late stage evolution of the dense phase until it reaches minimum

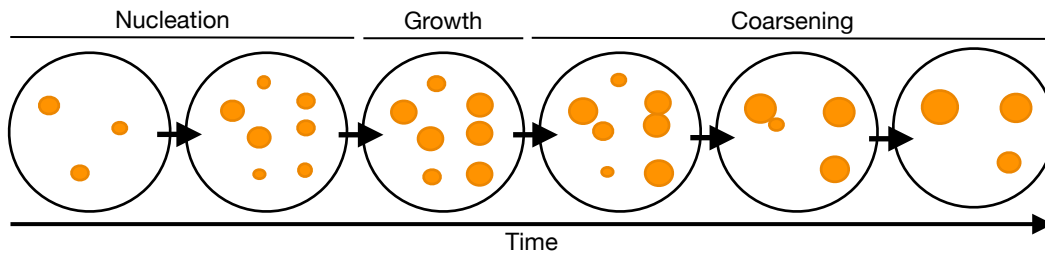


FIGURE 1.1: **Schematic of stages during the evolution of an emulsion:** During nucleation, which is the first stage of phase separation, droplets form. After nucleation, due to high supersaturation, each droplet grows, and no droplets dissolve. During growth, the supersaturation decreases such that the concentrations approach the equilibrium values. When the supersaturation is low the size differences between the droplets drive coarsening. Smaller droplets dissolve, while larger ones grow on their expense. If two droplets are in the physical vicinity, they fuse.

of its surface free energy [1]. The end of this process is associated with the thermodynamic equilibrium.

This work is dedicated to the physics of emulsion coarsening kinetics. We will discuss the effect of different conditions the system can be exposed to and their impact on the longtime coarsening kinetics. In the introduction, we will first discuss the possible kinetic pathways of coarsening and the difference between fusion and Ostwald ripening. Later, we will make an excursion to the biology of the cell, to learn the importance of emulsions in biology and what are the biologically relevant conditions emulsions can be exposed to. In the second part of the introduction we will discuss the physics of phase separation as well as coarsening kinetics of passive emulsions.

1.1 Kinetic pathways of coarsening: Fusion and Ostwald ripening

There are two kinetic pathways of coarsening. If two droplets are in the physical vicinity, they can fuse into one droplet. The resulting droplet will have approximately the same volume as the sum of the two original droplets. Its surface area will be smaller than the combined surface areas of the two droplets. The surface area contribution to the free energy will be thus lowered [3, 4]. If droplets are sparsely distributed in the solution, and do not come into physical contact, there is a further mechanism of coarsening possible: Ostwald ripening, which is driven by gradients of concentration between the droplets.

In 1897 Wilhelm Ostwald was the first to observe this coarsening phenomenon in HgO droplets [5, 6]. The phenomenon of coarsening in which diffusional growth of larger drops happens at the expense of smaller drops, which eventually dissolve, has been called by his name: Ostwald ripening. Besides liquid-liquid systems, it is observed in liquid-vapor mixtures, such as droplets in clouds, or solid-liquid mixtures found in metallurgy or geology. It has importance in material sciences for processes like ageing of metallic alloys, liquid and solid state sintering, deoxidation of steel melts or in geology when studying aging or growth of phenocrysts and crystals in solid rock.

In the early 1960s, Ostwald ripening gained a lot of interest, through the first quantitative description of this phenomenon by Lifshitz and Slyozov [7] and independently by Wagner [8]. Their derivation of a unique self-similar evolution of the droplet size distribution function and its moments for Ostwald ripening kinetics has been known as LSW-theory. Self-similar means that the distribution function has the same shape at all times. In the same paper Wagner [8] derived asymptotic solution for coarsening kinetics considering that growth might be limited by the interface-kinetics and not only the process of diffusion. The theory of Ostwald ripening has been revisited many times, the works of Vorhees [2, 9], Marquess and Ross [1, 10], and Niethammer [11, 12, 13, 14] explore the validity of assumptions made in the LSW-theory from the experimental observations as well as its mathematical rigorous.

Although there are many studies of the classical LSW-theory, coarsening kinetics for emulsions with matter supply has yet to be explored in detail. This work aims to extend the theory of Ostwald ripening to systems with matter supply in the dilute phase. Of particular interest is the application of such coarsening theory to cell biology, where matter supply in the form of protein expression, chemical reactions or exchange of material with an external reservoir can happen. In the last decade, droplets and the study of emulsions became very important due to the discovery of membraneless organelles in cells.

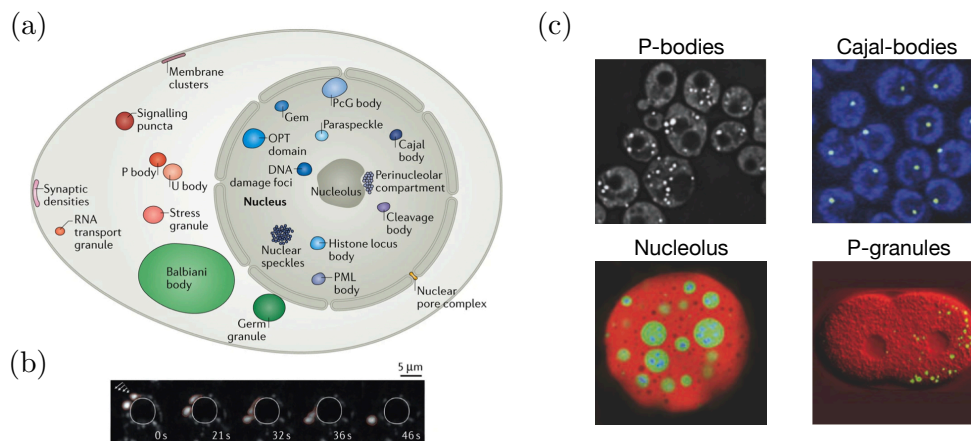


FIGURE 1.2: **Classification of membraneless organelles in cells:** (a): Schematic of the numerous condensates in the nucleus, cytoplasm, and membranes of eukaryotic cells. Taken from [15]. (b): A montage of live time-lapse imaging of P granules under shear force (arrows, top left). The condensates behave like liquid droplets: They deform, drip and fuse around a nucleus. Taken from [15]. (c): Examples of different condensates in cells, P-bodies [16], Cajal-bodies [17], Nucleolus [18] and P-granules [19]. Modified from [20].

1.2 Emulsions in biology and at the molecular origin of life

In the following, we discuss the relevance of phase separation in cell biology and at the molecular origin of life. In particular, we will introduce state-of-the-art knowledge about coarsening kinetics of emulsions in cells and in studying protocells.

1.2.1 Phase separation and its kinetics in cell biology

Cell biology faces the challenge of maintaining control over its complex cellular processes in space and time, despite the diversity and richness of its biochemical constituents. Cells localize their chemical components in distinct environments. These cellular subunits, called organelles, are differently formed parts of the cell that coexist with the cell's environment. There are two types of organelles in cells: Membrane-bound organelles surrounded by a selectively permeable membrane and membraneless organelles which lack a physical barrier between their internal components and the surrounding medium. The classic membrane-bound organelles are e.g., endoplasmic

reticulum, Golgi apparatus, nucleus. The examples of membraneless organelles, Fig. 1.2(a),(c), include RNA-protein granules as nucleoli, Cajal bodies, PML bodies in nucleus, as well as stress granules and germ granules in the cytoplasm [15].

Membranes are impermeable to most biological macromolecules, and transport through organelle's boundaries is regulated by membrane channels [21, Chapt. 11]. Membraneless organelles (biomolecular condensates) need another way to maintain and control their composition. Liquid-liquid phase separation is a mechanism that facilitates the formation, composition, physical and biochemical properties of membraneless organelles.

Biomolecular condensates are liquid-like [19], Fig. 1.2(b), and form by phase separation from the cytoplasm [19, 22, 15, 23]. They control biochemical reactions [24], biological signal control, and processing [25] in cells. Membraneless organelles typically comprise proteins and RNA [26], and despite their dynamic nature, many of these condensates can maintain their overall size and shape for minutes or hours while exchanging their components with the surrounding cytoplasm or nucleoplasm on time scales of seconds.

It has been confirmed that droplets in cells coarsen through fusion and through diffusion limited Ostwald ripening [27]. In experiments, the dissolution of small droplets indicates Ostwald ripening that happens in parallel to fusion [27, 28]. In cells, both processes are present and nonnegligible, and dependent on the conditions inside the cell, their effect on the droplet coarsening kinetics may differ. For example, coarsening of droplets surrounded by a chromatin network is highly influenced by the viscoelastic properties of the surroundings. In some cases fusion can be completely inhibited by the chromatin-dense environment, and droplet can only grow through diffusive transport of molecules [29]. Another interesting example is for the P granules of *Caenorhabditis elegans*, which are coated by MEG-3 proteins, that form a cluster on their surface. This local condition at the interface, changes the coarsening behaviour of the droplets, which again slows down fusion [30]. Although fusion in such conditions is inhibited droplets still coarsen and we should explore the theory of coarsening kinetics determined by the exchange of droplet material in the absence of physical contact.

Studying the dynamics and morphology of the individual condensates in cells is crucial to understand the biophysical properties of biomolecular condensates. However, it is a challenging task, since cells are very dynamic and undergo division, which limits the observation times.

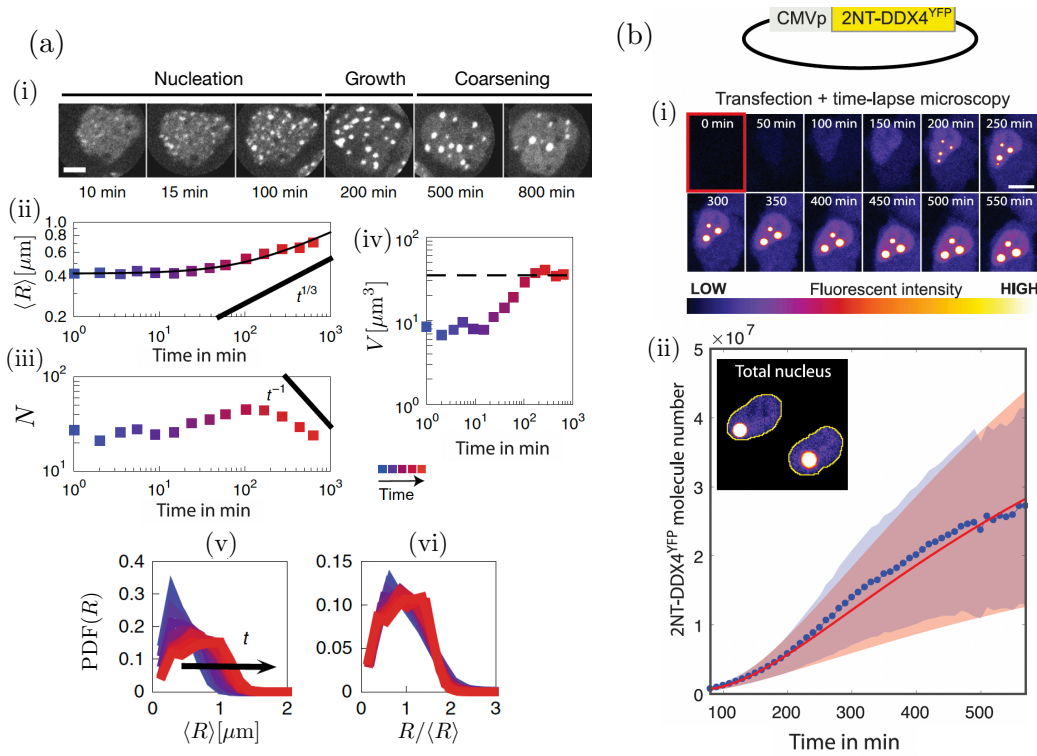


FIGURE 1.3: **Biophysical properties of condensates:** (a): Analysis of 53BP1-GFP droplets in NIH2/4 cells. (i): Representative images from live-cell microscopy of 53BP1-GFP condensate formation and kinetics (scale bar, $5\mu\text{m}$). (ii) Temporal evolution of the average radius. (iii): Temporal evolution of the average number of droplets per nucleus. (iv): Temporal evolution of the total volume of condensates per nucleus. (v): Probability distribution function $\text{PDF}(R)$ of foci radius measured at different time points (logarithmically spaced between 1min and 700min) (vi): $\text{PDF}(R)$ as in (v), with both axes rescaled with the average radius $\langle R \rangle$. Modified from [31]. (b): Analysis of 2NT-DDX4^{YFP} condensate kinetics in HeLa cells. (i): Time-lapse microscopy of a typical cell initiating expression of 2NT-DDX4^{YFP} protein and its phase separation after transfection and plasmid incorporation. (ii): Mean and variance of 2NT-DDX4^{YFP} total molecule numbers as a function of time. Model parameters were estimated from the time-lapse data (blue) by using statistical methods. Corresponding model behaviors are shown in red. Modified from [25].

Pessina et al. in Ref. [31], studied the dynamics of condensates formed through liquid-liquid phase separation of 53BP1 protein into droplets in NIH2/4 cell line. The cells in the experiment were irradiated, i.e., exposed to radiation from an X-ray source to create enough DNA damage that the cells could no longer divide. After the initial nucleation and growth stage, when the number and total volume of the condensed phase increase, it was possible to observe late-time coarsening, with a decrease in the total number of droplets, but an increase in average radius while the total volume of 53BP1 droplets

per nucleus was constant, Fig. 1.3(a). The estimated scaling laws of the number and the average radius were consistent with both Ostwald ripening and fusion. Since the majority of droplets was disappearing without physical contact, suggesting Ostwald ripening to be the dominant process [31]. What is more, a collapse of all of the distribution function curves onto an invariant distribution is observed for late times, $t > 100\text{min}$, Fig. 1.3(a)(vi). The feature of self-similarity is a strong indication for Ostwald ripening driving the coarsening process in the experiment.

The challenge in studying coarsening kinetics in cells is in deducing the precise scaling exponent and prefactor and whether they exist for the average radius, the number density of droplets, or the total droplet phase volume. Furthermore, the LSW-theory with the $t^{1/3}$ scaling law of the average radius [32] requires conditions of low volume density of the droplet phase and a conservation of the total droplet material. The latter does not have to always apply to cells.

For example, in Ref. [25] the liquid-like droplets, composed of 2NT-DDX4^{YFP} proteins are formed inside the nuclei of HeLa cells. The total number of 2NT-DDX4^{YFP} protein molecules expressed in the total nuclei is increasing over time, Fig. 1.3(b), which is an indication that cells in general do not have to conserve the total amount of droplet material [33]. In general, cells are open systems and we should include the changes of the total droplet material in the studies of coarsening behaviour.

1.2.2 Model systems for membraneless organelles

To understand the physicochemical principles underlying the functioning of membraneless organelles, we need detailed studies in both living cells and model systems [34].

Complex coacervates have shown great potential as model systems in chemical sciences for such active compartments [34]. In addition to being stable over a broad range of physicochemical conditions, coacervate droplets are able to spatially localise and up-concentrate different molecules [35, 36] and support biochemical reactions [37, 38, 39]. Coacervation describes the condensation of polymeric molecules into a liquid state. The phenomenon was first observed in mixed solutions of oppositely charged biopolymers and in solutions of isoelectric proteins with (poly)phenols [26, 40]. Complex coacervation is a process of condensation of oppositely charged molecules, as opposed to simple coacervation, which involves a single self-associating

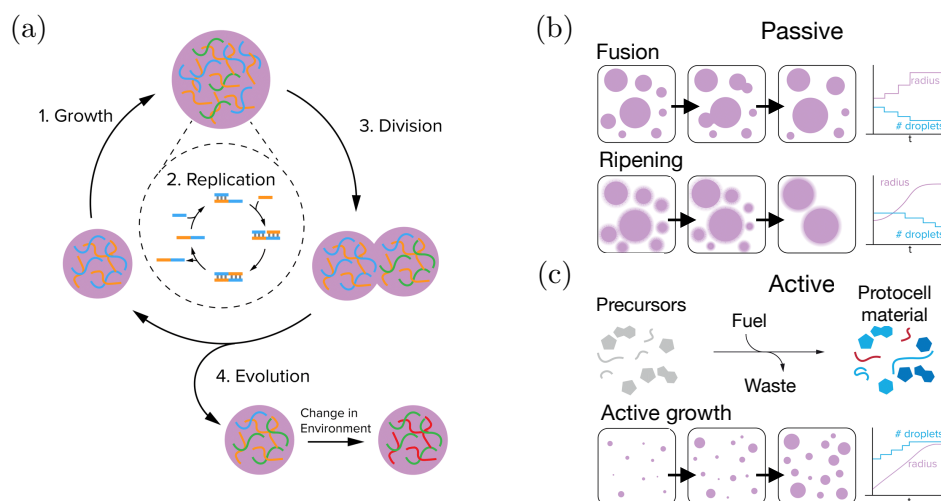


FIGURE 1.4: **A schematic of protocell cycle and active kinetics:** (a): A minimal model of the protocell cycle necessary to give rise to evolution. A system should be able to grow, replicate and divide. Evolution also requires its response to the changes in the environment. (b): Passive growth kinetics of coacervates. In passive systems coacervates can grow by fusion and Ostwald ripening. During passive growth, the number of protocells decreases, which is not desired in order to sustain a population. (c): Active growth, which uses an active reaction that converts precursor molecules to protocell molecules after input of fuel. This coarsening pathway could facilitate the robustness of the population. Taken from [44].

molecule [34]. The mechanism of coacervate formation is liquid-liquid phase separation [41, 42]. The study of the physicochemical properties of coacervates is currently at focus due to its accessibility in the lab and the possibility for experimental studies of systems having features resembling membraneless organelles but in the setting outside of the cell. Already in the 1920's Oparin first suggested that coacervation could have been a way to bring prebiotic molecules together and form a protocell [43]. Thus, studying coacervates can help elucidate the cellular evolution at the origin of life.

1.2.3 Emulsions in the study of protocells

Recently, researchers in Ref. [37] proved for the first time that coacervates facilitate RNA catalysis. This effect is coupled with selective recruitment and release of RNA without additional energy input. These features could have been significant on early Earth where concentrations of RNA, their building blocks, and other molecules may have been low [37].

The defining life features of modern cells are often divided into hallmarks, such as growth, division, information processing, and compartmentalization,

Fig. 1.4(a), [44, 45]. In recent years, many chemical systems have been reported in which one or more of these hallmarks have been reconstituted, as steps on the way to creating a living, viable protocell (a primitive cell) [44, 46]. The (proto)cellular growth, which happens due to the exchange of reactants between the compartment and its surroundings, must be different from coarsening kinetics of closed systems, like Ostwald ripening, where there is no exchange of material with the environment. Moreover, during Ostwald ripening and fusion, the total number of droplets decreases as the average size increases, Fig. 1.4(b). In the model of protocells, the decrease in the number of droplets, which model the protocells, is not desired. Protocells need to survive and replicate, for their evolution the control of their sizes and numbers are vital.

Active growth has been proposed as an alternative mechanism to passive growth [44]. By keeping the system away from relaxing toward thermodynamic equilibrium, protocells could grow while also controlling their number [47, 48]. The conditions for active growth could be achieved by an external energy input, such as a chemical reaction or a concentration gradient [49], e.g., a chemical reaction that converts precursor molecules to protocell material after input of energy [44], Fig. 1.4(c). These conditions must be incorporated in the theoretical descriptions of the coarsening kinetics of emulsions to study which processes and what kind of chemical reactions should be used to achieve controlled growth.

We now understand why it is important to study droplet coarsening kinetics under conditions of active growth. To discuss the theoretical descriptions of coarsening kinetics of emulsions, we should first revisit the theory of liquid-liquid phase separation.

1.3 Physics of liquid-liquid phase separation

In the following, we will introduce the basics of liquid-liquid phase separation, which we need in discussing coarsening kinetics of binary mixtures. We will closely follow the work on the physics of active emulsions in Ref. [49].

1.3.1 Thermodynamics of phase separation

Phase separation refers to the spontaneous partitioning of a system into subsystems with distinct macroscopic properties [49]. We consider a binary mixture of molecules A and B , with $N_{A/B}$ representing the total number of A and

B molecules respectively. The Helmholtz free energy of a homogeneous binary mixture of volume V , can be expressed in the canonical ensemble by the internal energy E and the entropy S ,

$$F = E - TS. \quad (1.1)$$

The following thermodynamic quantities are related to the derivatives of the free energy F :

The entropy $S = -\partial F/\partial T|_{V,N_A,N_B}$, the pressure $p = -\partial F/\partial V|_{T,N_A,N_B}$ and the chemical potentials $\mu_A = \partial F/\partial N_A|_{T,V,N_B}$ and $\mu_B = \partial F/\partial N_B|_{T,V,N_A}$.

For simplicity, we focus here on an incompressible binary system with constant molecular volume ν of the components. Together with constant volume V , it implies the conservation of the sum of the total number of molecules A and B . The relevant thermodynamic quantities are the exchange chemical potential $\bar{\mu}$ and the osmotic pressure Π are [49, 50, 51],

$$\bar{\mu} = \frac{\partial F}{\partial N_A} \Big|_{T,V} = - \frac{\partial F}{\partial N_B} \Big|_{T,V}, \quad (1.2a)$$

$$\Pi = \frac{\partial F}{\partial V} \Big|_{T,N_A}. \quad (1.2b)$$

Using the free energy density, $f(\phi) = F/V$, with the volume fraction of A molecules, $\phi = N_A\nu/V$, we can rewrite,

$$\bar{\mu} = \nu \frac{\partial f}{\partial \phi} \Big|_T, \quad (1.3a)$$

$$\Pi = -f + \phi \nu \frac{\partial f}{\partial \phi} \Big|_T. \quad (1.3b)$$

The Flory-Huggins free energy density describes such binary mixture, and is given by [53, 50]

$$f_{\text{mix}}(\phi) = \frac{k_B T}{\nu} [\phi \ln \phi + (1 - \phi) \ln(1 - \phi) + \chi \phi(1 - \phi)], \quad (1.4)$$

where the volume fraction of B molecules is $(1 - \phi)$. The Flory-Huggins free energy density captures the competition between the mixing entropy $S = -k_B V/\nu(\phi \ln \phi + (1 - \phi) \ln(1 - \phi))$ and the molecular interactions characterised by the parameter χ . The parameter χ is the Flory-Huggins interaction parameter, which characterizes the molecular interactions between the components A and B of the mixture. [54, 55].

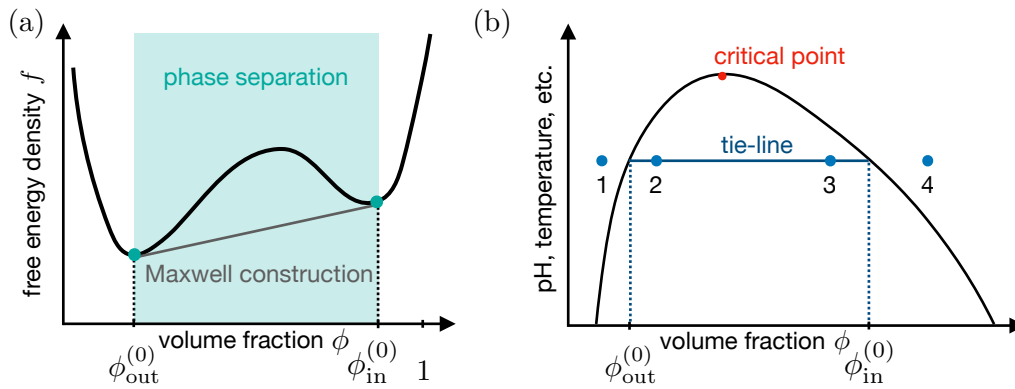


FIGURE 1.5: **Schematic free energy and phase diagram for a binary mixture:** (a): Sketch of an asymmetric free energy density $f(\phi)$ for an incompressible binary mixture as a function of volume fraction ϕ . The gray line indicates the common tangent method in the Maxwell construction. Modified from [49]. (b): Schematic of a phase diagram indicated by the coexistence line (black), which separates the one-phase and two-phase states as a function of conditions such as temperature, pH, etc. At volume fractions below equilibrium value (1) or above (4), the system is in the one-phase regime. At any condition within the two-phase regime (2,3), the system demixes into a dilute phase $\phi_{\text{out}}^{(0)}$ and a dense phase $\phi_{\text{in}}^{(0)}$. All conditions on a single tie-line (blue line) result in two phase systems with fixed conditions. Modified from [52].

If the free energy density has a non-convex shape, the global free energy F can be minimized by forming two different domains. The state for a given volume is thermodynamically stable, if it corresponds to a minimum of the global free energy F . If the molecular interactions, captured by parameter χ in Eq. (1.4), dominate the entropic terms, the free energy density is concave, $f''(\phi) > 0$, with a shape as in Fig. 1.5(a). Within this range, the homogeneous state is not stable. On the other hand, a state with two coexisting different domains is stable [49].

The realization of an inhomogeneous system is a state of two different volume fractions corresponding to in/out phases, $\phi_{\text{in}}, \phi_{\text{out}}$. The free energy can be rewritten as, $F \simeq V_{\text{in}}f(\phi_{\text{in}}) + V_{\text{out}}f(\phi_{\text{out}})$, with the volumes of the phases, $V_{\text{in}}, V_{\text{out}}$, satisfying the volume conservation, $V = V_{\text{in}} + V_{\text{out}}$, and the particle number conservation implying further $\phi_{\text{in}}V_{\text{in}} + \phi_{\text{out}}V_{\text{out}} = \phi V$. The inhomogeneous state is stable if it corresponds to a minimum of the free energy F consistent with the imposed constraint. To find this minimum, we take a derivative of F with respect to ϕ_{in} and V_{in} , Fig. 1.5(a). Setting the expressions to zero, we obtain:

$$0 = f'(\phi_{\text{in}}^{(0)}) - f'(\phi_{\text{out}}^{(0)}), \quad (1.5a)$$

$$0 = f(\phi_{\text{in}}^{(0)}) - f(\phi_{\text{out}}^{(0)}) + (\phi_{\text{out}}^{(0)} - \phi_{\text{in}}^{(0)})f'(\phi_{\text{out}}^{(0)}). \quad (1.5b)$$

The equilibrium volume fractions of the two coexisting phases are denoted by $\phi_{\text{in/out}}^{(0)}$. Comparing Eq. (1.5) with Eq. (1.3b), we see that equation Eq. (1.5a) corresponds to the balance of the exchange chemical potentials between phases, $\bar{\mu}_{\text{in}}|_{\phi=\phi_{\text{in}}^{(0)}} = \bar{\mu}_{\text{out}}|_{\phi=\phi_{\text{out}}^{(0)}}$, where Eq. (1.5b) is the balance of the osmotic pressures between the two phases, $\Pi_{\text{in}}|_{\phi=\phi_{\text{in}}^{(0)}} = \Pi_{\text{out}}|_{\phi=\phi_{\text{out}}^{(0)}}$. These conditions graphically correspond to a common tangent to the two points of the free energy density. The method of finding the equilibrium volume fractions is known as Maxwell's construction or construction of the convex hull [49]. The gray line in Fig. 1.5(a) visualises this construction.

Each value of a control parameter, e.g. temperature, pressure, etc., gives corresponding values of $\phi_{\text{in}}^{(0)}$ and $\phi_{\text{out}}^{(0)}$. For varying the control parameter, we can depict the equilibrium concentrations on a phase diagram. The phase diagram, Fig. 1.5(b), shows the coexistence region of the two phases. The separation into two phases with volume fractions $\phi_{\text{in}}^{(0)}$ and $\phi_{\text{out}}^{(0)}$ is only possible when the average volume fraction $\bar{\phi}$ fulfills $\phi_{\text{out}}^{(0)} < \bar{\phi} < \phi_{\text{in}}^{(0)}$. Outside this region, phase separation is not possible, and only the homogeneous state is stable. The coexistence line (black) in Fig. 1.5(b) separates the homogeneous and inhomogeneous regimes and corresponds to the binodal. Within the binodal curve is located a spinodal, which indicates the limit of local phase stability. Compositions between the spinodal and binodal curves, while not thermodynamically stable, are robust against small fluctuations.

1.3.2 Interface effects on phase equilibrium

Until now, we did not analyze the energetic contributions of the interface separating the two phases. Only in the thermodynamic limit, where the system and the volumes of the phases are infinitely large, the energetic contribution of the interface is negligible compared to the energetic contributions of the bulk phases. For droplets, due to their finite sizes, the effects of the curvature are, in general, non-negligible.

To determine the concentration profile that connects the two phases, we define a flat interface. For an expanded system to infinity, we can keep the position and concentration value of the interface fixed. The interface of the coexisting phases follows a $\tanh(x)$ profile, where the interfacial profile varies substantially within the interfacial width [49]. The contribution of the interface to the free energy is expressed through the surface tension γ [56].

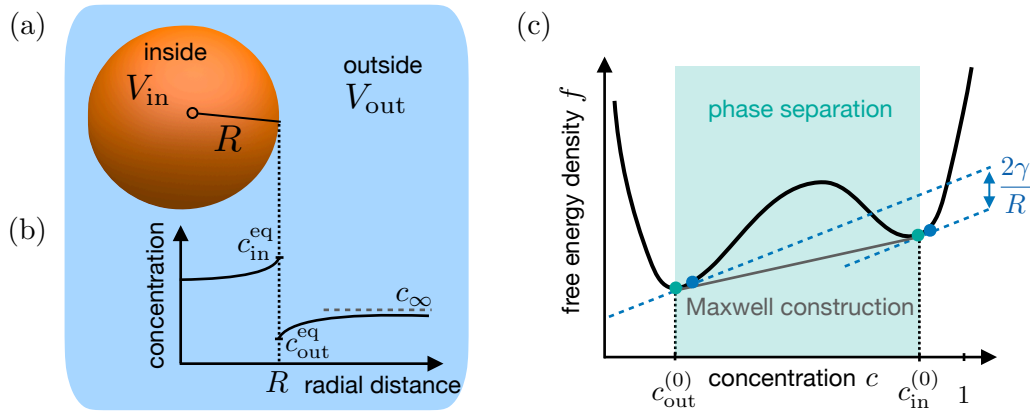


FIGURE 1.6: **Schematic concentration profile and phase diagram for finite interface effects:** (a) Single droplet of radius R representing the total dense phase volume V_{in} coexisting with the dilute phase, $(V - V_{in})$. (b) Schematic of a concentration profile of droplet material in the dense and dilute phase, given the interface conditions subject to curvature effect (Gibbs-Thomson relation). Far away from the droplet interface, the concentration is c_{∞} . (c) Sketch of a free energy density profile, where we see the shift in the equilibrium concentrations due to the Laplace pressure. Modified from [49].

Using $\phi_{in/out} = \nu c_{in/out}$, the free energy for a droplet of radius R , Fig. 1.6(a), is

$$F = V_{in}c_{in} + (V - V_{in})c_{out} + 4\pi R^2\gamma, \quad (1.6)$$

where $V_{in} = 4\pi R^3/3$, is the volume of the droplet phase and V the total system volume. The conservation of the total particle number, $V\bar{c} = \text{const}$, gives a condition for the concentration outside $c_{out} = (V\bar{c} - V_{in}c_{in})/(V - V_{in})$. In the following we consider the case where the surface tension γ is constant and independent of the interface curvature [49, 57, 58].

Analogously to minimising the free energy in Eq. 1.5, we take a derivative of F with respect to c_{in} and V_{in} , and the equilibrium conditions read then

$$0 = f'(c_{in}^{eq}) - f'(c_{out}^{eq}), \quad (1.7a)$$

$$0 = f(c_{in}^{eq}) - f(c_{out}^{eq}) + (c_{out}^{eq} - c_{in}^{eq})f'(c_{out}^{eq}) + \frac{2\gamma}{R}, \quad (1.7b)$$

where $c_{in/out}^{eq}$ are the equilibrium concentration in/outside the droplet, depicted by blue markers in Fig. 1.6(c). The additional term in the Eq. (1.7b) of the pressure balance, $2\gamma/R$, is the Laplace pressure. In the Maxwell construction, this term corresponds to the shift of the tangents Fig. 1.6(c)(blue dashed line). The effect of the Laplace pressure disappears in the thermodynamic limit, where $R \rightarrow \infty$. The Gibbs-Thomson relations, capture the effect of the

Laplace pressure on the equilibrium concentrations $c_{\text{in/out}}^{\text{eq}}$,

$$c_{\text{in}}^{\text{eq}} = c_{\text{in}}^{(0)} \left(1 + \frac{\ell_{\gamma,\text{in}}}{R} \right), \quad (1.8a)$$

$$c_{\text{out}}^{\text{eq}} = c_{\text{out}}^{(0)} \left(1 + \frac{\ell_{\gamma,\text{out}}}{R} \right), \quad (1.8b)$$

where $c_{\text{in/out}}^{(0)}$ are the equilibrium concentrations in the thermodynamic limit in the condensed and dilute phase, respectively. The capillary lengths $\ell_{\gamma,\text{in/out}}$ characterize the effect of the Laplace pressure. In the limit of strong phase separation with $c_{\text{in}}^{(0)} \gg c_{\text{out}}^{(0)}$, the impact of the Laplace pressure on the equilibrium concentration inside the droplet can be neglected, i.e. $c_{\text{in}}^{\text{eq}} \simeq c_{\text{in}}^{(0)}$. Furthermore, in the limit when the conditions of the outside phase are dilute, the capillary length is determined by the surface tensions γ , such that [32]

$$\ell_{\gamma,\text{out}} = \frac{2\gamma}{k_{\text{B}}T c_{\text{in}}^{(0)}}, \quad (1.9)$$

which only holds for the free energy density we have defined in Eq. (1.4). The concentration profile of a single droplet with the boundary conditions at the interface from the Gibbs–Thomson relations Eq. (1.8), is depicted in Fig. 1.6(a). The concentration far away from the droplet interface is c_{∞} .

The above discussion gives us a model of a single droplet in a binary mixture. Coarsening refers to a behavior of emulsions, which are composed of many droplets. In the following, we will classify emulsions through the condition of conservation law, which we will also refer to in later sections.

1.4 Classification of emulsions by matter supply

The classical LSW-theory describes coarsening kinetics of emulsions with conserved total amount of droplet material. Droplet material refers to the molecules of the type which phase separate into droplets. Due to phase separation the droplet material is enriched within the droplets and is present at a lower concentration in the phase outside the droplets. This work aims to extend the theory of Ostwald ripening to systems with broken conservation law of the total droplet material. This setting is relevant in the application of the theory of droplet coarsening to cells. As we have discussed in Subsect. 1.2, in cells the droplet building blocks can be constantly expressed, changing thus the total amount of droplet material available for droplets to grow. In the coarsening kinetics, we are interested in the late stage of emulsion kinetics

when droplets exchange material with each other without affecting the dilute concentration, which is close to equilibrium.

Passive emulsions are closed systems where the total droplet material is set by the initial condition and does not change. LSW-theory applies to passive emulsions. We will discuss the theory of coarsening for passive emulsions in the next Subsect. 1.5.

In this thesis we break the conservation of the total droplet material. **Emulsions with matter supply** refer to open binary mixtures with a supply of droplet material, which only affects the dilute phase. We restrict ourselves to the special case of a matter supply that is homogeneous in space. In an experimental realization, the emulsion would be surrounded from the outside by a matter reservoir in such a way so that the supplied matter would homogeneously spread throughout the emulsion, i.e., matter entering at the long edges of the container which embeds the emulsion. We consider matter supply that can be time-dependent, where the concentration of the droplet material in the dilute phase is constant. Furthermore, we will discuss a constant matter supply. Chapt. 3 is devoted to these cases.

As an example of **chemically-active emulsions** we focus in this thesis on binary mixtures with a fuel-driven out-of-equilibrium chemical reaction in the dilute phase. Such systems are inspired by experimentally studied emulsions in the Boekhoven lab [59, 60]. They investigate reaction cycles consisting of a reaction in which upon consumption of fuel, the precursor molecules becomes activated to droplet material. As discussed in Subsect. 1.2, such reaction cycles are explored in coacervates and give a premise of active emulsions, which in contrary to passive emulsions, could exhibit size control. The coarsening kinetics of this system will be discussed in Chapt. 4.

1.5 Coarsening kinetics of passive emulsions

In this section, we will explore the theory of coarsening kinetics of passive emulsions. We will discuss the effect of growth limited by diffusion or the interface-kinetics on the emulsion kinetics. We will see the main assumptions leading to Ostwald ripening in the diffusion limited mass transport. We will learn about the scaling laws and the statistics of growth in passive emulsions, as well as about the self-similarity of the droplet size distribution function. The following discussion is based on known theory of coarsening of passive emulsions and we will follow the seminal paper from Carl Wagner Ref. [8].

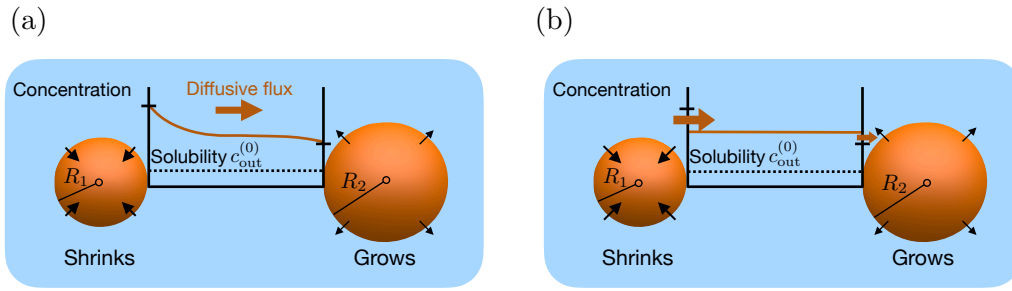


FIGURE 1.7: **Schematic for droplet growth in a rate limiting process:** (a): Diffusion limited growth of droplets. Concentration difference between two droplets results from the curvature dependence of the Gibbs-Thomson relation. Material from the smaller droplet is transported through diffusive flux to the larger droplet until its dissolution. (b): Interface-kinetics limited growth. When the interface-kinetics is slower than diffusion, droplets exchange material due to the difference between the concentration at the interface and the average concentration in the dilute phase.

The goal of this section is to gain a general intuition for the problem and learn about the main results for passive emulsions from Ref. [8] and Ref. [7]. Chapt. 2.

1.5.1 Diffusion limited and interface-kinetics limited coarsening

The droplet material is distributed between the dilute and the droplet phase, with the average concentration in the dilute phase $c(t)$. We consider a system with a homogeneous concentration of the droplet phase, which is the equilibrium value $c_{\text{in}} = c_{\text{in}}^{(0)}$. The conservation of the droplet material reads

$$\bar{c}V = c_{\text{in}}^{(0)}V_{\text{in}}(t) + c(t)(V - V_{\text{in}}(t)), \quad (1.10)$$

where $V_{\text{in}}(t)$ is the total droplet phase volume. Taking the time derivative of both sides, and using the definition of a passive emulsion, $\bar{c}V = \text{const}$ gives [8]

$$\frac{d}{dt}c(t) = -c_{\text{in}}^{(0)}\frac{d}{dt}\frac{V_{\text{in}}(t)}{V}, \quad (1.11)$$

where we have further used the assumption for the droplet phase volume, $V_{\text{in}}(t) \ll V$, i.e. droplets phase being a very small volume fraction of the whole system. If there is just a single droplet of radius R , the total droplet phase volume is $V_{\text{in}}(t) = 4\pi R^3(t)/3$. The changes of the droplet phase volume

$V_{\text{in}}(t)$ come from the changes in the radius $R(t)$, $\dot{V}_{\text{in}} = 4\pi R(t)^2 \dot{R}(t)$. For a system composed of more than one droplet, $V_{\text{in}}(t)$ can be computed from the average volume $\langle V(t) \rangle$ and the total droplet number $N(t)$, $V_{\text{in}}(t) = \langle V(t) \rangle N(t)$, such that

$$\frac{d}{dt}c(t) = -\frac{c_{\text{in}}^{(0)}}{V} \frac{d}{dt} \left(N(t) \langle V(t) \rangle \right). \quad (1.12)$$

To find the solution of $c(t)$ in Eq. (1.12), we need to know what is the droplet growth law, $\dot{R}(t)$.

There are two asymptotic regimes which define the droplet growth law, $\dot{R}(t)$, in a phase-separated system: diffusion limited and interface-kinetics limited regime, Fig. 1.7.

In liquids, mass transport occurs by diffusion [49, 2]. If diffusion with a diffusion coefficient D is slow compared to the surface transport of molecules and any other mass transport in the system, then the gradient of concentration of the droplet material at the droplet interface will dictate the amount of material that diffuses into or out of the droplet [61]. The growth law in the **diffusion limited** regime is

$$\frac{d}{dt}R(t) = \frac{D}{R} \frac{c(t) - c_{\text{out}}^{\text{eq}}(R)}{c_{\text{in}}^{(0)}}, \quad (1.13)$$

where $c_{\text{out}}^{\text{eq}}(R)$ is the concentration from the Gibbs-Thomson condition, Eq. (1.8).

In the limit of low supersaturation, the competition between the droplets for the droplet material dominates the system's dynamics. Any gradients of the chemical potential in the dilute phase will drive the material transport within the solution, Fig. 1.7(a). A droplet of a smaller radius $R_1 < R_2$ has a higher curvature and, thus, the effect of the Laplace pressure is higher. Using the Gibbs-Thomson relation Eq. (1.8) we can conclude that $c_{\text{out}}^{\text{eq}}(R_1) \gg c_{\text{out}}^{\text{eq}}(R_2)$, Fig. 1.7(a). The resulting concentration difference between the two droplets drives the material transport from a smaller droplet to the larger one. The smaller droplet will start to dissolve, since $c(t) < c_{\text{out}}^{\text{eq}}(R_1)$, while the larger droplet grows. When the small droplet finally disappears, the number of droplets $N(t)$ decreases by one, $(N(t) - 1)$, and the volume of the droplet of radius R_2 , incorporated the whole volume of the droplet R_1 . This process is called Ostwald ripening.

Another regime of droplet growth corresponds to slow relaxation kinetics to the local equilibrium at the droplet interface, Fig. 1.7(b). If the relaxation speed k is slower than the diffusion of molecules across the concentration

gradients in the solution, and if there is a jump of a chemical potential at the droplet interface, the droplet grows according to the **interface-kinetics limited** law [8]. The molecular fluxes in the interface-kinetics limited regime for phase-separated system have been discussed for flat interfaces [62, 63, 64, 65]. We will highlight the theory model by Langer and Sekerka of the departure from local equilibrium with moving interface [66] for the derivation of droplet growth in Chapt. 2. In the interface-limited kinetics, if the interface is moving very slowly on the time scale associated with diffusion, then there is no composition gradient in the outside phase, Fig.1.7(b). Droplets grow due to the difference of the concentration at the interface and that in the solution $c(t)$, with the droplet growth law [8]

$$\frac{d}{dt}R(t) = k \frac{c(t) - c_{\text{out}}^{\text{eq}}(R)}{c_{\text{in}}^{(0)}}, \quad (1.14)$$

where k is the relaxation speed toward the local equilibrium at the interface. Notice that due to the dominating volume versus area effects, the growth laws in Eq. (1.13) and Eq. (1.14) differ in their dependence on the radius R . In Ref. [8] we find a single equation which combines both processes,

$$\frac{d}{dt}R(t) = \frac{kD}{D + kR(t)} \frac{c_{\text{out}}^{(0)}}{c_{\text{in}}^{(0)}} \left(\varepsilon(t) - \frac{\ell_\gamma}{R(t)} \right), \quad (1.15)$$

where we have used the Gibbs-Thomson relation, Eq. (1.8), for $c_{\text{out}}^{\text{eq}}(R)$, and introduced supersaturation $\varepsilon(t) = (c(t) - c_{\text{out}}^{(0)})/c_{\text{out}}^{(0)}$. The capillary length we consider, $\ell_{\gamma,\text{out}} = \ell_\gamma$. By varying the ratio $kR(t)/D$, we can switch between diffusion limited ($kR(t) \gg D$) and interface-kinetics limited regime ($kR(t) \ll D$).

To derive the coarsening kinetics and the scaling laws of the average radius $\langle R(t) \rangle$, the first step is to find a solution of Eq. (1.12). In the dilute limit, close to equilibrium, when droplets compete between each other for the droplet material, the changes of the concentration $c(t)$ are negligible compared to the droplet growth, which implies a quasi-static approximation $\dot{c}(t) \simeq 0$. In this approximation the solution of Eq. (1.12) is

$$c(t) = c_{\text{out}}^{(0)} \left(1 + \ell_\gamma \frac{1}{\langle R(t) \rangle} \right) \quad \text{diffusion limited}, \quad (1.16a)$$

$$c(t) = c_{\text{out}}^{(0)} \left(1 + \ell_\gamma \frac{\langle R(t) \rangle}{\langle R^2(t) \rangle} \right) \quad \text{interface-kinetics limited}, \quad (1.16b)$$

where ℓ_γ is the capillary length, and by $\langle \bullet \rangle$ we indicate the moments of the distribution function $\mathcal{N}(R, t)$ which describes the statistics of droplet sizes. The derivation of these solutions will be discussed in more detail in Chapt. 2 and can be found in Ref. [8]. What is important to notice at this point, is that the average concentration $c(t)$ captures at each time t the evolution of the whole emulsion. Every distinct droplets which grows according to Eq. (1.15), is coupled through the supersaturation $\varepsilon(t)$ to all other droplets in the emulsion. The fixed-point of the growth law $\dot{R}(t)$, is the critical radius, which can be expressed through the supersaturation and the capillary length, $R_c(t) = \ell_\gamma/\varepsilon(t)$. From Eq. (1.16b) follows that $R_{c,\text{diff}} = \langle R(t) \rangle$ and $R_{c,\text{int}} = \langle R^2(t) \rangle / \langle R(t) \rangle$.

Lifshitz, Slyozov and Wagner have separately derived the asymptotic droplet size distribution function $\mathcal{N}(R, t)$ and its moments for passive emulsions in the diffusion limited [7, 8] and interface-kinetics limited regime [8]. The asymptotic coarsening solution of the average radius is

$$\langle R(t) \rangle = \left(\frac{4 D c_{\text{out}}^{(0)} \ell_\gamma t}{9 c_{\text{in}}^{(0)}} \right)^{1/3} \quad \text{diffusion limited,} \quad (1.17a)$$

$$\langle R(t) \rangle = \frac{8}{9} \left(\frac{k c_{\text{out}}^{(0)} \ell_\gamma t}{2 c_{\text{in}}^{(0)}} \right)^{1/2} \quad \text{interface-kinetics limited,} \quad (1.17b)$$

are depicted in Fig. 1.8. The critical radius $R_{c,\text{diff/int}}$, given its initial value at time $t = 0$, $R_{c,\text{diff/int}}(0)$, in the diffusion limited and interface-kinetics limited case is

$$R_{c,\text{diff}} = \left(R_{c,\text{diff}}(0)^3 + \frac{4 D c_{\text{out}}^{(0)} \ell_\gamma t}{9 c_{\text{in}}^{(0)}} \right)^{1/3}, \quad (1.18a)$$

$$R_{c,\text{int}} = \left(R_{c,\text{int}}(0)^2 + \frac{k c_{\text{out}}^{(0)} \ell_\gamma t}{2 c_{\text{in}}^{(0)}} \right)^{1/2}, \quad (1.18b)$$

respectively. The supersaturation, due to its dependence on the critical radius, follows $c(t) \propto R_c^{-1}(t)$, and we can see the evolution of the supersaturation profile according to this prediction in Fig. 1.8(b). We can also make a simple estimation for the total number of droplets, $N(t) = V_{\text{in}}(t)/\langle V(t) \rangle$. Coarsening in passive emulsions refers to a stage when the supersaturation is very low, and the total droplet phase volume is approximately constant, $V_{\text{in}} \simeq \text{const}$. We can approximate the average volume $\langle V(t) \rangle \propto \langle R(t) \rangle^3$, such

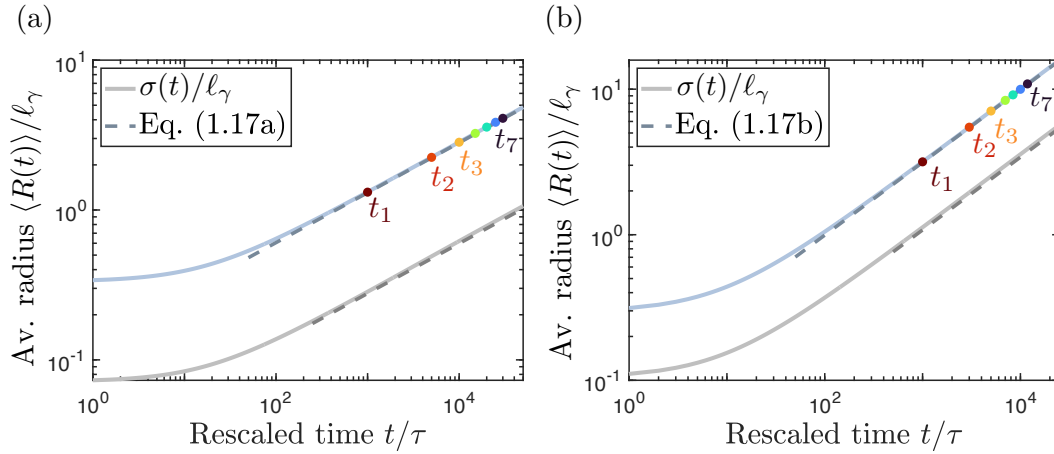


FIGURE 1.8: **Temporal evolution of the average radius and standard deviation in passive emulsions:** The plots are depicted on a log-log scale, the time t is rescaled by $\tau = \ell_\gamma^2/D$ and the radius by ℓ_γ , see Eq. (1.22). The dots corresponds to a time series of measurements we will later refer to. (a): Diffusion limited coarsening kinetics of passive emulsions. The average radius (light blue solid line) follows the theoretical LSW-prediction with the scaling $t^{1/3}$. The rescaled standard deviation $\sigma(t)/\ell_\gamma$ (grey solid line) is increasing indicating a broadening distribution function. (b): Interface-kinetics limited coarsening kinetics of passive emulsions. The average radius follows the $t^{1/2}$ law. The standard deviation (grey solid line) increases.

that the scaling law of the total droplet number

$$N(t) \propto \begin{cases} t^{-1} & \text{diffusion limited,} \\ t^{-3/2} & \text{interface-kinetics limited.} \end{cases} \quad (1.19)$$

The results for the number density $n(t) = N(t)/V$ following the scaling laws (dashed-lines) from Eq. (1.19), are depicted in Fig.1.9(a).

In the results sketched above, every moment contains the droplet size distribution function $\mathcal{N}(R, t)$. The droplet size distribution function $\mathcal{N}(R, t)$, which we will define and discuss in Chapt. 3, obeys a continuity equation [67],

$$\partial_t \mathcal{N}(R, t) = -\partial_R \left(\mathcal{N}(R, t) \frac{d}{dt} R(t) \right), \quad (1.20)$$

if we plug in Eq. (1.15),

$$\partial_t \mathcal{N}(R, t) = -\frac{c_{\text{out}}^{(0)}}{c_{\text{in}}^{(0)}} \partial_R \left(\mathcal{N}(R, t) \frac{kD}{D + kR(t)} \left(\varepsilon(t) - \frac{\ell_\gamma}{R(t)} \right) \right). \quad (1.21)$$

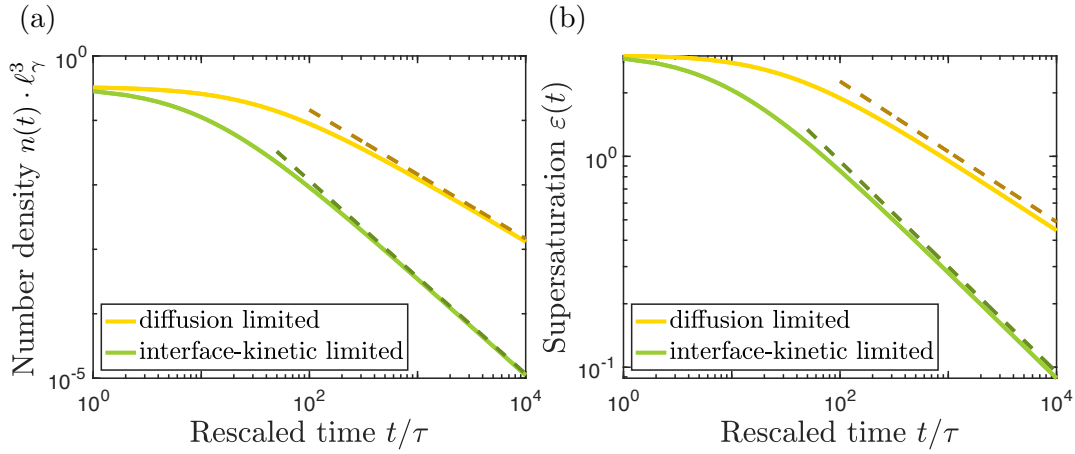


FIGURE 1.9: Temporal evolution of the number of droplets and supersaturation in passive emulsions: The plots are depicted on a log-log scale. The dashed lines correspond to the analytic derivations in the LSW-theory, Eq. (1.19) and Eq. (1.18), respectively. The time t is nondimensionalized by $\tau = \ell_\gamma^2/D$, Eq. (1.22). (a): Number of droplets decays with t^{-1} in the diffusion limited regime (yellow) and with $t^{-3/2}$ in the interface-kinetics limited regime (green). (b): Supersaturation $\varepsilon(t) \propto R_c^{-1}(t)$, decreases since the concentration $c(t)$ converges to the equilibrium $c_{\text{out}}^{(0)}$.

Numerically we solve nondimensionalized Eq. (1.21) using conservation law Eq. (1.11). The nondimensionalisation of the variables is a transformation

$$t \rightarrow t/(\ell_\gamma^2/D) \quad (1.22a)$$

$$R \rightarrow R/\ell_\gamma, \quad (1.22b)$$

such that the nondimensional form of Eq. (1.15) is

$$\frac{d}{dt}R(t) = \frac{k}{1 + k R(t)} \frac{c_{\text{out}}^{(0)}}{c_{\text{in}}^{(0)}} \left(\varepsilon(t) - \frac{1}{R(t)} \right), \quad (1.23)$$

where $k = k \cdot \ell_\gamma/D$ is also nondimensional. For the numerical calculations we chose: $\ell_\gamma = 1\mu\text{m}$, $D = 10^8\mu\text{m}^2/\text{s}$, $c_{\text{in}}^{(0)} = 200\text{mM}$, $c_{\text{out}}^{(0)} = 1\text{mM}$. For the diffusion limited case the choice of $k = 10^{20}\mu\text{m}/\text{s}$ and for the interface-kinetics $k = 10^2\mu\text{m}/\text{s}$.

1.5.2 Universal coarsening kinetics of passive emulsions

We have seen that for conserved emulsions, the average radius, the supersaturation, and the number density of droplets evolve during the coarsening kinetics with universal power laws. The exponents of the power laws are independent of the material, the system's history, and the amplitudes depend

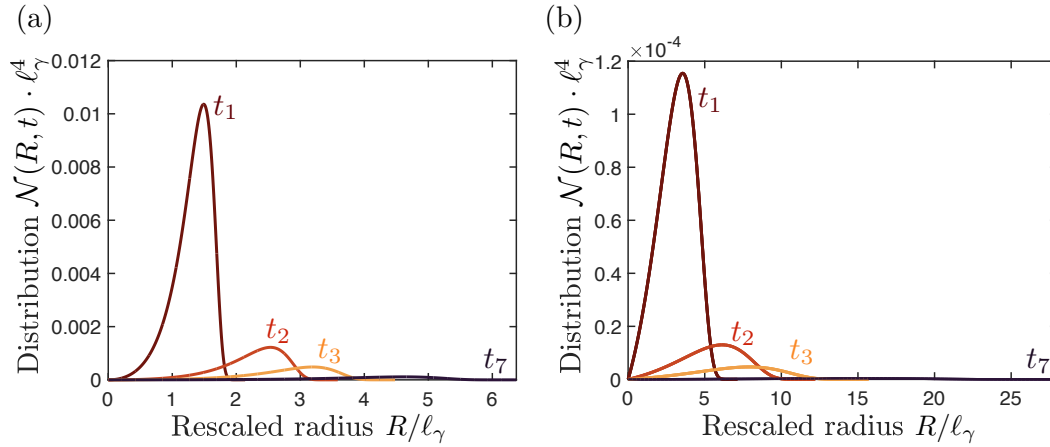


FIGURE 1.10: **Temporal evolution of the droplet size distribution function in passive emulsions:** We depict the droplet size distribution function for the first three time points ($t_1/\tau, t_2/\tau, t_3/\tau$) and the last measured time point t_7/τ during the evolution of the system in Fig. 1.8. We see that the distribution function broadens during the coarsening kinetics. (a): Diffusion limited regime. (b): Interface-kinetics limited regime. For the numerical calculations we use the same parameters as in Fig. 1.8. The radius R is rescaled by ℓ_γ . The color code for the different times corresponds to the color code used in Fig. 1.8.

on a few material constants but are also independent of initial conditions [10].

The most intriguing feature of the LSW-theory is the universal, self-similar nature of the coarsening process at long times [2]. The distribution function $\mathcal{N}(R, t)$ can be separated into a time-dependent and radial-dependent part, such that Eq. (1.20) can be solved using an ansatz $\mathcal{N}(R, t) = g(t)h(\rho)$, where the dimensionless radius, $\rho = R/R_c$, is time-invariant [8]. The universal behaviour is a direct result of the droplet material conservation law, $\bar{c}V = \text{const}$, on the longtime solution of the continuity equation, Eq. (1.20) and the kinetic equations Eq. (1.12), Eq. (1.15), [1]. It means that at all times, the distribution function can be rescaled to one universal shape. The distribution functions measured at different times t , Fig. 1.10, can be collapsed onto one curve, by rescaling the radius R to $\rho = R/R_c$ and the amplitude of distribution function by $R_c^4(t)$, Fig. 1.11.

The solution of droplet size distribution function $\mathcal{N}(R, t)$ in the diffusion limited regime is [8],

$$\mathcal{N}(\rho, t) = \begin{cases} \frac{C_{\text{diff}}}{R_c(t)^4} \rho^2 \left(\frac{3}{3+\rho}\right)^{7/3} \left(\frac{1}{1-\frac{2}{3}\rho}\right)^{11/3} \exp\left(\frac{-2\rho}{3-2\rho}\right), & \rho = \frac{R}{R_c(t)} \leq \frac{3}{2}, \\ 0, & \rho > \frac{3}{2}, \end{cases} \quad (1.24)$$

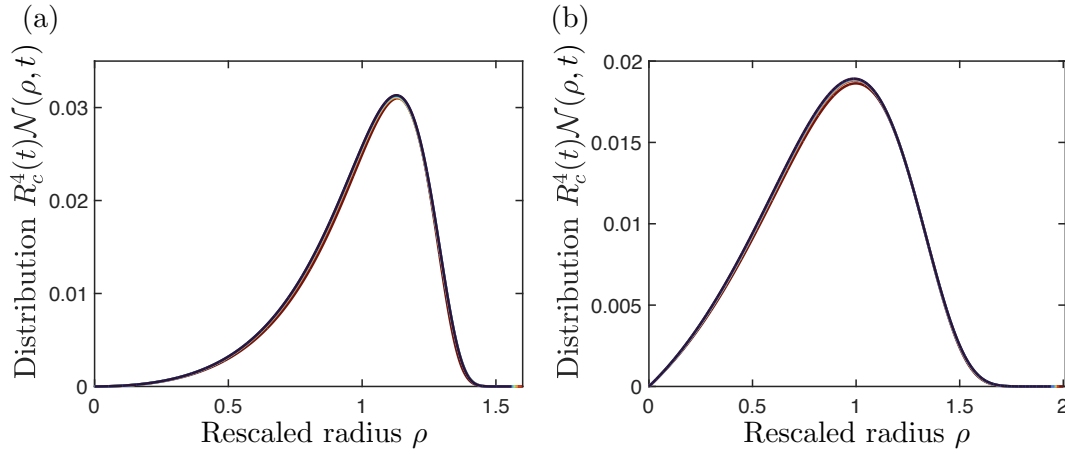


FIGURE 1.11: **Collapse of the distribution function:** The distribution functions measured at different time points from Fig. 1.8 can be collapsed on a self-similar shape by rescaling the radius R by $R_c(t)$, $\rho = R/R_c$, and the amplitude of distribution function by $R_c^4(t)$, to multiply out the time dependence of $g(t) \propto R_c^{-4}(t)$. (a): Diffusion limited regime. The distribution function becomes zero at $\rho = 1.5$. (b): Interface-limited regime. The distribution function becomes zero at $\rho = 2$. The color code for the curves on the collapse corresponds to the color scheme used to indicate the time points in Fig. 1.8.

For the interface-kinetics limited case [8],

$$\mathcal{N}(\rho, t) = \begin{cases} \frac{C_{\text{int}}}{R_c(t)^4} \rho \left(\frac{2}{2-\rho} \right)^5 \exp\left(\frac{-3\rho}{2-\rho}\right), & \rho = \frac{R}{R_c(t)} \leq 2, \\ 0, & \rho > 2, \end{cases} \quad (1.25)$$

in both cases $g(t) = C_{\text{diff/int}} R_c(t)^{-4}$. The constant $C_{\text{diff/int}}$ is determined by the initial condition of the droplet size distribution function. We can show that the time dependence of the moments of the distribution function is a function of the length scale $R_c(t)$ which we choose for the radius $\rho = R/R_c$. A k -th moment of the distribution function is defined as

$$\langle R^k(t) \rangle = \frac{\int_0^\infty R^k \mathcal{N}(R, t) dR}{\int_0^\infty \mathcal{N}(R, t) dR}. \quad (1.26)$$

By plugging in the ansatz $\mathcal{N}(R, t) = g(t)h(\rho)$, and using $\rho = R/R_c$, we find that the k -th moment scales as a k -th power of the critical radius,

$$\langle R^k(t) \rangle = R_c^k(t) \frac{\int_0^\infty \rho^k h(\rho) d\rho}{\int_0^\infty h(\rho) d\rho}. \quad (1.27)$$

The variance $\sigma^2(t)$ tells us about the behavior of the distribution function. Performing the steps before, for $\sigma^2(t)$, gives us

$$\begin{aligned}\sigma^2(t) &= \langle R^2(t) \rangle - \langle R(t) \rangle^2 \\ &= \frac{\int_0^\infty R^2 \mathcal{N}(R, t) dR}{\int_0^\infty \mathcal{N}(R, t) dR} - \left(\frac{\int_0^\infty R \mathcal{N}(R, t) dR}{\int_0^\infty \mathcal{N}(R, t) dR} \right)^2 \\ &= R_c^2(t) \left(\frac{\int_0^\infty \rho^2 h(\rho) d\rho}{\int_0^\infty h(\rho) d\rho} - \left(\frac{\int_0^\infty \rho h(\rho) d\rho}{\int_0^\infty h(\rho) d\rho} \right)^2 \right).\end{aligned}\quad (1.28)$$

For the solutions of $h(\rho)$ in Eq. (1.24) and Eq. (1.25), the difference of the integrals in the brackets is always positive. The distribution function is broadening, and the variance increases as $R_c^2(t)$. For passive emulsions, a significant result which also follows from Eq. (1.27) is that $\langle R(t) \rangle_{\text{diff}} = R_{c,\text{diff}}(t)$, and $\langle R(t) \rangle_{\text{int}} = (8/9)R_{c,\text{int}}(t)$. The average radius is equal to or slightly below the critical radius respectively.

The universal self-similar nature made Ostwald ripening an interesting process as a premise for a wide variety of two-phase mixtures. For example, fusion does not reflect this feature of universality, and its statistics depend on the initial conditions. Although the scaling of the average radius for fusion is the same as for Ostwald ripening, with $\langle R(t) \rangle \propto t^{1/3}$, the droplet size distribution function is not self-similar. The rate of fusion depends on time, and due to no upper bound in the radial domain, the distribution function has a long tail. We now have all the knowledge and intuition about the theory of coarsening for passive emulsions necessary to proceed in the following chapters with the new theory of coarsening for emulsions with matter supply.

1.6 Scope of this thesis

Extending the theory of coarsening kinetics of passive emulsions to systems with matter supply is crucial to our understanding of the evolution of emulsions in living cells and in vitro.

Chapt. 2 is dedicated to the theory of droplet growth in systems with a broken conservation law of the total droplet material. Some definitions introduced in Subsect. 1.5 were often postulated in the literature but not derived. We will discuss and derive in detail the droplet growth law where the growth rate limiting process can be diffusion or the relaxation to local equilibrium at the droplet interface. Furthermore, we will discuss the droplet material

conservation law and how it can be broken through matter supply. We will derive droplet size distribution function in systems where the conservation law of the total droplet material is broken. The question we will attempt to answer is: Are there new universality classes of emulsions with matter supply? This discussion will be the basis for Chapt. 3, where we will derive and study coarsening kinetics of emulsions corresponding to a specific class of matter supply.

In Chapt. 3, we will explore novel coarsening laws for emulsions with matter supply. We will discuss a constant matter supply and a time-dependent supply, which maintains constant supersaturation. We will derive the scaling of moments of the droplet size distribution function and its kinetics. The questions we are interested in are:

- Are there new longtime coarsening kinetics for emulsions with matter supply?
- When is the coarsening kinetics for emulsions with matter supply universal?

The preliminary results of Chapt. 3 and the comparison to passive emulsions are summarized in Tab. 1.1.

Chapt. 4 is devoted to chemically-active emulsions in which droplet material supply is controlled through a chemical reaction cycle. Precursor molecules under fuel consumption become activated to droplet material which can spontaneously deactivate to precursor molecules. We will discuss under which conditions we can write the mass action law for such a system and how does the modified conservation law look like. We will link the model to an experimental realization. The experimental realization will allow us to study coarsening in chemically-active emulsions for precursors and droplet building blocks spanning a wide range of physicochemical properties under different conditions of fuel supply. We will explore:

- Which parameters of the chemical reaction cycle influence the coarsening kinetics and in which way?
- Is the coarsening kinetics in chemically-active emulsions universal?
- What is the effect of the chemical reaction cycle on the short-time and long-time evolution of the chemically-active emulsions?

In the summary part of the thesis Chapt. 5, we will summarize the results and discuss the possible outlook. Furthermore, we will discuss the relevance of

Supply / Growth process	Diffusion limited	Interface-kinetics limited
Passive <i>no supply</i>	$\langle R(t) \rangle = \left(D \frac{4}{9} \frac{\ell_\gamma c_{\text{out}}^{(0)}}{c_{\text{in}}^{(0)}} t \right)^{1/3}$ broadening	$\langle R(t) \rangle = \frac{8}{9} \left(k \frac{\ell_\gamma c_{\text{out}}^{(0)}}{2c_{\text{in}}^{(0)}} t \right)^{1/2}$ broadening
Time-dependent <i>constant supersaturation</i>	$\langle R(t) \rangle = \left(2 \frac{D\varepsilon c_{\text{out}}^{(0)}}{c_{\text{in}}^{(0)}} t \right)^{1/2}$ narrowing	$\langle R(t) \rangle = \left(\frac{k\varepsilon c_{\text{out}}^{(0)}}{c_{\text{in}}^{(0)}} t \right)$ constant width
Constant supply	$\langle R(t) \rangle = \xi_{\text{diff}} \left(D \frac{4}{9} \frac{\ell_\gamma c_{\text{out}}^{(0)}}{c_{\text{in}}^{(0)}} t \right)^{1/3}$ broadening - narrowing	$\langle R(t) \rangle = \xi_{\text{int}} \frac{8}{9} \left(k \frac{\ell_\gamma c_{\text{out}}^{(0)}}{2c_{\text{in}}^{(0)}} t \right)^{1/2}$ broadening

TABLE 1.1: **Summary of coarsening kinetics in emulsions with different matter supply:** Table summarising asymptotic scaling laws for the average radius $\langle R(t) \rangle$, and whether the distribution function is narrowing or broadening in emulsions under different constraints. We differentiate between the two processes that define the growth law, diffusion limited and interface-kinetics limited. The passive results have been discussed in Chapt. 1, and the novel results for emulsions with supply will be derived in Chapt. 3. We will there derive and discuss the parameter $\xi_{\text{diff/int}}$, which under some conditions can be independent of the supply.

the results from the perspective of emulsions in biology and at the molecular origin of life.

Chapter 2

Theory of droplet growth in emulsions with broken conservation law

In this chapter, we derive a complete model for emulsion kinetics, in which the conservation of the total droplet material can be broken. We start with a single droplet in a binary mixture, where we consider the departure from the local equilibrium at the phase interface. We will derive the droplet growth law, which in an asymptotic regime will correspond to a diffusion limited or the interface-kinetics limited growth. The work of Langer and Sekerka in Ref. [66], about a departure from the local equilibrium at the flat interface of a binary mixture, will be of importance in our discussion. The growth laws discussed in the introduction, especially Eq. (1.17a) and Eq. (1.17b), will emerge in our derivation as asymptotic limits of the rate limiting processes.

In the second part of the chapter, we will extend the model from a single droplet to an emulsion with a general matter supply term in the dilute phase that breaks the droplet material conservation law. We will introduce the droplet size distribution function $\mathcal{N}(R, t)$ first as a sum over an ensemble of droplets to later discuss the results in the continuum limit. We will derive how a single droplet grows in an emulsion with matter supply. In the last part of the chapter, we will attempt to find an analytical solution of the droplet size distribution function for emulsions with matter supply. We will highlight the general features of the distribution function and discuss the predictions of Sugimoto in Ref. [68, 69], who suggested possible regimes of narrowing and broadening distribution function based on the relation between the average and the critical radius.

2.1 Effective droplet model

In Sect. 1.3, we learned that for a two-phase system, there exist equilibrium volume fractions, $\phi_{\text{in}}^{(0)}$, $\phi_{\text{out}}^{(0)}$ of the two phases. Since the volume fraction ϕ is continuous in space, the free energy must interpolate between the concentration of dilute and dense phases. The free energy accounts for the contribution of spatial inhomogeneities of the concentration profile across the interface.

We assume that at each position \mathbf{r} , at time t , the two-phase system is described by a scalar variable $c(\mathbf{r}, t)$, which corresponds to the local concentration of the droplet material solution, whose molecular volume, ν is independent of composition throughout the whole system and $c = \phi/\nu$. For each value of $c(\mathbf{r}, t)$, the coarse-grained free energy functional is of the form [49, 66, 70]

$$F[c] = \int d^3r \left[f_0(c) + f_{\text{mix}}(c) + \frac{\kappa}{2} |\nabla c(\mathbf{r}, t)|^2 \right], \quad (2.1)$$

where f_{mix} follows Eq. (1.4) and f_0 is the free energy of the pure system before mixing [49]. Furthermore, $\kappa = k_B T \chi \nu^{5/3}$, and characterises the concentration inhomogeneities in the free energy. The stationary solutions to Eq. (2.1) subject to the constraint of the overall conservation of molecules are sketched in Fig. 2.1(a). In the limit of strong phase separation, the interaction parameter χ in $f_{\text{mix}}(c)$ is high, leading to a large relative difference $(c_{\text{in}}^{(0)} - c_{\text{out}}^{(0)})/c_{\text{out}}^{(0)}$ for equilibrium concentrations. The interfacial width, δ_R , in this limit is of the order of the molecular size $\nu^{1/3}$.

We want to formulate the dynamical aspects of the model, describing how it reaches its equilibrium state. The particle conservation is expressed by a continuity equation, which describes the transport of a conserved quantity, which is the concentration $c(\mathbf{r}, t)$,

$$\partial_t c + \nabla \cdot \mathbf{j} = 0, \quad (2.2)$$

where \mathbf{j} is the particle flux. Solving the above equation is generally non-trivial due to the non-linear nature of the problem. For the system we consider, there is a sharp jump in the concentration value at the thin interface. In regions inside the coexisting phases and far away from the interface, we can thus linearize the concentrations $c_{\text{in/out}}$ around the uniform equilibrium values, $c_{\text{in/out}}^{(0)}$. We arrive at a diffusion equation, valid in phases $\alpha = \text{in/out}$, and reads [71]

$$\partial_t c \simeq D_\alpha \nabla^2 c, \quad (2.3)$$

where $D_\alpha = k_B T (\partial \mu_\alpha / \partial c)_{c_\alpha^{(0)}}$, is a diffusion coefficient inside and outside the droplet phase ($\alpha = \text{in/out}$). For the flux of molecules, it follows,

$$\mathbf{j}_\alpha = -D_\alpha \nabla c. \quad (2.4)$$

Furthermore, we need a condition at the interface of the phases. Usually, one can assume local phase equilibrium at the interface, which corresponds to the chemical potential of the two phases being in balance at the interface,

$$\mu^{\text{eq}} := \mu_{\text{in}} = \mu_{\text{out}}, \quad (2.5)$$

where the chemical potential at the interface $\mu_\alpha = \left. \frac{\partial f}{\partial c} \right|_{c=c_\alpha^{\text{eq}}}$. The chemical potential can be expressed in terms of the activity coefficient γ_α , the concentration c_α and the reference chemical potential μ_α^0 [72, 73, 74, 75]

$$\mu_\alpha = \mu_\alpha^0 + k_B T \log(\gamma_\alpha c_\alpha). \quad (2.6)$$

The direct effect of the local equilibrium condition, Eq. (2.5), is that the partition coefficient $P = c_{\text{in}}^{\text{eq}} / c_{\text{out}}^{\text{eq}}$, can be expressed in terms of the activity coefficients of both phases at equilibrium,

$$P = \frac{\gamma_{\text{out}}^{\text{eq}}}{\gamma_{\text{in}}^{\text{eq}}}. \quad (2.7)$$

which reflects that the partitioning of the molecules in the two phases is determined by the composition dependence of activity coefficients $\gamma_\alpha^{\text{eq}}$, [76]. We will explore the effects of the departure from local equilibrium at the interface in Subsect. 2.1.1.

Before we continue, it is worth discussing the time and length scales relevant to our problem. The shape of a droplet is parameterized in the spherical coordinate system (r, ϕ, θ) , by $\mathbf{R}(\phi, \theta; t) = \mathcal{R}(\phi, \theta; t) \mathbf{e}_r$. From now on, we will, for simplification, consider a spherically symmetric system, such that $\mathcal{R}(\phi, \theta; t) = R(t)$, and we parameterize the coordinate system accordingly. The interfacial width is small ($\delta_R \propto \nu^{1/3}$), Fig. 2.1(a), we may assume that the time $\tau_\delta = \delta_R^2 / D$ required for the interface profile to relax across the phases is smaller or compared to the time $\tau_D = l_D^2 / D$ required for diffusion processes associated with a length scale l_D . We assume that the smoothing of the interface profile will take place in a time much shorter than that required for the displacement of the interface. If the interface moves with velocity v , it follows that $\tau_\delta v \ll \delta_R$ [66]. These assumptions simplify the concentration profile

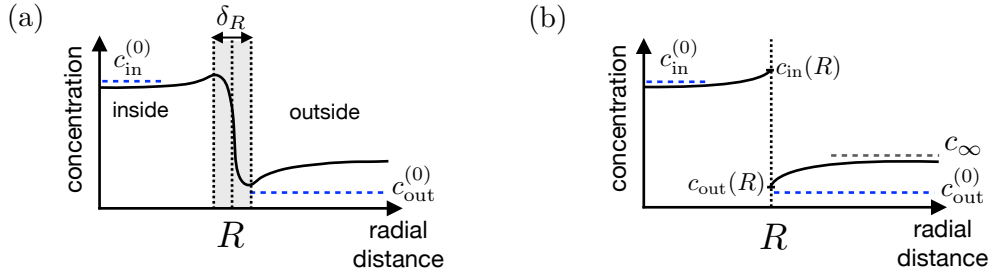


FIGURE 2.1: **Schematic of the concentration profile for the inside and outside phase across the interface:** (a): Concentration of droplet material across the phases with a tanh-profile across the interface. In bulk, away from the interface, we indicate the equilibrium concentrations $c_{in/out}^{(0)}$. (b): In the effective droplet model at the sharp interface we approximate the concentration profile by the respective boundary conditions for both phases, with $c_{in/out}(R)$ at the droplet's interface and c_{∞} far away from the interfaces.

across the two-phase system to the **effective droplet model**, where the finite interfacial width is replaced by a sharp interface and the boundary condition for the concentration in both phases at $r = R$, $c_{in/out}(r = R) = c_{in/out}(R)$, Fig. 2.1(b). In the effective droplet model, the concentration far away from the droplet interface is $c(r \rightarrow \infty) = c_{\infty}$.

2.1.1 Interface kinetics with local departure from equilibrium

In this section, we discuss the propagation of the interface R with a velocity v and consider the local departure from equilibrium at the interface. The case of small interfacial width δ_R compared to the curvature, which we have discussed above, implies $\delta_R/R \rightarrow 0$. We decide to derive the movement of the interface in a 1D system corresponding to a flat interface. The results hold for higher dimensions i.e., for spherically symmetric systems in the limit of sharp interface limits, as showed by Elder et al. in Ref. [77].

We define a frame of reference moving with a velocity v , which is defined by the equation $r' = r - \int_0^t v(t') dt'$. The concentration $c(r', t)$ in that reference frame evolves with [66]

$$\partial_t c(r', t) - v \partial_{r'} c(r', t) = \partial_t c(r, t). \quad (2.8)$$

In the moving reference frame, the continuity equation Eq. (2.2) holds, such that $\partial_t c(r', t) = -\partial_{r'} \tilde{j}(r', t)$. We also use Eq. (2.2) for the conservation law in

the center of mass reference,

$$-\partial_{r'}\tilde{j}(r', t) - v \partial_{r'}c(r', t) = -\partial_r j(r, t). \quad (2.9)$$

The conservation law in the reference frame of the moving interface implies, $\partial_t c(r', t) = 0$ and thus $\partial_{r'}\tilde{j} = 0$. The flux is constant, $\tilde{j} = \text{const}$ across the interface. The condition for both phases at the interface is, $\tilde{j}_{\text{in}} = \tilde{j}_{\text{out}}$. Integrating both sides of Eq. (2.9) across the interface $r = R$,

$$j_{\text{out}}|_R - v c_{\text{out}}(R) = j_{\text{in}}|_R - v c_{\text{in}}(R), \quad (2.10)$$

The interface moves at a velocity v [77, 66],

$$v(R) = \frac{j_{\text{in}}|_R - j_{\text{out}}|_R}{c_{\text{in}}(R) - c_{\text{out}}(R)}. \quad (2.11)$$

We want to relate the interface fluxes measured at in a reference frame which is the interface at rest, to the chemical potential differences $\Delta\mu_{\text{in}}$ and $\Delta\mu_{\text{out}}$ across the interface. The rate of entropy production, due to interface fluxes, per unit area of interface is [66, 78]

$$T\dot{S} = j_{\text{in}}\Delta\mu_{\text{in}} + j_{\text{out}}\Delta\mu_{\text{out}}, \quad (2.12)$$

where $\Delta\mu_{\text{in}} = (\mu_{\text{in}} - \mu^*)$, $\Delta\mu_{\text{out}} = (\mu^* - \mu_{\text{out}})$. The reference chemical potential at the interface, μ^* , corresponds in the linear order to the equilibrium chemical potential, $\mu^* \simeq \mu^{\text{eq}}$, determined by the tangent to the free energy minima in the Maxwell-construction Fig. 1.6(b). The fluxes $j_{\alpha}|_R$ at the interface can be expressed through their respective conjugate generalized forces $\Delta\mu_{\alpha}$ and be written as

$$j_{\text{in}}|_R = k_{\text{in}} \left(e^{\mu_{\text{in}}/k_{\text{B}}T} - e^{\mu^*/k_{\text{B}}T} \right), \quad (2.13a)$$

$$j_{\text{out}}|_R = k_{\text{out}} \left(e^{\mu^*/k_{\text{B}}T} - e^{\mu_{\text{out}}/k_{\text{B}}T} \right), \quad (2.13b)$$

where we chose an expression that suffices the detailed balance of rates [79]. The coefficients k_{α} with units $[k_{\alpha}] = \text{concentration} \cdot \text{length}/\text{time}$, characterize the relaxation of the chemical potentials to the reference μ^* at the interface R . The boundary conditions for the fluxes follow from Eq. (2.4). In spherically symmetric coordinates, with $j_{\alpha} = \mathbf{j}_{\alpha} \cdot \mathbf{e}_r$ considering that there is no polar and

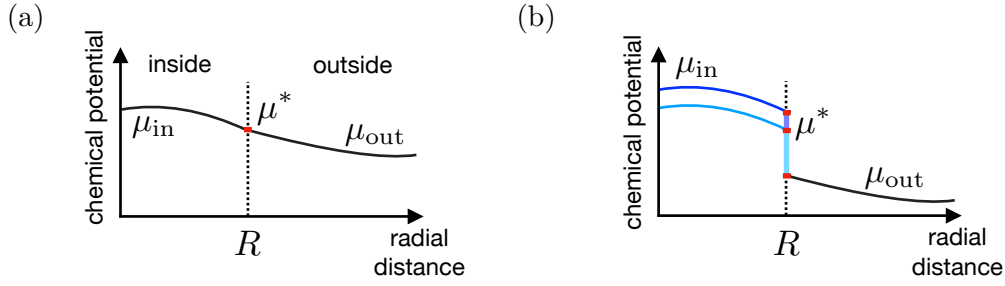


FIGURE 2.2: **Schematics of the chemical potential profile across the phases:** (a): The chemical potentials $\mu_{in/out} = \mu^*$ are equal at the interface, which corresponds to the phase equilibrium at the droplet interface. (b): Scenario with a jump in the chemical potential profile at the interface. Dark-blue line corresponds to the scenario, when both the inside and the outside phase mismatch the reference potential μ^* . The light-blue line shows a scenario when the inside is at equilibrium $\mu_{in} = \mu^*$, but for the outside there is a mismatch in the chemical potential $\mu_{out} \neq \mu^*$.

azimuthal dependence of the fields, the boundary condition reads,

$$j_{in}|_R = -D_{in} \nabla c_{in}|_R, \quad (2.14a)$$

$$j_{out}|_R = -D_{out} \nabla c_{out}|_R. \quad (2.14b)$$

2.1.2 Cases of departure from the local equilibrium at the droplet interface

In the following, we consider cases of the departure from the local equilibrium at the droplet interface. We will first look at the scenario when there is no departure, and the condition of phase equilibrium at the interface holds. We will compare the resulting movement of the interface to a case of asymmetric departure from the local equilibrium at the interface when only the outside phase is not at equilibrium.

Suppose the chemical potentials in the inside and outside phases at the interface are equal to the reference chemical potential $\mu_{out} = \mu_{in} = \mu^*$. This is a condition of local phase equilibrium at the interface, Fig. 2.2(a). In this case, since the fluxes in Eq. (2.13) have to be finite, we calculate them from the boundary condition Eq. (2.14). The equation for the movement of the interface Eq. (2.11) becomes

$$v(R) = \frac{-D_{in} \nabla c_{in}|_R + D_{out} \nabla c_{out}|_R}{c_{in}(R) - c_{out}(R)}. \quad (2.15)$$

The gradient of the concentrations in both phases at the interface determines the growth of the droplet. This case corresponds to **diffusion limited** growth.

If the interface is not locally at the equilibrium in both phases, there is a jump of the chemical potentials at the interface, Fig. 2.2(b). Using Eq. (2.6), we can rewrite the expression for the local fluxes at the interface

$$j_{\text{in}}|_R = k_{\text{in}} \left((\gamma_{\text{in}} c_{\text{in}})|_R - \gamma_{\text{in}}^{\text{eq}} c_{\text{in}}^{\text{eq}} \right), \quad (2.16a)$$

$$j_{\text{out}}|_R = k_{\text{out}} \left(\gamma_{\text{out}}^{\text{eq}} c_{\text{out}}^{\text{eq}} - (\gamma_{\text{out}} c_{\text{out}})|_R \right). \quad (2.16b)$$

Notice, that k_{α} , for $\alpha = \text{in/out}$ is a molecular flux per unit area of the interface, and does not depend on the composition.

As discussed earlier, at phase equilibrium, the partition coefficient P can be expressed in terms of the activity coefficients, Eq. (2.7). The fluxes can be thus simplified to

$$j_{\text{in}}|_R = k_{\text{in}} \gamma_{\text{in}}^{\text{eq}} P \left(\frac{(\gamma_{\text{in}} c_{\text{in}})|_R}{\gamma_{\text{in}}^{\text{eq}} P} - c_{\text{out}}^{\text{eq}} \right), \quad (2.17a)$$

$$j_{\text{out}}|_R = k_{\text{out}} \gamma_{\text{in}}^{\text{eq}} P \left(c_{\text{out}}^{\text{eq}} - \frac{(\gamma_{\text{out}} c_{\text{out}})|_R}{\gamma_{\text{in}}^{\text{eq}} P} \right). \quad (2.17b)$$

We have rewritten the fluxes in terms of the equilibrium conditions and the concentrations at the interface. The above scenario corresponds to a case when both μ_{in} and μ_{out} depart from the local equilibrium μ^* , depicted in Fig. 2.2(b) (dark blue line).

The asymmetric departure from local equilibrium can also happen, e.g., if for one of the phases only, the relaxation to equilibrium has not been reached. Consider a situation like the one depicted in Fig. 2.2(b) (light blue line). For the inside phase $\mu_{\text{in}} = \mu^*$ at the interface. In this case, $(\gamma_{\text{in}} c_{\text{in}})|_R = \gamma_{\text{in}}^{\text{eq}} c_{\text{in}}^{\text{eq}}$, and the flux $j_{\text{in}}|_R = -D_{\text{in}} \nabla c_{\text{in}}|_R$ is controlled by diffusion. We can rewrite Eq. (2.13b) for the flux in the outside phase

$$j_{\text{out}}|_R = k_{\text{out}} \left(\gamma_{\text{in}}^{\text{eq}} c_{\text{in}}^{\text{eq}} - (\gamma_{\text{out}} c_{\text{out}})|_R \right), \quad (2.18)$$

and expand $(\gamma_{\text{out}} c_{\text{out}})|_R$ around the equilibrium value up to the second order,

$$(\gamma_{\text{out}} c_{\text{out}})|_R \simeq \gamma_{\text{out}}^{\text{eq}} c_{\text{out}}^{\text{eq}} + \left(\frac{\partial \gamma_{\text{out}}}{\partial c_{\text{out}}} \Big|_{\text{eq}} c_{\text{out}}^{\text{eq}} + \gamma_{\text{out}}^{\text{eq}} \right) (c_{\text{out}}(R) - c_{\text{out}}^{\text{eq}}). \quad (2.19)$$

Since $\gamma_\alpha^{\text{eq}}$ and its derivatives are in the dilute regime constants, we can incorporate them into the coefficient k_{out} , which becomes a speed of relaxation towards the equilibrium at the interface. The flux in Eq. (2.18) becomes

$$j_{\text{out}}|_R = k_{\text{out}}(c_{\text{out}}^{\text{eq}} - c_{\text{out}}(R)). \quad (2.20)$$

The corresponding growth law, Eq. (2.11), is composed of a diffusive flux and an interface-kinetics controlled material transport,

$$v(R) = \frac{-D_{\text{in}} \nabla c_{\text{in}}|_R - k_{\text{out}}(c_{\text{out}}^{\text{eq}} - c_{\text{out}}(R))}{c_{\text{in}}(R) - c_{\text{out}}(R)}. \quad (2.21)$$

If the interface-kinetics contribution dominates the growth kinetics in Eq. (2.21), this leads to the **interface-kinetics** controlled growth.

2.1.3 Constant conditions inside the droplet

We discuss here a spherical droplet of radius $R(t)$ in a spherically symmetric system. We assume no polar or azimuthal dependence of the concentration field. Throughout this thesis, we focus on the case where the inside phase has fast relaxation towards equilibrium and there are no spatial inhomogeneities, $\nabla^2 c_{\text{in}}(r, t) = 0$. The flux inside the droplet vanishes $\partial_r c_{\text{in}}(r)|_{r=0} = 0$. Furthermore, for strong phase separation, when $c_{\text{in}}^{(0)} \gg c_{\text{out}}^{(0)}$, we can neglect the curvature effects in the Gibbs-Thomson relation for the inside, such that $c_{\text{in}}^{\text{eq}} \simeq c_{\text{in}}^{(0)}$. In this case we can set $c_{\text{in}} = c_{\text{in}}^{(0)}$, which implies $j_{\text{in}} = 0$. The equation for the movement of the interface simplifies to

$$v(R) = \frac{-j_{\text{out}}|_R}{c_{\text{in}}^{(0)} - c_{\text{out}}(R)}, \quad (2.22)$$

where $j_{\text{out}}|_R$ is given by Eq. (2.20) with the boundary condition Eq. (2.14b).

2.1.4 Quasi-static approximation and the concentration profile

To derive the droplet's growth dynamics, since the concentration profile inside is flat, we only need to know the concentration profile in the outside phase. We employ the quasi-static approximation, which assumes that the droplet radius varies slowly, such that at each (coarse-grained) time point of the droplet dynamics, we can neglect the transient of the diffusion equation,

Eq. (2.3) [49]. The diffusion equation simplifies to the Laplace equation,

$$0 \simeq \nabla^2 c_{\text{out}}(r; t) = \frac{1}{r^2} \frac{\partial}{\partial r} \left(r^2 \frac{\partial c_{\text{out}}}{\partial r} \right). \quad (2.23)$$

Since we have relaxed to a stationary solution, the time t here is a parameter determining the boundary condition but not the time dependence of the concentration. We consider a single droplet embedded in a large system, with concentration far away from the droplet interface, c_∞ , set by the condition at the system's boundary. Given the concentration at the droplet's interface $c_{\text{out}}(R)$, we have two boundary conditions for Eq. (2.23),

$$c_{\text{out}}(r = R) = c_{\text{out}}(R), \quad (2.24a)$$

$$\lim_{r \rightarrow \infty} c_{\text{out}}(r) = c_\infty. \quad (2.24b)$$

The solution of the Laplace equation for $r \geq R$, given the above conditions is

$$c_{\text{out}}(r) = c_\infty + (c_{\text{out}}(R) - c_\infty) \frac{R}{r}, \quad (2.25)$$

whereas due to the constant conditions inside, for $r < R$, $c_{\text{in}}(r) = c_{\text{in}}^{(0)}$.

2.1.5 Asymptotic relaxation at the interface

Constant conditions inside the droplet imply that we will only encounter coefficients relevant to the outside phase. Thus, we can drop the index "out" for parameters like the diffusion constant D , relaxation speed k , or when discussing the concentration profile outside.

In our model, the concentration at the boundary in the outside phase, $c(R)$, is still undetermined. Setting Eq. (2.20) equal to the boundary condition Eq. (2.14b) and using the solution in Eq. (2.25), gives

$$c(R) = \frac{D c_\infty + k R(t) c^{\text{eq}}(R)}{D + k R(t)}, \quad (2.26)$$

where we have indicated the dependence of $c^{\text{eq}}(R)$ on R from the Gibbs-Thomson relation. Wagner has also showed this solution [8], but the exact derivation was missing. Comparison of D to $kR(t)$ gives us two asymptotic regimes, which we can distinguish by $\beta = kR(t)/D$, such that: for $kR(t) \gg D$, in the diffusion limited regime ($\beta \rightarrow \infty$), the concentration $c(R)$

is determined by the Gibbs-Thomson relation,

$$\lim_{\beta \rightarrow \infty} c(R) = c^{\text{eq}}(R). \quad (2.27)$$

For $kR(t) \ll D$, which corresponds to the interface-kinetics limited regime ($\beta \rightarrow 0$), the concentration $c(R)$ is determined by the condition at the system's boundary far away from the droplet's interface,

$$\lim_{\beta \rightarrow 0} c(R) = c_{\infty}, \quad (2.28)$$

where we have used L'Hôpital's rule to perform the limit of Eq. (2.26). We reach the two asymptotic regimes by varying the ratio $\beta = kR(t)/D$, which tells about the relaxation speed to the local equilibrium at the interface compared to the diffusion in the bulk.

Plugging in the solution for $c(R)$, i.e., Eq. (2.26) into the growth law Eq. (2.22),

$$v(R) = \frac{kD}{D + kR(t)} \frac{(c_{\infty} - c^{\text{eq}})}{c_{\text{in}}^{(0)}}, \quad (2.29)$$

where we have assumed strong phase separation, such that $c_{\text{in}}^{(0)} \gg c(R)$, at all times. This result corresponds to the growth law discussed in Eq. (1.15). By varying $kR(t)$ to D , the growth law for a single droplet is corresponding either to the interface-kinetics limited growth law Eq. (1.14), or the diffusion limited regime Eq. (1.13).

2.2 Statistics of growth in emulsions

Until now, we have studied the behavior of a single droplet embed in an infinite system, with the constant concentration at the system's boundary c_{∞} . For emulsions, we need to define a system composed of many droplets sharing an average concentration in the dilute phase, which will be controlled by the external matter supply.

In the following, we will derive mathematical tools to describe emulsions from a perspective of a discrete sum over an ensemble of droplet radii, Subsect. 2.2.1, and later in Subsect. 2.2.2 by taking a continuum limit. By introducing matter supply, we will find how it affects the single droplet growth law and the evolution of emulsion. The derivation of emulsion kinetics in a discrete picture, is partially inspired by the discussion of Ostwald ripening in passive emulsions in the lecture notes of Martin Grant [80] and the notes

of James S. Langer in Ref. [71]. We expanded this discussion to the interface-kinetics limited growth of droplets and to matter supply. We focus only on emulsions with constant conditions inside the droplets.

2.2.1 Derivation of emulsion growth kinetics for each droplet

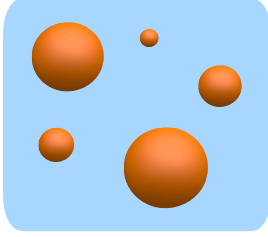


FIGURE 2.3: **Schematic of emulsion:** Emulsion is composed of many droplets coexisting with a dilute phase.

Emulsion is composed of many droplets coexisting with a dilute phase. We define a set of droplets labeled $i = 1, 2, 3, \dots, M$, each of radius $R_i(t)$, centered at positions \mathbf{r}_i . The droplet size distribution function in the discrete description is

$$\mathcal{N}(R, t) = \frac{1}{V} \sum_{i=1}^{N(t)} \delta(R - R_i), \quad (2.30)$$

where the total number of droplets is $N(t)$. Any k -th moment of the distribution is defined as

$$\langle R^k(t) \rangle = \frac{\sum_{i=1}^M R_i^k(t)}{N(t)}. \quad (2.31)$$

The units of the droplets size distribution function in Eq. (2.30) are $[\mathcal{N}] = \text{length}^{-4}$.

We treat droplets as reservoirs of droplet material, with constant concentration $c_{\text{in}}^{(0)}$. The material exchanged by each droplet with its environment due to its volumetric changes is

$$c_{\text{in}}^{(0)} \frac{d}{dt} \left(\frac{4\pi}{3} R_i^3(t) \right) = 4\pi Q_i(t), \quad (2.32)$$

where $Q_i(t)$ is a sink (or source) term of the droplet material due to droplet growth. The contributions from all droplets through the sink and source terms is a sum of the volumetric changes for all droplets, i.e., the sum of Eq. (2.32) over all droplets i , such that

$$c_{\text{in}}^{(0)} \sum_{i=1}^{N(t)} \frac{d}{dt} \left(\frac{4\pi}{3} R_i^3(t) \right) = 4\pi \sum_{i=1}^{N(t)} Q_i(t). \quad (2.33)$$

In the vector notation Fig. 2.4, a vector \mathbf{r}_i is pointing from the origin of the frame of reference to the center of a droplet i , Fig. 2.4(a). The radius of droplet i is given by $R_i = |\mathbf{r} - \mathbf{r}_i|$. The concentration field of the droplet material

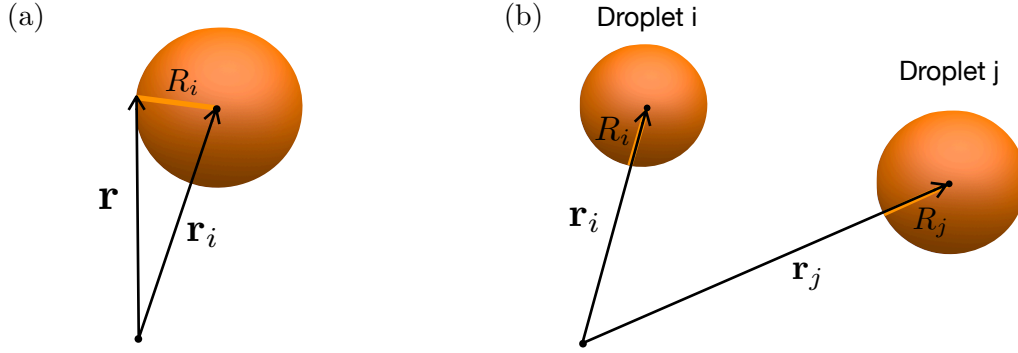


FIGURE 2.4: **Schematic of the coordinate system:** (a) Vector \mathbf{r}_i points from the origin (dot) to the center of a droplet i . Radius $R_i = |\mathbf{r} - \mathbf{r}_i|$. (b): Two droplets i and j . The vectors point from the origin, which is represented by a dot.

in the dilute phase at position \mathbf{r} is $c_{\text{out}}(\mathbf{r}, t)$. The conservation law for the concentration field, $c_{\text{out}}(\mathbf{r}, t)$ in absence of any additional matter supply, is

$$\partial_t c_{\text{out}}(\mathbf{r}, t) = D \nabla^2 c_{\text{out}}(\mathbf{r}, t) - 4\pi \sum_{i=1}^{N(t)} Q_i(t) \delta(\mathbf{r} - \mathbf{r}_i), \quad (2.34)$$

where the last term describes the distributed source associated with growing droplets [71]. We introduce a matter supply term $J_c(t)$, an additional source term that is spatially homogeneous and contributes homogeneously to the dilute phase. Without matter supply $J_c(t)$, the total amount of the droplet material in the system would be conserved and bound by the initial condition. The conservation law for the concentration field $c_{\text{out}}(\mathbf{r}, t)$ in the presence of matter supply, is

$$\partial_t c_{\text{out}}(\mathbf{r}, t) = D \nabla^2 c_{\text{out}}(\mathbf{r}, t) - 4\pi \sum_{i=1}^{N(t)} Q_i(t) \delta(\mathbf{r} - \mathbf{r}_i) + J_c(t). \quad (2.35)$$

Since $J_c(t)$ is a homogeneous matter supply and we can assume droplets being distributed homogeneously, we can incorporate $J_c(t)$ into the sum over i . We can consider the contribution of $J_c(t)$ to a sink source per droplet volume $V/N(t)$ for each droplet i ,

$$\partial_t c_{\text{out}}(\mathbf{r}, t) = D \nabla^2 c_{\text{out}}(\mathbf{r}, t) - 4\pi \sum_{i=1}^{N(t)} \left(Q_i(t) - \frac{J_c(t)V}{4\pi N(t)} \right) \delta(\mathbf{r} - \mathbf{r}_i), \quad (2.36)$$

which we can write in the form of Eq. (2.34) by substituting $Q(t)$ with

$$\tilde{Q}_i(t) = Q_i(t) - \frac{J_c(t)V}{4\pi N(t)}. \quad (2.37)$$

Employing the quasi-static assumption, $\partial_t c_{\text{out}}(\mathbf{r}, t) \simeq 0$, allows us to find a quasi-static solution for $c_{\text{out}}(\mathbf{r}; t)$, where the time dependence t arises due to the boundary conditions of the solution. We need to solve the differential equation,

$$D \nabla^2 c_{\text{out}}(\mathbf{r}; t) = 4\pi \sum_{i=1}^{N(t)} \tilde{Q}_i(t) \delta(\mathbf{r} - \mathbf{r}_i), \quad (2.38)$$

For problems like Coulomb's law above, we can use a theorem [81, p.50], $\nabla^2(1/|\mathbf{x}|) = -4\pi\delta(\mathbf{x})$. The solution of Eq. (2.38) in spherically symmetric coordinates is,

$$c_{\text{out}}(\mathbf{r}; t) = -\frac{1}{D} \sum_{i=1}^{N(t)} \frac{\tilde{Q}_i(t)}{|\mathbf{r} - \mathbf{r}_i|} + A. \quad (2.39)$$

Far away from growing interface in a finite system, the concentration is set by a homogeneous value $c_\infty(t)$. Due to this condition $A = c_\infty(t)$. Note that the time in the solution $c(\mathbf{r}; t)$ arises only due to the boundary conditions of the quasi-stationary solution. The contribution to the dilute concentration at the droplet's interface is given by term $\tilde{Q}_i(t)$. Note that we assume that droplets are point-like object far from one another that the diffusion field is not affected by any distortions in their shapes [71].

Integrating Eq. (2.38) over the dilute phase, assuming that at system's boundary there are no fluxes of droplet material,

$$0 = \sum_{i=1}^{N(t)} \tilde{Q}_i(t). \quad (2.40)$$

Using the definition of $\tilde{Q}_i(t)$, Eq. (2.37), it follows that

$$\sum_{i=1}^{N(t)} Q_i(t) = \frac{J_c(t)V}{4\pi}. \quad (2.41)$$

The effect of this result is visible when we look at Eq. (2.33). In the presence of matter supply, the total droplet phase volume changes according to added material.

Without matter supply, the exchanged material between the droplets would always balance, such that no material would be lost to the dilute phase but also there would be no change in the total droplet phase volume. The sum of

the sink and sources from all the droplets must balance, $\sum_{i=1}^{N(t)} Q_i(t) = 0$, for $J_c(t) = 0$, such that for two droplets i and j Fig. 2.4(b), $Q_i = -Q_j$.

To consider how droplets in an emulsion with matter supply grow, we should first determine the growth law of a single droplet. Given the solution $c_{\text{out}}(\mathbf{r}; t)$, we can write modified version of the growth law Eq. (2.29), in which we recognize that the i -th droplet actually sees the field $c_{\text{out}}(\mathbf{r}_i; t)$ as opposed to simply c_∞ . The equation for $\dot{R}_i(t)$, using Eq. (2.29) and Eq. (2.39),

$$\dot{R}_i(t) = \frac{kD}{D + k R_i(t)} \frac{1}{c_{\text{in}}^{(0)}} \left(-\frac{1}{D} \sum_{\substack{j=1 \\ j \neq i}}^{N(t)} \frac{\tilde{Q}_j(t)}{|\mathbf{r}_i - \mathbf{r}_j|} + c_\infty(t) - c^{\text{eq}}(R_i) \right). \quad (2.42)$$

This equation has been obtained by Wein and Cahn for the diffusion controlled coarsening in passive emulsions in Ref. [82], see also [71]. In the dilute limit of very distant droplets from each other, the term $|\mathbf{r}_i - \mathbf{r}_j| \rightarrow \infty$, which is precisely the criterion for validity of the mean-field approximation. In that case, the term with the sum vanishes, and we can consider droplets growing just through the far away concentration shared by all droplets, $c_\infty(t)$

$$\dot{R}_i(t) = \frac{kD}{D + k R_i(t)} \frac{1}{c_{\text{in}}^{(0)}} \left(c_\infty(t) - c^{\text{eq}}(R_i) \right). \quad (2.43)$$

Combining the condition of the overall droplet phase volume growth, Eq. (2.33) and the result for the sum over all sink and source terms in the presence of matter supply $J_c(t)$, Eq. (2.41) gives us

$$4\pi c_{\text{in}}^{(0)} \sum_{i=1}^{N(t)} R_i(t)^2 \dot{R}_i(t) = J_c(t), \quad (2.44)$$

where we have incorporated the total system volume into $J_c(t) = V J_c(t)$, see Eq. (2.41). Substituting the growth law $\dot{R}_i(t)$ Eq. (2.43),

$$\sum_{i=1}^{N(t)} R_i^2(t) \frac{c_\infty(t) - c^{\text{eq}}(R_i)}{D + k R_i(t)} = \frac{J_c(t)}{4\pi k D}. \quad (2.45)$$

In the limit of the diffusion $kR_i \gg D$, or the interface-kinetics limited regime, $kR_i \ll D$, we distinguish two asymptotic solutions for the supersaturation

respectively,

$$\frac{c_\infty(t) - c^{(0)}}{c^{(0)}} = \frac{J_c(t)(4\pi D c^{(0)})^{-1} + \ell_\gamma N(t)}{\sum_{i=1}^{N(t)} R_i(t)} \quad \text{for } kR_i \gg D, \quad (2.46a)$$

$$\frac{c_\infty(t) - c^{(0)}}{c^{(0)}} = \frac{J_c(t)(4\pi k c^{(0)})^{-1} + \ell_\gamma \sum_{i=1}^{N(t)} R_i(t)}{\sum_{i=1}^{N(t)} R_i^2(t)} \quad \text{for } kR_i \ll D, \quad (2.46b)$$

where we have used the Gibbs-Thomson relation, $c^{\text{eq}}(R) = c^{(0)}(1 + \ell_\gamma/R)$. Using the definition of a k -th moment Eq. (2.31), and rewriting for the supersaturation $\varepsilon(t) = (c_\infty(t) - c^{(0)})/c^{(0)}$,

$$\varepsilon(t) = \frac{J_c(t)(4\pi D N(t)c^{(0)})^{-1} + \ell_\gamma}{\langle R(t) \rangle} \quad \text{for } kR \gg D, \quad (2.47a)$$

$$\varepsilon(t) = \frac{J_c(t)(4\pi k N(t)c^{(0)})^{-1} + \ell_\gamma \langle R(t) \rangle}{\langle R^2(t) \rangle} \quad \text{for } kR \ll D. \quad (2.47b)$$

In the growth law for each droplet

$$\dot{R}(t) = \frac{kD}{D + kR(t)} \frac{c^{(0)}}{c_{\text{in}}^{(0)}} \left(\varepsilon(t) - \frac{\ell_\gamma}{R(t)} \right), \quad (2.48)$$

the information about the whole emulsion is encoded through $\varepsilon(t)$. In the absence of matter supply $J_c = 0$, the concentration shared by all droplets depends only on the distribution of droplet sizes through its first and second moment, respectively, as it is known for passive emulsions. The critical radius $R_c(t)$ is a fixed point of equation $\dot{R}(t) = 0$, thus $R_c(t) = \ell_\gamma/\varepsilon(t)$. For the two asymptotic regimes,

$$R_c(t) = \frac{\langle R(t) \rangle}{J_c(t)(4\pi D N(t)c^{(0)}\ell_\gamma)^{-1} + 1} \quad \text{for } kR \gg D, \quad (2.49a)$$

$$R_c(t) = \frac{\langle R^2(t) \rangle}{J_c(t)(4\pi k N(t)\ell_\gamma c^{(0)})^{-1} + \langle R(t) \rangle} \quad \text{for } kR \ll D, \quad (2.49b)$$

It is possible to describe the coupling between the droplets and the evolution of emulsion with matter supply using discrete formalism. We have seen how the coupling of droplets through the shared supersaturation $\varepsilon(t)$ influences the growth of every distinct droplet in the system. Only by fixing the supersaturation to be a constant, and thus breaking the dependence on the moments of the distribution function, droplets would be decoupled from each other.

2.2.2 Continuum theory for emulsion kinetics

The time derivative of the droplet size distribution function, Eq. (2.30), is

$$\frac{\partial}{\partial t} \mathcal{N}(R, t) = \frac{1}{V} \sum_{i=1}^{N(t)} \frac{\partial}{\partial t} \delta(R - R_i(t)). \quad (2.50)$$

The right hand side of the equation above can be rewritten as

$$\sum_{i=1}^{N(t)} \frac{dR_i(t)}{dt} \frac{\partial}{\partial R_i} \delta(R - R_i(t)) = - \sum_{i=1}^{N(t)} \frac{dR_i(t)}{dt} \frac{\partial}{\partial R} \delta(R - R_i(t)), \quad (2.51)$$

where we have used the property of the Dirac delta function, which directly follows from its integral definition, $\delta(x-a) = (1/2\pi) \int_0^\infty e^{ip(x-a)} dp$. Since $\dot{R}_i(t)$ has no dependence on R , we can use the product rule and write the partial derivative $\partial/\partial R$ outside the sum over i ,

$$- \sum_{i=1}^{N(t)} \frac{dR_i(t)}{dt} \frac{\partial}{\partial R} \delta(R - R_i(t)) = - \frac{\partial}{\partial R} \sum_{i=1}^{N(t)} \frac{dR_i(t)}{dt} \delta(R - R_i(t)). \quad (2.52)$$

Bringing Eq. (2.50) and Eq. (2.52) together, gives a continuity equation, which is obeyed by the droplet size distribution function,

$$\frac{\partial}{\partial t} \mathcal{N}(R, t) + \frac{\partial}{\partial R} \left(\frac{\partial R}{\partial t} \mathcal{N}(R, t) \right) = 0. \quad (2.53)$$

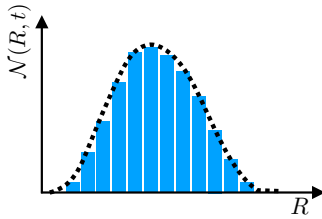


FIGURE 2.5: **Schematics of the droplet size distribution function:** The distribution function is a continuous function in radial space.

The droplet size distribution function $\mathcal{N}(R, t)$ in the discrete system, Fig. 2.5 (histogram, blue bars of width ΔR), can be replaced by a continuous function defined in space R , Fig. 2.5 (black dashed line). We introduce $\mathcal{N}(R, t)$ by taking the step size ΔR in the discrete description to be infinitesimally small and counting the number density of droplets between radius R and $R + \Delta R$,

$$\mathcal{N}(R, t) = \lim_{\Delta R \rightarrow 0} \frac{n(R, R + \Delta R, t)}{\Delta R}. \quad (2.54)$$

The droplet number density is defined as,

$$n(t) = \int_0^\infty \mathcal{N}(R, t) dR, \quad (2.55)$$

where the radius $R \in [0, \infty)$. The dimensions of the droplet size density function are $[\mathcal{N}(R, t)] = \text{length}^{-4}$.

Since we do not consider nucleation of droplets, the droplet number density $n(t)$ can only change due to droplets dissolving. If we integrate the continuity equation Eq. (2.53) we obtain

$$\int_0^\infty \frac{d}{dt} \mathcal{N}(R, t) dR = - \int_0^\infty \frac{\partial}{\partial R} (\dot{R}(t) \mathcal{N}(R, t)) dR. \quad (2.56)$$

Using the definition of the droplet number density, Eq. (2.55) and assuming that the droplet size distribution function vanishes at infinity, we find how the droplet number density changes in time

$$\frac{d}{dt} n(t) = - \left(\dot{R}(t) \mathcal{N}(R, t) \right) \Big|_{R=0}. \quad (2.57)$$

The droplet number density changes only due to events of dissolution at $R = 0$. Furthermore, the k -th moment of the distribution, Eq. (2.31), is defined as

$$\langle R^k(t) \rangle = \frac{\int_0^\infty R^k(t) \mathcal{N}(R, t) dR}{\int_0^\infty \mathcal{N}(R, t) dR}, \quad (2.58)$$

and we define the droplet phase volume fraction $\Phi(t)$ as

$$\Phi(t) = \int_0^\infty \frac{4\pi}{3} R^3(t) \mathcal{N}(R, t) dR. \quad (2.59)$$

We can immediately see that the transition from the discrete picture, where the distribution function was a Dirac delta function, Eq. (2.30), to continuum corresponds to the transition

$$\frac{d}{dt} \sum_{i=1}^{N(t)} \frac{4\pi}{3} R_i^3(t) \delta(\mathbf{r} - \mathbf{r}_i) \rightarrow \frac{d}{dt} \int_0^\infty \frac{4\pi}{3} R^3(t) \mathcal{N}(R, t) dR. \quad (2.60)$$

We can thus very simply rewrite the conservation law in Eq. (2.35) in the continuum limit. For this we replace the sum over all sink and source terms of the droplet material, which was defined in Eq. (2.33) through the volumetric changes of all droplets, by the droplet phase volume fraction $\Phi(t)$, such that the conservation law becomes

$$\partial_t c_{\text{out}}(\mathbf{r}, t) = D \nabla^2 c_{\text{out}}(\mathbf{r}, t) - c_{\text{in}}^{(0)} \frac{d}{dt} \int_0^\infty \frac{4\pi}{3} R^3(t) \mathcal{N}(R, t) dR + J_c(t). \quad (2.61)$$

At this point, we can use the argument of time scale separation. Droplets

grow by the exchange of material between each other, and they pick additional material through the matter supply $J_c(t)$. The growth of droplets in the quasi-static approximation is much slower than the diffusion of concentration profiles $c_{\text{out}}(\mathbf{r}, t)$ away from droplets. There is a separation of timescales such that there is a balance between $\partial_t c_{\text{out}}(\mathbf{r}, t) = D \nabla^2 c_{\text{out}}(\mathbf{r}, t)$ and, the balance between

$$0 \simeq -c_{\text{in}}^{(0)} \int_0^\infty 4\pi R^2(t) \dot{R}(t) \mathcal{N}(R, t) dR + J_c(t). \quad (2.62)$$

from which also follows a condition for the time derivative of the droplet phase volume fraction $\Phi(t)$ (Eq. (2.59)),

$$\frac{d}{dt} \Phi(t) = \frac{J_c(t)}{c_{\text{in}}^{(0)}}. \quad (2.63)$$

This equations is the continuum analog to Eq. (2.41). In the absence of matter supply $J_c(t) = 0$, droplets can only grow by exchanging material with each other. In the presence of $J_c(t)$, growth and volumetric changes are dictated by matter supply.

As we have learned in the previous discussion, to calculate the growth of each droplet in an emulsion, we need to calculate the supersaturation as a function of the whole emulsion. We again use the droplet growth law Eq. (2.29) for the condition in Eq. (2.62) to solve for the quasi-static solution of the supersaturation $\varepsilon(t) = (c_\infty(t) - c^{(0)})/c^{(0)}$. We use the Gibbs-Thomson relation for $c^{\text{eq}}(R) = c^{(0)}(1 + \ell_\gamma/R)$, Eq. (1.8). The solution for the supersaturation is

$$\varepsilon(t) = \frac{\ell_\gamma \int_0^\infty \left(\frac{R}{D+kR} \right) \mathcal{N}(R, t) dR + J_c(t) (4\pi k D c^{(0)})^{-1}}{\int_0^\infty \left(\frac{R^2}{D+kR} \right) \mathcal{N}(R, t) dR}. \quad (2.64)$$

The growth law for a distinct droplet of radius $R(t)$ embed in an emulsion of supersaturation $\varepsilon(t)$ with matter supply $J_c(t)$ is

$$\dot{R}(t) = \frac{kD}{D+kR(t)} \frac{c^{(0)} \ell_\gamma}{c_{\text{in}}^{(0)}} \left(\frac{\int_0^\infty \left(\frac{RN(R,t)}{D+kR} \right) dR + J_c(t) (4\pi k D \ell_\gamma c^{(0)})^{-1}}{\int_0^\infty \left(\frac{R^2 N(R,t)}{D+kR} \right) dR} - \frac{1}{R(t)} \right). \quad (2.65)$$

We introduce a new variable $\beta = kR/D$, which tells us about the ratio of the two rate limiting processes: Diffusion and interface-kinetics. If diffusion is the limiting process, $D \ll kR$ and $\beta \rightarrow \infty$. Otherwise, $D \gg kR$ implies $\beta \rightarrow 0$. Thus, we can distinguish two asymptotic results for the critical radius

$R_c(t; \beta)$,

$$R_c(t; \infty) = \frac{\int_0^\infty R \mathcal{N}(R, t) dR}{\int_0^\infty \mathcal{N}(R, t) dR + J_c(t) (4\pi D \ell_\gamma c^{(0)})^{-1}}, \quad (2.66a)$$

$$R_c(t; 0) = \frac{\int_0^\infty R^2 \mathcal{N}(R, t) dR}{\int_0^\infty R \mathcal{N}(R, t) dR + J_c(t) (4\pi k \ell_\gamma c^{(0)})^{-1}}. \quad (2.66b)$$

Without matter supply, when $J_c(t) = 0$, we retrieve the classical results, with $R_c(t; \infty) = \langle R(t) \rangle$ and $R_c(t; 0) = \langle R^2(t) \rangle / \langle R(t) \rangle$.

By using the appropriate limits, the growth law simplifies to

$$\dot{R}(t; \infty) = \frac{D}{R(t)} \frac{c^{(0)} \ell_\gamma}{c_{\text{in}}^{(0)}} \left(\frac{\int_0^\infty \mathcal{N}(R, t) dR + J_c(t) (4\pi D \ell_\gamma c^{(0)})^{-1}}{\int_0^\infty R \mathcal{N}(R, t) dR} - \frac{1}{R(t)} \right), \quad (2.67a)$$

$$\dot{R}(t; 0) = k \frac{c^{(0)} \ell_\gamma}{c_{\text{in}}^{(0)}} \left(\frac{\int_0^\infty R \mathcal{N}(R, t) dR + J_c(t) (4\pi k \ell_\gamma c^{(0)})^{-1}}{\int_0^\infty R^2 \mathcal{N}(R, t) dR} - \frac{1}{R(t)} \right), \quad (2.67b)$$

where we have also introduced a parameter β , $\dot{R}(t; \beta)$. We have retrieved all results as discussed in the discrete derivation in Subsect. 2.2.1. We will use these equations directly in Chapt. 3 to discuss the effect of different matter supply scenarios on the coarsening kinetics of emulsions. In the following, we will discuss the separation ansatz for the droplet size distribution function and the time dependence of the critical radius $R_c(t)$.

2.2.3 Separation ansatz for the droplet size distribution function

Since we do not consider nucleation of droplets or droplets being added to the system, the change in the droplet number density $n(t)$ comes only from the dissolution of droplets, which happens for $R \leq R_c(t)$. We have derived the law for the droplet number density change in Eq. (2.57), which is

$$\frac{d}{dt} n(t) = \dot{R}(t) \mathcal{N}(R, t) \Big|_{R=0}. \quad (2.68)$$

Using the part of the growth law $\dot{R}(t)$, Eq. (2.67), which is valid for $R \leq R_c(t)$, we obtain [8]

$$\frac{dn(t)}{dt} = \frac{kD}{(D + k R(t))} \frac{\ell_\gamma c^{(0)}}{R(t) c_{\text{in}}^{(0)}} \mathcal{N}(R, t) \Big|_{R=0}. \quad (2.69)$$

This holds both for passive emulsions and emulsions with matter supply, since $J_c(t)$ only contributes in the growth law for $R > R_c(t)$. The condition for the droplet number density will determine the radial dependence of the droplet size distribution function $\mathcal{N}(R, t)$.

For passive emulsions, the final state of the coarsening process is just one droplet. Thus, for passive emulsions the droplet number density $n(t)$ will decrease. If the droplet number density decreases, Eq. (2.69) should be finite. In order to counteract the divergence at $R = 0$ in the two asymptotic cases of diffusion or interface-kinetics limited growth, where $\beta \rightarrow \infty$ and $\beta \rightarrow 0$, with $\beta = kR(t)/D$ respectively, the dependence on the radius R of the droplet size distribution function in passive emulsions is

$$\mathcal{N}(R, t; \infty) \propto R^2(t), \quad (2.70a)$$

$$\mathcal{N}(R, t; 0) \propto R(t). \quad (2.70b)$$

The separation ansatz for the droplet size distribution function is, $\mathcal{N}(\rho, t) = g(t)h(\rho)$ [8], where the rescaled radius $\rho = R(t)/l_c(t)$, is scaled by a length scale $l_c(t)$. The normalization condition is $h(\rho = 0) = 1$.

For passive emulsions, given the condition in Eq. (2.70) which holds for small values of R , it follows that $\mathcal{N}(\rho, t; \infty) = \rho^2 \tilde{h}(\rho; \infty)g(t; \infty)$, and $\mathcal{N}(\rho, t; 0) = \rho \tilde{h}(\rho; 0)g(t; 0)$. In passive emulsions the choice of the length scale is the critical radius $l_c(t) = R_c(t)$. Depending on the time dependence of the droplet number density $n(t)$, in Eq. (2.69), the dependence on the radius R of the droplet size distribution function might differ.

The time-dependent part of the separation ansatz $g(t)$ can be defined through any moment. The typical choice is to define it through the droplet phase volume fraction $\Phi(t)$, Eq. (2.59), such that [8]

$$g(t) = \frac{3\Phi(t)}{4\pi l_c(t)^4 \int_0^\infty \rho^3 h(\rho) d\rho}. \quad (2.71)$$

Without matter supply $\dot{\Phi}(t) = 0$, which follows from Eq. (2.63), and in passive emulsions, the droplet phase volume fraction $\Phi(t)$ is constant. For systems with matter supply, this is not the case anymore, and we need to take into account that $g(t)$ can have, in general, a nontrivial dependence on the time t .

Applying the separation ansatz to the the continuity equation, Eq. (2.53), we can attempt to solve for the analytical solution of the droplet size distribution

function $\mathcal{N}(R, t)$. We will see that it is not possible to find a complete analytical solution for emulsions with matter supply. However, we will work in the analytical approach as far as possible and discuss the final results compared to passive emulsions in the LSW-theory.

2.3 Analytical solution of the droplet size distribution function for emulsions with matter supply

The correctness of the separation ansatz for the droplet size distribution function can be checked, if, after using the continuity equation Eq. (2.53), we can separate the radial and temporal contributions from each other. In the following, we will discuss the separation ansatz $\mathcal{N}(\rho, t) = g(t)h(\rho)$, with $\rho = R(t)/l_c(t)$ and $g(t) \propto \Phi(t)l_c^{-4}(t)$, from Eq. (2.71). We do not determine yet the length scale $l_c(t)$, which is a length scale of choice.

We are interested how the matter supply $J_c(t)$ influences the validity of the separation ansatz and if it is possible to solve for the droplet size distribution function. Note that in our derivation the important condition is that the matter supply is homogeneous in space. Otherwise, we would need to take into account the fluctuations in the diffusion profile of the concentration field and the growth law might change as well. We focus here on a class of matter supply, that can be defined through the power law time dependence, such that $J_c(t)/(c_{\text{in}}^{(0)}) = \tilde{J}_c \cdot t^\alpha$, with α determining the power law. We can write the droplet phase volume fraction using the result in Eq. (2.63),

$$\Phi(t) = \Phi(0) + \frac{\tilde{J}_c}{\alpha + 1} \cdot t^{\alpha+1}. \quad (2.72)$$

The continuity equation is

$$\partial_t \mathcal{N}(R, t) = \partial_R(\dot{R}(t)\mathcal{N}(R, t)). \quad (2.73)$$

The left-hand side of the continuity equation, using the ingredients discussed above, is

$$\partial_t \mathcal{N}(R, t) = \dot{l}_c(t)l_c^{-5}(t)\Phi(t) \left(-4h(\rho) - \rho h'(\rho) + h(\rho)l_c(t) \frac{\dot{\Phi}(t)}{\Phi(t)} \right). \quad (2.74)$$

Using $\Phi(t) \propto t^{\alpha+1}$ and thus $\dot{\Phi}(t)/\Phi(t) = (\alpha + 1)t^{-1}$,

$$\partial_t \mathcal{N}(R, t) = \dot{l}_c(t) l_c^{-5}(t) \Phi(t) \left(-4h(\rho) - \rho h'(\rho) + (\alpha + 1)h(\rho) l_c(t) t^{-1} \right). \quad (2.75)$$

For $\alpha = -1$, the last term in the sum will always vanish, and we can separate the left-hand side of the continuity equation as a product of a time-dependent and radial-dependent function. Furthermore, as long as the time dependence of the length scale $l_c(t)$ is such that in the asymptotic limit $t \rightarrow \infty$, which is valid in the regime of coarsening

$$\lim_{t \rightarrow \infty} (l_c(t) t^{-1}) = 0, \quad (2.76)$$

we can neglect the last term of the sum. In passive emulsions, this term was not present due to $\dot{\Phi} = 0$. If in emulsions with matter supply there is a length scale that fulfills the condition in Eq. (2.76), we can choose it to separate the left-hand side of the continuity equation into

$$\partial_t \mathcal{N}(R, t) = \dot{l}_c(t) l_c^{-5}(t) \Phi(t) F(\rho, h(\rho)). \quad (2.77)$$

We will now, analogously, rewrite the right-hand side of the continuity equation Eq. (2.73). We distinguish between the two asymptotic regimes of growth limited by diffusion $\beta \rightarrow \infty$ or interface-kinetics, $\beta \rightarrow 0$. The growth laws $\dot{R}(t; \beta)$ (Eq. (2.67)) are:

$$\dot{R}(t; \infty) = \frac{v_{\text{diff}}}{R(t)} \left(\frac{1}{R_c(t)} - \frac{1}{R(t)} \right), \quad (2.78a)$$

$$\dot{R}(t; 0) = v_{\text{int}} \left(\frac{1}{R_c(t)} - \frac{1}{R(t)} \right), \quad (2.78b)$$

where we have used v_{diff} and v_{int} ,

$$v_{\text{diff}} = \frac{D c^{(0)} \ell_\gamma}{c_{\text{in}}^{(0)}}, \quad (2.79a)$$

$$v_{\text{int}} = \frac{k c^{(0)} \ell_\gamma}{c_{\text{in}}^{(0)}}. \quad (2.79b)$$

The units are $[v_{\text{diff}}] = \text{length}^3/\text{time}$ and $[v_{\text{int}}] = \text{length}^2/\text{time}$. Using the growth laws we can write for the right-hand side of the continuity equation

in the two regimes, such that for the diffusion limited regime,

$$\begin{aligned} \partial_R(\dot{R}(t; \infty)\mathcal{N}(R, t; \infty)) &= \\ &= \frac{v_{\text{diff}}\Phi(t)}{l_c^4(t)} \left(\frac{h'(\rho)}{l_c(t)} (R_c^{-1}(t)R^{-1}(t) - R^{-2}(t)) - \frac{h(\rho)}{R_c(t)R^2(t)} + \frac{2h(\rho)}{R^3(t)} \right), \end{aligned} \quad (2.80a)$$

and for the interface-kinetics limited regime,

$$\partial_R(\dot{R}(t; 0)\mathcal{N}(R, t; 0)) = \frac{v_{\text{int}}\Phi(t)}{l_c^4(t)} \left(\frac{h'(\rho)}{l_c(t)} (R_c^{-1}(t) - R^{-1}(t)) - \frac{h(\rho)}{R^2(t)} \right). \quad (2.80b)$$

To simplify the calculations further, one can substitute $R(t) = \rho l_c(t)$. We immediately see that if there exists a time-dependent critical radius, a choice of $l_c(t) = R_c(t)$ is the right choice to separate the temporal and radial parts of the equations even further. The substitution for the choice of $l_c(t)$ results in

$$\partial_R(\dot{R}(t; \infty)\mathcal{N}(R, t; \infty)) = \frac{v_{\text{diff}}\Phi(t)}{R_c^7(t)} \left(h'(\rho)(\rho^{-1} - \rho^{-2}) - h(\rho)\rho^{-2}(1 - 2\rho^{-1}) \right), \quad (2.81a)$$

$$\partial_R(\dot{R}(t; 0)\mathcal{N}(R, t; 0)) = \frac{v_{\text{int}}\Phi(t)}{R_c^6(t)} \left(h'(\rho)(1 - \rho^{-1}) - h(\rho)\rho^{-2} \right). \quad (2.81b)$$

We were able to separate the equation into temporal and ρ dependent parts,

$$\partial_R(\dot{R}(t; \infty)\mathcal{N}(R, t; \infty)) = \frac{v_{\text{diff}}\Phi(t)}{R_c^7(t)} G(\rho, h(\rho); \infty), \quad (2.82a)$$

$$\partial_R(\dot{R}(t; 0)\mathcal{N}(R, t; 0)) = \frac{v_{\text{int}}\Phi(t)}{R_c^6(t)} G(\rho, h(\rho); 0), \quad (2.82b)$$

where $G(\rho, h(\rho); \beta)$ captures the dependence on ρ and $h(\rho)$.

Combining both sides of the continuity equation, Eq. (2.75) and Eq. (2.81), and using $l_c(t) = R_c(t)$ gives us

$$\dot{R}_c(t; \infty)R_c^2(t; \infty) = v_{\text{diff}} \frac{G(\rho, h(\rho); \infty)}{F(\rho, h(\rho))}, \quad (2.83a)$$

$$\dot{R}_c(t; 0)R_c(t; 0) = v_{\text{int}} \frac{G(\rho, h(\rho); 0)}{F(\rho, h(\rho))}. \quad (2.83b)$$

Integrating both sides of the equations above over the time t gives a solution for the critical radius in the diffusion and interface-kinetics limited regime,

for emulsions with matter supply

$$R_c(t; \infty) = (3 v_{\text{diff}} t \Lambda_\infty)^{1/3}, \quad (2.84a)$$

$$R_c(t; 0) = (2 v_{\text{int}} t \Lambda_0)^{1/2}, \quad (2.84b)$$

which, up to a yet undetermined constant $\Lambda_\beta = G(\rho, h(\rho); \beta)/F(\rho, h(\rho))$. Notice that the assumption we made to neglect the term $R_c(t)t^{-1}$ in Eq. (2.75) can be now verified. The contribution of this term, given Eq. (2.81) leads to $R_c(t; \infty) \propto t^{1/2}$ and $R_c(t; 0) \propto t^{2/3}$. Both of these results on the other hand, will in the asymptotic limit fulfil the condition Eq.(2.76), becoming negligible again. Even if matter supply leads to a different time-dependence of the critical radius than the one in Eq. (2.84b), as long as the critical radius is not constant, this effect would be transient.

A very important result, is that in both cases the functional form of Λ_β , which must be a constant number, is exactly the same as in passive emulsions. Following Bray in Ref. [32], who considered diffusion limited case only, we can write for $\rho = R/R_c$

$$\frac{d\rho}{dt} = \frac{1}{R_c} \dot{R} - \frac{R}{R_c} \dot{R}_c. \quad (2.85)$$

The growth law in Eq. (2.78) and the results for $R_c(t; \beta)$ in Eq. (2.84b) imply for the two asymptotic cases $\beta \rightarrow \infty$ and $\beta \rightarrow 0$,

$$\frac{d}{dt}\rho = \frac{1}{3\Lambda_\infty t} (\rho^{-1} - \rho^{-2} - \Lambda_\infty \rho), \quad (2.86a)$$

$$\frac{d}{dt}\rho = \frac{1}{2\Lambda_0 t} (1 - \rho^{-1} - \Lambda_0 \rho). \quad (2.86b)$$

For the behaviour of ρ to be physical, we need to find Λ_β such that ρ does not diverge. The expression in brackets has a shape of an inverted parabola, and a choice of Λ_β for which there is a stable fixed point that is reached as a power law and not exponentially quickly is a right one. Through a graphical method we find a solution when there is a single fixed point, $\Lambda_\infty = 4/27$ [32] and $\Lambda_0 = 1/4$. Given this results, the critical radius for emulsions with matter supply behaves exactly like in passive emulsions, both in the scaling exponent and in the scaling prefactor (see Eq. (1.18)),

$$R_c(t; \infty) = \left(\frac{4 D c^{(0)} \ell_\gamma}{9 c_{\text{in}}^{(0)}} t \right)^{1/3}, \quad (2.87a)$$

$$R_c(t; 0) = \left(\frac{k c^{(0)} \ell_\gamma}{2 c_{\text{in}}^{(0)}} t \right)^{1/2}. \quad (2.87b)$$

The only part of the droplet size distribution function we are missing is $h(\rho)$. Wagner in Ref. [8] used the results in Eq. (2.84b) and Eq. 2.83b, which can be combined into $\Lambda_\beta F(\rho, h(\rho)) = G(\rho, h(\rho); \beta)$. To simplify expression after the integration over ρ , he has used the condition which holds for passive emulsions that $R_c(t; \infty) = \langle R(t; \infty) \rangle$ and $R_c(t; 0) = \langle R^2(t; 0) \rangle / \langle R(t; 0) \rangle$. With matter supply, see Eq. (2.66), this does not hold. Furthermore, the condition for the solution of $h(\rho)$ was that the droplet phase volume fraction $\Phi(t)$ is constant thus $h(\rho)$ cannot be non-zero for arbitrary large ρ . With matter supply it is not anymore the case.

Before we finalize this chapter and move to Chapt. 3, in which we analyse the droplet size distribution function numerically, we will shortly determine the kinetics of the droplet size distribution function through the prediction of its narrowing and broadening regimes. We should remember, that the derivation we have done above, holds only for systems where the distribution function broadens and when the critical radius is not constant. If the distribution function narrows, or the critical radius is constant, the separation ansatz $\mathcal{N}(R, t) = g(t)h(\rho)$, with $\rho = R/R_c$ is not valid anymore.

2.4 Prediction of a broadening and narrowing zone of the droplet size distribution function

An important feature of the distribution function $\mathcal{N}(R, t)$ is if the distribution function broadens or narrows in time. If it broadens, it spans over time a larger domain of droplet radii; if it narrows, the domain of droplet sizes focuses around one value, corresponding to a size control mechanism. Sugimoto in Ref. [69] has proposed a simple approximation for the standard deviation and its time behavior given the growth laws in Eq. (2.67).

Sugimoto in Ref. [69] approximates the standard deviation $\sigma(t) \simeq \Delta R = (R_2 - R_1)$, as a distance between two radii $R_2 > R_1$. The growth laws Eq. (2.67) in terms of the critical radii are: $\dot{R}(t; \infty) = v_{\text{diff}}(1/R_c(t) - 1/R)/R$, $\dot{R}(t; 0) = v_{\text{int}}(1/R_c(t) - 1/R)$, with $v_{\text{diff}} = D c^{(0)} \ell_\gamma / c_{\text{in}}^{(0)}$ and $v_{\text{int}} = k c^{(0)} \ell_\gamma / c_{\text{in}}^{(0)}$ respectively. Taking the radial derivative of both equations gives us

$$d \left(\frac{dR(t; \infty)}{dt} \right) = \frac{v_{\text{diff}}}{R^2} \left(\frac{2}{R} - \frac{1}{R_c(t)} \right) dR, \quad (2.88a)$$

$$d \left(\frac{dR(t; 0)}{dt} \right) = \frac{v_{\text{int}}}{R^2} dR. \quad (2.88b)$$

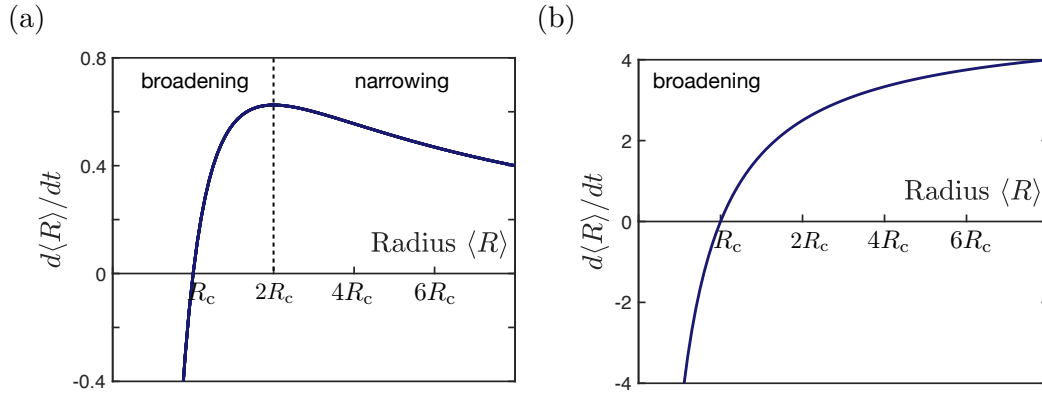


FIGURE 2.6: **Narrowing and broadening zones in the growth rate of the average radius:** (a): Diffusion limited regime. The broadening and narrowing zone corresponds to $\langle R \rangle < 2R_c$ and $\langle R \rangle > 2R_c$ respectively. The $1/R$ term in the growth law allows for a competition between the Gibbs-Thomson effects and the critical radius R_c . (b): Interface-kinetics limited regime. There is no regime for which the distribution function could narrow. Due to the lack of the extra $1/R$ term in the growth law, there is no competition between the Gibbs-Thomson effects and the critical radius R_c . Due to the Gibbs-Thomson term dominating the temporal evolution of the standard deviation there is only broadening possible. Modified from Sugimoto [68].

Replacing $dR \rightarrow \Delta R$, and $R \rightarrow \langle R \rangle$, we obtain an approximation for the temporal change of the standard deviation ΔR ,

$$\left. \frac{d\Delta R}{dt} \right|_{\text{diff}} = \frac{v_{\text{diff}}}{\langle R \rangle^2} \left(\frac{2}{\langle R \rangle} - \frac{1}{R_c(t; \infty)} \right) \Delta R, \quad (2.89a)$$

$$\left. \frac{d\Delta R}{dt} \right|_{\text{int}} = \frac{v_{\text{int}}}{\langle R \rangle^2} \Delta R. \quad (2.89b)$$

We see, that for the diffusion limited regime, the standard deviation broadens, i.e., $d\Delta R/dt > 0$ if $\langle R \rangle < 2R_c(t; \infty)$. It can narrow if the average radius is large enough, such that $\langle R \rangle > 2R_c(t; \infty)$. For passive emulsions, which we have discussed in Sect. 1, we have $\langle R \rangle = R_c(t; \infty)$, and the distribution function will always broaden. The two zones are depicted in Fig. 2.6(a).

For the interface-kinetics limited regime, the interesting result is that the distribution function does not have a narrowing zone, i.e., $d\Delta R/dt > 0$ for all R , Fig. 2.6(b). Although the distribution function for the interface-kinetics limited regime cannot narrow, we will show cases where due to matter supply, the broadening is reduced, and we reach a constant standard deviation.

2.5 Summary

We have derived the law for the movement of the droplet interface, which considers local departure from equilibrium at the phase boundary. We have derived the statistics of the droplet sizes in emulsions with matter supply. We have learned that the supply changes the competition between the droplets and enters the droplet growth law through the critical radius. Finally, we have attempted to solve analytically for the droplet size distribution function and found when the separation ansatz holds and why for emulsions with matter supply a complete analytical solution is not possible to be found. We have revisited the prediction of narrowing and broadening zones of the distribution function and the condition for the two regimes to exist. In the interface-kinetics growth regime, narrowing cannot occur. Narrowing is however possible in the diffusion limited regime, if the ratio of the critical to the the average radius exceeds a value of 2. This chapter is a theoretical basis to discuss results of coarsening kinetics of emulsions with different matter supply scenarios in the next chapters. There, using numerical tools we will discuss the behavior of the distribution function and the power laws governing the average radius and the droplet number density to make a comparison with passive emulsions.

Chapter 3

Coarsening kinetics of emulsions with matter supply

We want to study the effect of matter supply on the distribution of droplet sizes and the coarsening kinetics. Since we cannot find the complete analytical solution to the problem, we will use numerical tools to discuss the solution of the droplet size distribution function and make a comparison to passive emulsions. Clark et al. in Ref. [83] revisited the prediction of Sugimoto in Ref. [68]. They found a minimum matter supply needed for the distribution function in the diffusion limited regime to narrow for emulsions with constant matter supply. In a continuation of this study, Vollmer et al. in Ref. [84] explored the evolution of the droplet size distribution function in such systems. In their results, the size distribution does not approach to a universal shape, but rather depends on the initial conditions [84].

In the light of what we have learned in the previous chapter, we will start our discussion with a constant matter supply and discuss the coarsening kinetics of emulsions below and above the threshold from [83] in both diffusion and interface-kinetics limited regimes. We will look at the universality of the distribution function at late times in both regimes. In the second part of the chapter, we will choose to supply matter in such a way as to keep the supersaturation constant. It corresponds to a choice of a time-dependent matter supply. Here we will also discuss the scaling laws that govern the evolution of the emulsion, the average radius, and the droplet number density. We will address the question of self-similarity of the droplet size distribution function in such systems.

The numerical tools used in this chapter were optimized and developed with helpful discussion and hints from Thomas Tushar Dutta and Efe Ilker.

3.1 Emulsions with constant matter supply

We want to discuss coarsening kinetics of emulsions with constant matter supply. For this, we start with a modified conservation law Eq. (2.61), which for fast diffusion of concentration profiles in the dilute phase compared to the droplet growth kinetics, can be rewritten for a homogeneous concentration of the droplet material in the dilute phase $c(t)$. We have for simplicity dropped the subscript in $c_\infty(t)$. For the matter supply, we replace $J_c(t)$ by a constant matter supply rate J_c . The conservation law is

$$\frac{dc(t)}{dt} = -c_{\text{in}}^{(0)} \frac{d}{dt} \int_0^\infty \frac{4\pi}{3} R^3(t) \mathcal{N}(R, t) dR + J_c. \quad (3.1)$$

The same modification of a constant supply is introduced in Eq. (2.63), which describes the temporal evolution of the droplet phase volume fraction $\Phi(t)$. The droplet phase volume fraction evolves now according to,

$$\frac{d}{dt} \Phi(t) = \frac{J_c}{c_{\text{in}}^{(0)}}, \quad (3.2)$$

from which it directly follows that $\Phi(t) = \Phi(0) + tJ_c/c_{\text{in}}^{(0)}$, grows linearly.

Following the results in Subsect. 2.2.2 (Eq. (2.64)), the supersaturation, $\varepsilon(t) = (c(t) - c^{(0)})/c^{(0)}$, for constant matter supply is,

$$\varepsilon(t) = \ell_\gamma \frac{\int_0^\infty \left(\frac{R}{D+kR} \right) \mathcal{N}(R, t) dR + J_c (4\pi D k \ell_\gamma c^{(0)})^{-1}}{\int_0^\infty \left(\frac{R^2}{D+kR} \right) \mathcal{N}(R, t) dR}, \quad (3.3)$$

and the growth law (Eq. (2.65)) for a droplet in an emulsion with constant matter supply is

$$\dot{R}(t) = \frac{kD}{D+kR(t)} \frac{c^{(0)} \ell_\gamma}{c_{\text{in}}^{(0)}} \left(\frac{\int_0^\infty \left(\frac{RN(R, t)}{D+kR} \right) dR + J_c (4\pi D k \ell_\gamma c^{(0)})^{-1}}{\int_0^\infty \left(\frac{R^2 N(R, t)}{D+kR} \right) dR} - \frac{1}{R(t)} \right). \quad (3.4)$$

The critical radius $R_c(t)$ is the fixed point of the growth law, $\dot{R} = 0$, and is also defined through the supersaturation $\varepsilon(t) = \ell_\gamma/R_c(t)$. We again use $\beta = kR/D$ to distinguish between the diffusion and interface-kinetics limited regime. In the asymptotic limit, we have two cases: diffusion limited case when $D \ll kR(t)$, ($\beta \rightarrow \infty$), and the interface-kinetics limited case when $D \gg kR(t)$, ($\beta \rightarrow 0$). The critical radius, Eq. (2.66), for an emulsion with

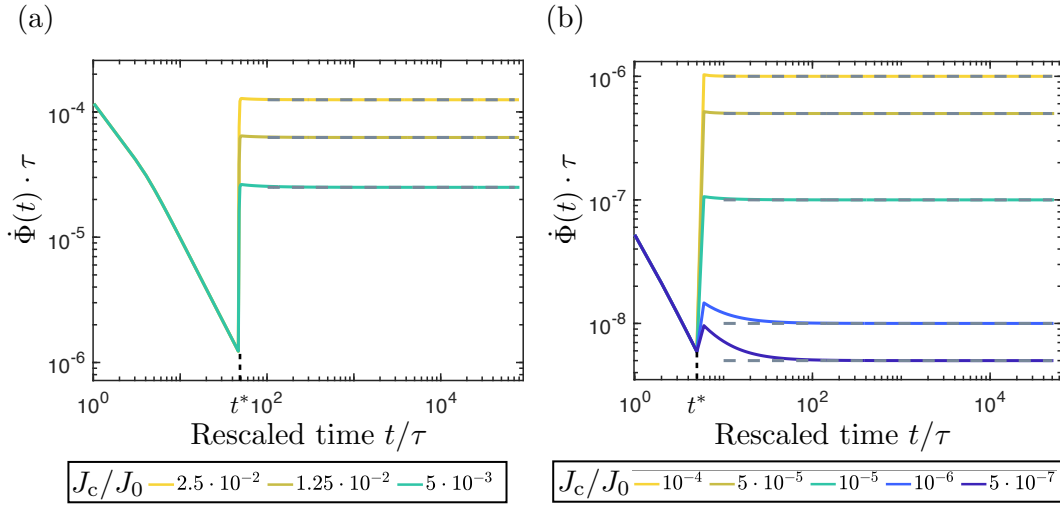


FIGURE 3.1: **Constant rate of change of the droplet phase volume fraction:** Rate of change of the droplet phase volume fraction as a function of matter supply J_c . The rate of change of the volume fraction, $\dot{\Phi}(t)$, follows the relation in Eq. (3.2) (grey dashed line) as soon as the supply is switched on. The values of matter supply J_c used are expressed in the units of $J_0 = c^0/\tau$, with the color code corresponding to the legend below each plot. The time t is rescaled by $\tau = \ell_\gamma^2/D$. (a): Diffusion limited and (b): Interface-kinetics limited regime.

constant matter supply is

$$R_c(t; \infty) = \frac{\int_0^\infty R \mathcal{N}(R, t; \infty) dR}{\int_0^\infty \mathcal{N}(R, t; \infty) dR + J_c (4\pi D \ell_\gamma c^{(0)})^{-1}}, \quad (3.5a)$$

$$R_c(t; 0) = \frac{\int_0^\infty R^2 \mathcal{N}(R, t; 0) dR}{\int_0^\infty R \mathcal{N}(R, t; 0) dR + J_c (4\pi k \ell_\gamma c^{(0)})^{-1}}, \quad (3.5b)$$

where $\mathcal{N}(R, t; \beta)$ is the droplet size distribution function in the two regimes distinguished by β .

In the following, we will use the tools discussed in Sect. 1.5.1 and solve the continuity equation Eq. (1.21) of the droplet size distribution function for the conservation law in Eq. (3.1). We use the same parameters as discussed for the numerical method in Subsect. 1.5.1 with the nondimensionalization in Eq. (1.22) and the growth law in Eq. (1.23). In our study, we initialize the emulsion as passive emulsion first, and ensure it has started the passive coarsening. At time t^* we switch the matter supply J_c . Once we switch on the matter supply, we study the effect of the different values of the supply J_c on the two asymptotic cases: diffusion limited and interface-kinetics limited growth. The results depicted in Fig. 3.1 show exactly the expected relation between the droplet phase volume fraction $\Phi(t)$ and the supply J_c .

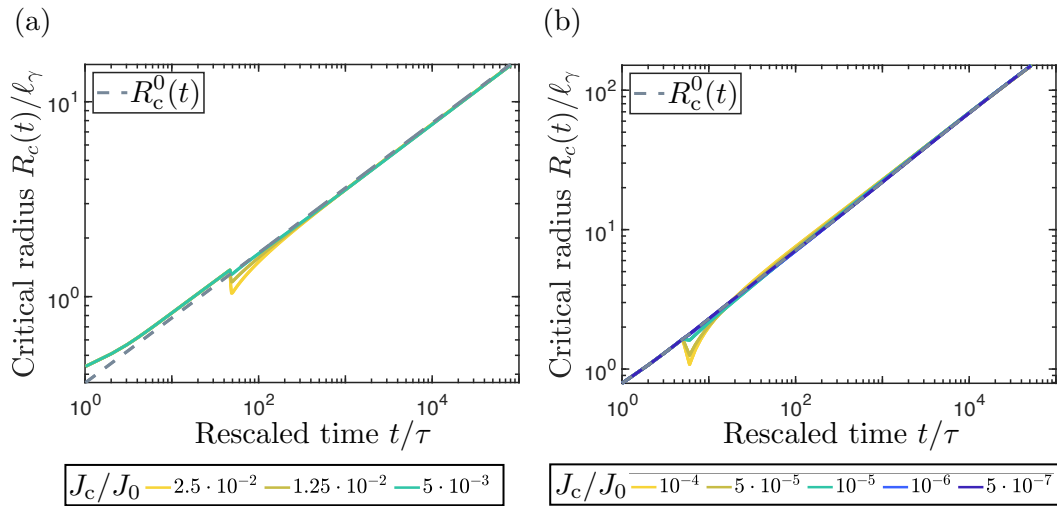


FIGURE 3.2: **Convergence of the critical radius in emulsions with matter supply to the passive solution:** The critical radius for emulsions with matter supply, despite the supply converges to the result of passive emulsions (grey dashed line). It is consistent with the results in Eq. (2.87b). (a): Diffusion limited regime. (b): Interface-kinetics limited regime. The time t is rescaled according to Eq. (1.22) with $\tau = \ell_\gamma^2/D$, the length with ℓ_γ , for the matter supply $J_0 = c^{(0)}/\tau$. The color code of the matter supply corresponds to the legend below each plot.

3.1.1 Supply-independent acceleration of coarsening in emulsions with constant matter supply

We want to find how the average radius and the droplet number density change for emulsions with matter supply and if they are governed by a different scaling law than in passive emulsions. We have learned in Sect. 2.3 that if the droplet size distribution function is broadening, even for emulsions matter supply, the solution of the critical radius is the same as in passive emulsions $R_c^0(t)$, Eq. (2.87b). We check if this condition is fulfilled for the choice of matter supply we have made in the diffusion and interface-kinetics limited regime, see Fig. 3.2(a) and (b) respectively. We see that in both cases the critical radius fulfills this prediction.

In the following, we use the same separation ansatz for the droplet size distribution function as before, $\mathcal{N}(R, t) = g(t)h(\rho)$ with the rescaled radius $\rho = R(t)/l_c(t)$, and a length scale of choice. We can assume that this ansatz holds as long as the distribution function is broadening and the critical radius is given by Eq. (2.87b). Using Eq. (2.71), the scaling function $g(t)$ for

emulsions with constant matter supply is

$$g(t) = \frac{3(\Phi(0) + t J_c/c_{\text{in}}^{(0)})}{4\pi l_c(t)^4 \int_0^\infty \rho^3 h(\rho) d\rho}, \quad (3.6)$$

where we have used how the droplet phase volume fraction $\Phi(t)$ changes in emulsions with constant matter supply Eq. (3.2). The droplet number density $n(t)$ using the separation ansatz is given by

$$n(t) = g(t) l_c(t) \int_0^\infty h(\rho) d\rho. \quad (3.7)$$

The average radius, which is defined as

$$\langle R(t) \rangle = \frac{\int_0^\infty R \mathcal{N}(R, t) dR}{\int_0^\infty \mathcal{N}(R, t) dR}, \quad (3.8)$$

can be rewritten given the separation ansatz,

$$\langle R(t) \rangle = l_c(t) \frac{\int_0^\infty \rho h(\rho) d\rho}{\int_0^\infty h(\rho) d\rho}. \quad (3.9)$$

Although we cannot solve analytically for the scaling function $h(\rho)$ and thus the integrals in Eq. (3.9), we can study them numerically. Since $R_c(t) = R_c^0(t)$, we choose $l_c(t) = R_c(t)$. The scaling law for the average radius will have the same time exponent for emulsions with constant matter supply as in passive emulsions. Depending on the regime, diffusion limited $\beta \rightarrow \infty$ or the interface-kinetics limited regime $\beta \rightarrow 0$, the average radius $\langle R(t; \beta) \rangle$,

$$\langle R(t; \infty) \rangle \propto t^{1/3}, \quad (3.10a)$$

$$\langle R(t; 0) \rangle \propto t^{1/2}. \quad (3.10b)$$

The prefactor of the scaling law is determined by the integrals of the scaling function $h(\rho; \beta)$ in Eq. (3.9), for $l_c(t) = R_c(t)$. The prefactor is given by

$$\frac{\langle R(t; \beta) \rangle}{R_c(t; \beta)} = \frac{\int_0^\infty \rho h(\rho; \beta) d\rho}{\int_0^\infty h(\rho; \beta) d\rho}, \quad (3.11)$$

which for passive emulsions was 1 ($\beta \rightarrow \infty$) and (8/9) ($\beta \rightarrow 0$) respectively [8]. In Fig. 3.3 we see the results of Eq. (3.11) for both regimes and different values of matter supply J_c . Surprisingly we find, that in the interface-kinetics

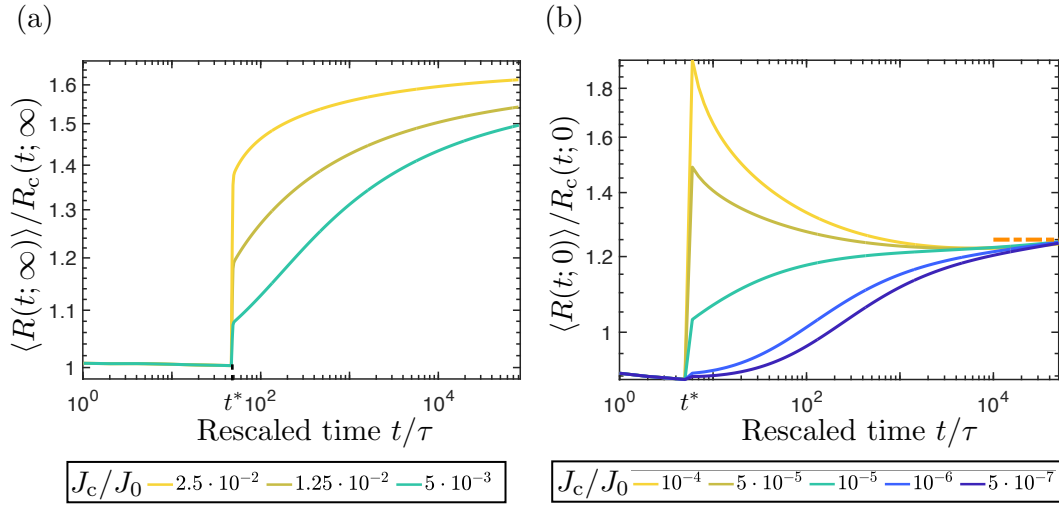


FIGURE 3.3: **Universality of the droplet size distribution function:** The ratio of the average radius to the critical radius. (a): In the diffusion limited regime, the ratio does not converge to a common value but seems dependent on the supply. (b): Interface-kinetics limited case. The ratio converges to the same number indicated by the orange dashed-dotted line (1.234). Since the ratio corresponds to the integrals of the radial part of the droplet size distribution function in Eq. (3.9), the convergence to the same number indicates that the droplet size distribution function is independent of the supply. The time t is nondimensionalized according to Eq. (1.22),

$$J_0 = c^{(0)}/\tau.$$

limited regime, Fig. 3.3(b), the ratio of the average to the critical radius converges to one value independent on the strength of the matter supply. The estimate of the value is $\langle R(t; 0) \rangle / R_c(t; 0) \simeq 1.234$ (orange dashed-dotted line in Fig. 3.3(b)). Thus, we conclude, that in the interface-kinetics limited regime, the droplet size distribution function behaves as if it would be independent of matter supply. Furthermore, it gives different results than in passive emulsions, and we expect the average radius to have a higher prefactor of the scaling law than the passive system. For emulsions with matter supply, in the interface-kinetics limited regime, we can compare the average radius to the passive emulsions by writing it as

$$\langle R(t; 0) \rangle = \xi_{\text{int}} \langle R(t; 0) \rangle_0, \quad (3.12)$$

with the constant shift $\xi_{\text{int}} = 1.234/(8/9) \simeq 1.39$, and the average radius of the passive emulsion,

$$\langle R(t; 0) \rangle_0 = \frac{8}{9} \left(\frac{k c^{(0)} \ell_\gamma t}{2 c_{\text{in}}^{(0)}} \right)^{1/2}. \quad (3.13)$$

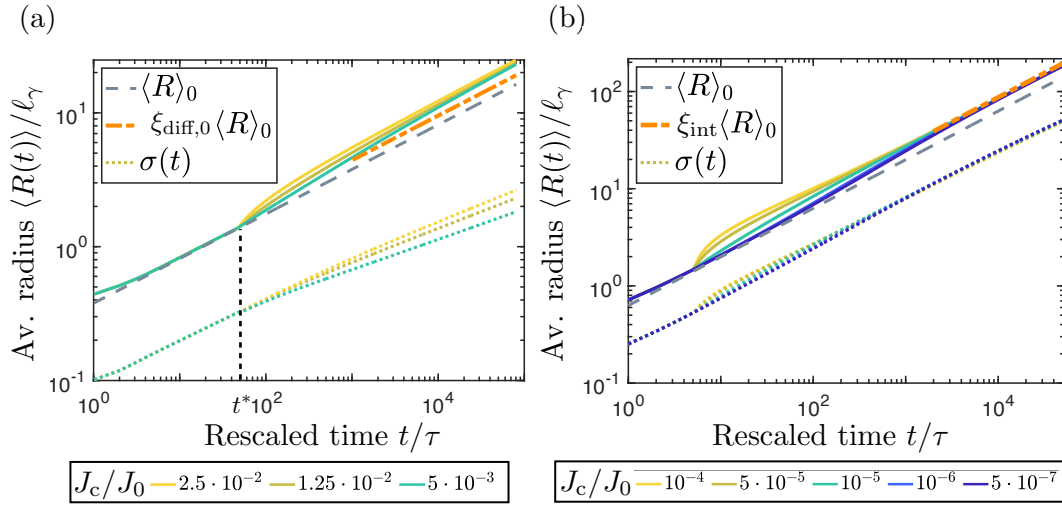


FIGURE 3.4: **Temporal evolution of the average radius for emulsions with constant matter supply:** (a) Average radius in the diffusion limited regime for different values of matter supply J_c . The orange dashed-dotted line corresponds to $\xi_{\text{diff},0} = 1.17$, the grey dashed line is the passive coarsening of Ostwald ripening. (b): Average radius in the interface-kinetics limited case. The acceleration of average radius compared to passive emulsions is independent of matter supply, with the orange dashed-dotted line corresponding to $\xi_{\text{int}} = 1.39$. In both regimes (a) and (b) the standard deviation is increasing (dotted line). The time t and radius R are nondimensionalized according to Eq. (1.22), with $\tau = \ell_\gamma^2/D$, and $J_0 = c^0/\tau$. The color code for the matter supply corresponds to the legend below each plot.

In Fig. 3.4(b) we see that the average radius for emulsions with matter supply in the interface-kinetics limited regime fulfills the condition in Eq. (3.13). There is an acceleration in the coarsening kinetics, which is independent of the supply rates.

On the other hand, in the diffusion limited regime, we do not find convergence of the ratio between the average radius and the critical radius to a common value, Fig. 3.3(a). We conclude that the distribution function is determined and depends on the matter supply J_c . Using the expression for the critical radius in the diffusion limited regime with matter supply Eq. (3.5a), we will try to estimate the effect of matter supply on the average radius. Given the definition of the average radius in Eq. (3.8), and $R_c(t) = R_c^0(t)$, we can rewrite Eq. (3.5a) for the average radius to find,

$$\langle R(t; \infty) \rangle = R_c^0(t; \infty) \left(1 + \frac{J_c (4\pi D \ell_\gamma c^{(0)})^{-1}}{n(t; \infty)} \right), \quad (3.14)$$

with $n(t; \infty)$ is the droplet number density (Eq. (3.7)) in the diffusion limited regime.

Due to $\langle R(t; \infty) \rangle_0 = R_c^0(t; \infty)$, in passive emulsions, we can immediately see, that in the presence of matter supply J_c , the average radius will be accelerated compared to passive emulsions. Using the definition of the droplet number density $n(t)$ in Eq. (3.7) and the scaling function $g(t)$ from Eq. (3.6), we can simplify the expression to,

$$\langle R(t; \infty) \rangle = R_c^0(t; \infty) \left(1 + \frac{4}{27} \frac{\int_0^\infty \rho^3 h(\rho; \infty) d\rho}{\int_0^\infty h(\rho; \infty) d\rho} \right), \quad (3.15)$$

where we have assumed that due to the linear growth of the droplet phase volume fraction, $\Phi(0) \ll tJ_c/c_{\text{in}}^{(0)}$, we can neglect $\Phi(0)$. For the length scale we have used, $l_c(t) = R_c^0(t; \infty)$ from Eq. (2.87b). The expression above only holds for $J_c \neq 0$. We replace the expression in the brackets by ξ_{diff} , which tells about the acceleration of coarsening of emulsions with matter supply compared to passive emulsions,

$$\langle R(t; \infty) \rangle = \xi_{\text{diff}} \langle R(t; \infty) \rangle_0. \quad (3.16)$$

Since, as we have already learned, the scaling function $h(\rho; \infty)$ depends on matter supply, and we cannot solve for it analytically, we cannot find the exact value and dependence on J_c of ξ_{diff} . We can, however estimate the expression in the brackets of the Eq. (3.15), using the scaling function of the passive emulsions in the diffusion limited regime Eq. (1.25). The lowest bound of the value of ξ_{diff} is then given by $\xi_{\text{diff},0} = 1.17$, and we expect the emulsions with constant matter supply in the diffusion limited regime to evolve with $\langle R(t; \infty) \rangle \geq \xi_{\text{diff},0} \langle R(t; \infty) \rangle_0$. In Fig. 3.4(a) we see the average radius in the diffusion limited regime for different values of matter supply. We find an agreement with our prediction, and the average radius fulfills the condition $\langle R(t; \infty) \rangle \geq \xi_{\text{diff},0} \langle R(t; \infty) \rangle_0$, (orange dashed-dotted line corresponds to $\xi_{\text{diff},0}$).

Analogously, we calculate the droplet number density $n(t; \beta)$ from Eq. (3.7). Using for the scaling function $g(t; \beta)$ Eq. (3.6), where we assume that due to the linear growth, $\Phi(0) \ll tJ_c/c_{\text{in}}^{(0)}$, we can neglect $\Phi(0)$, we can write

$$n(t; \beta) = \frac{3 J_c t}{4\pi c_{\text{in}}^{(0)} (R_c^0(t; \beta))^3} \frac{\int_0^\infty h(\rho; \beta) d\rho}{\int_0^\infty \rho^3 h(\rho; \beta) d\rho}, \quad (3.17)$$

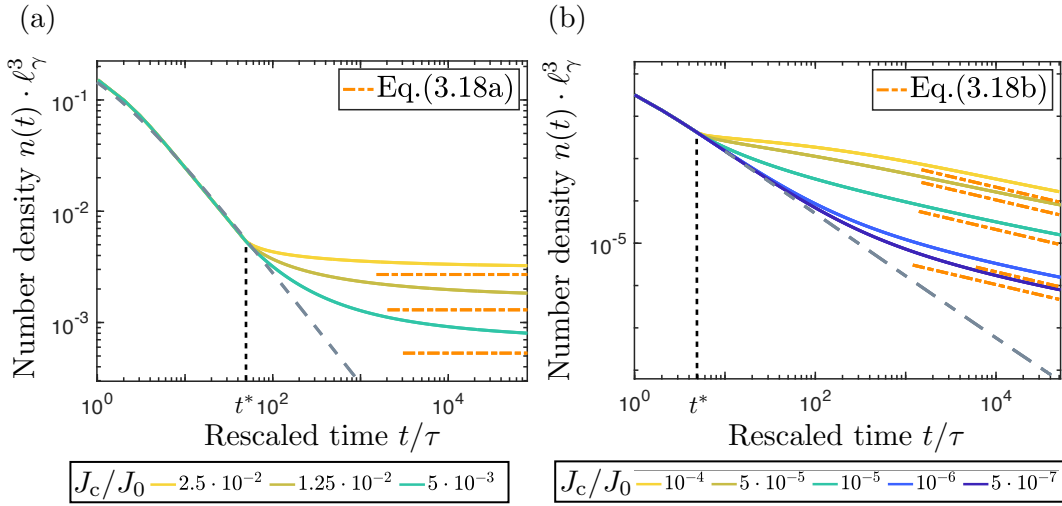


FIGURE 3.5: **New scaling laws of the droplet number density for emulsions with constant matter supply:** Droplet number density in the (a) diffusion limited and the (b) interface-kinetics limited case. In both cases, there is an agreement with the law derived in Eq. (3.18) (orange dashed-dotted lines). The droplet number density in passive emulsions follows an evolution depicted by grey dashed line. The time t is nondimensionalized according to Eq. (1.22), $J_0 = c^0/\tau$.

where we have used as the length scale $l_c(t) = R_c^0(t)$. Using the solution of the critical radius in the two regimes, Eq. (2.87b), we find

$$n(t; \infty) = \left(\frac{4}{9} \frac{3 J_c}{4\pi D \ell_\gamma c^{(0)}} \right) \frac{\int_0^\infty h(\rho; \infty) d\rho}{\int_0^\infty \rho^3 h(\rho; \infty) d\rho}, \quad (3.18a)$$

$$n(t; 0) = t^{-1/2} \left(\frac{3 J_c (c_{\text{in}}^{(0)})^{1/2}}{4\pi (k c^{(0)} \ell_\gamma / 2)^{3/2}} \right) \frac{\int_0^\infty h(\rho; 0) d\rho}{\int_0^\infty \rho^3 h(\rho; 0) d\rho}, \quad (3.18b)$$

In the diffusion limited regime, the number density and thus the total droplet number is constant, $n(t; \infty) \propto \text{const}$. This is due to the linear growth of the droplet phase volume fraction $\Phi(t)$ and the linear scaling of the average droplet volume $\langle V(t) \rangle \propto \langle R(t) \rangle^3$. In passive emulsions, due to the constant droplet phase volume fraction, $n(t; \infty)_0 \propto t^{-1}$. For the interface-kinetics limited case, the number density follows $n(t; 0) \propto t^{-1/2}$, where in the passive emulsions the dependence was $n(t; 0)_0 \propto t^{-3/2}$. Here too, the linear growth of the total droplet volume has an impact on the new scaling law. In Fig.3.5 we show the droplet number density in both regimes for different matter supplies. As a theoretical approximation we have used the results of Eq. (3.18). There, we have approximated the expression containing the integrals of the scaling function $h(\rho)$ to 1. This is motivated through the results of these integrals for passive emulsions which in both regimes is in the order of 1 (0.885

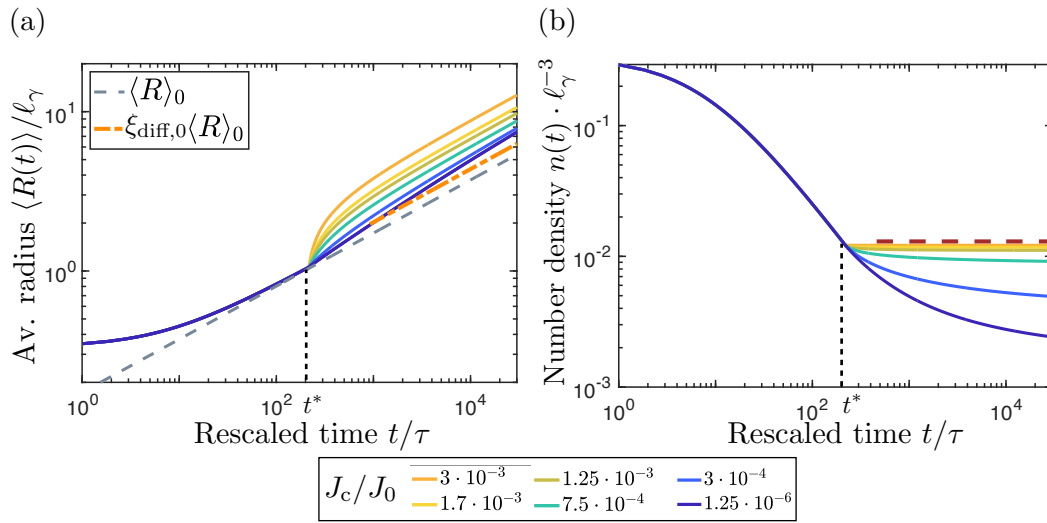


FIGURE 3.6: **Average radius and droplet number density in diffusion limited regime:** (a) Average radius follows a scaling law consistent with Eq. (3.16), with an increasing prefactor of the scaling law for higher supply rates. (b) Droplet number density approaches consistently to a constant following Eq. (3.18). For the two lowest values of the supply (blue and dark blue solid line), the number density is still not constant. Looking at the average radius for these cases, reveals that the system has not yet reached the regime of coarsening with a scaling of $t^{1/3}$. The time t and radius R are nondimensionalized according to Eq. (1.22), and $J_0 = c^0/\tau$.

and 1.045 respectively). It is not a rigorous approximation, and we can see that a higher value of this estimate would fit the results better.

3.1.2 Switch between a broadening and narrowing distribution function for increasing supply

Until now, we kept the matter supply J_c such that the distribution function was broadening. In Fig. 3.3, the dotted line depicts the standard deviation, which in both regimes is increasing. Inspired by the discussion of Sugimoto in Ref. [68], Clark et al. in Ref. [83] and Vollmer et al. in Ref. [84], we would like to explore the effect of increasing matter supply on our system. Furthermore, it is important to check beyond which regime the discussed assumptions and results in Subsect. 3.1.1 will break.

We study the same system as before, but now we introduce higher matter supply J_c . Note, that in this study we have increased the concentration inside, so the rates of matter supply used should not be quantitatively compared with the previous subsection. For the diffusion limited regime, the results of the average radius Fig. 3.6(a), show that as the matter supply becomes higher so does the prefactor in the scaling law of the average radius.

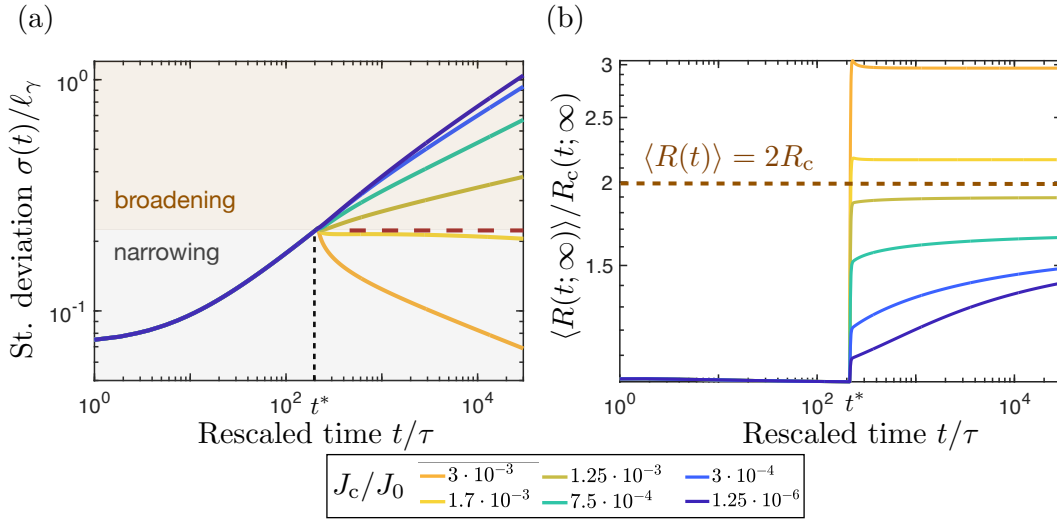


FIGURE 3.7: **Broadening and narrowing zones of the distribution function in diffusion limited regime:** (a): The standard deviation switches from increasing to decreasing function as we increase the matter supply J_c . The threshold between the two regimes (red dashed line) corresponds to a constant standard deviation and the supply from Eq. (3.19). (b) The ratio of the average to the critical radius for the narrowing distribution function corresponds to the condition $\langle R \rangle \leq 2R_c$. The time t is rescaled according to Eq. (1.22), $J_0 = c^{(0)}/\tau$.

The coarsening does not converge to any common value, and is always above the minimum threshold we have estimated, $\langle R(t; \infty) \rangle \geq \xi_{\text{diff},0} \langle R(t; \infty) \rangle_0$ with $\xi_{\text{diff},0} = 1.17$ (orange dashed-dotted line). The scaling exponent of the power law for the average radius does not change and the dependence on time t stays the same, $\langle R(t) \rangle \propto t^{1/3}$. The results in Fig. 3.6(b), reveal that for higher supplies, the system immediately reaches constant number density. The upper bound for the number density corresponds to $n(t^*; \infty)$, which is the number density at the time we switch the matter supply for the first time. Since we do not allow nucleation, $n(t; \infty) \leq n(t^*; \infty)$. In cases of higher matter supply the number density becomes independent of J_c and it only depends on the initial conditions of the system.

The standard deviation in Fig. 3.7(a) depicts a full range of broadening and narrowing scenarios. The standard deviation increases for lower values of J_c . There is a critical supply for which it becomes constant and beyond which the standard deviation decreases. The supply which corresponds to this threshold (red dashed line in Fig. 3.7(a)) is given by [83]

$$J_c \geq 4\pi n(t^*) D \ell_\gamma c^{(0)}. \quad (3.19)$$

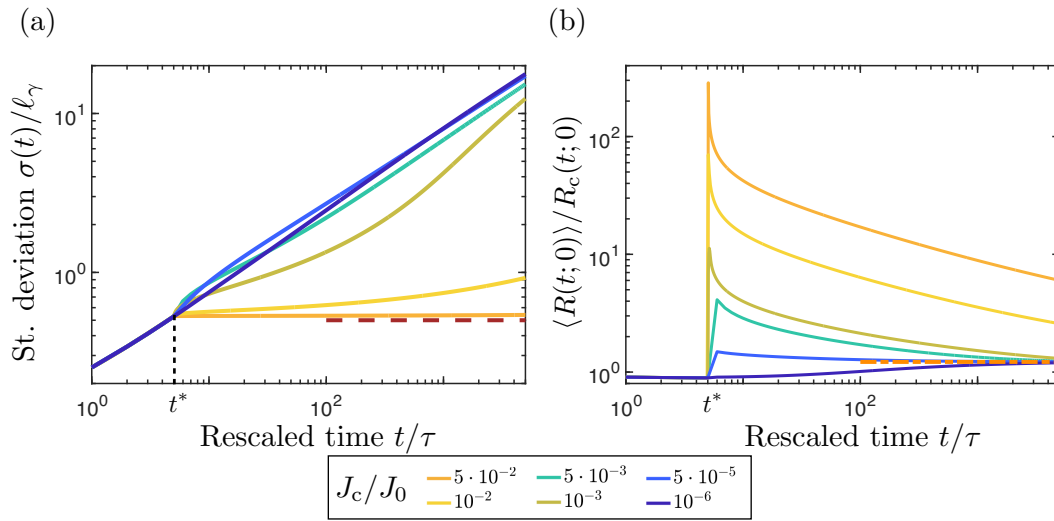


FIGURE 3.8: **Broadening distribution function in interface-kinetics limited regime:** (a): The standard deviation always increases even in the presence of higher matter supply J_c . For high supplies we reach a constant standard deviation (red dashed line). (b) The ratio of the average to the critical radius. For low matter supply the ratio converges to the prefactor $\langle R(t;0) \rangle / R_c(t;0) \simeq 1.234$ (orange dashed-dotted line). It indicates the universality of the distribution function. For higher supplies (orange and yellow solid lines) we do not converge to this value anymore. The time t is rescaled according to Eq. (1.22), $J_0 = c^{(0)}/\tau$

For any supply J_c fulfilling the condition in Eq. (3.19) the droplet size distribution function in the diffusion limited regime will narrow. The ratio of the average to the critical radius, $\langle R(t; \infty) \rangle / R_c(t; \infty)$, in Fig. 3.7(b), shows that the threshold in Eq. (3.19) corresponds to the estimation of Sugimoto Eq. (2.89). Narrowing in the diffusion limited regime happens if $\langle R(t; \infty) \rangle \geq 2R_c(t; \infty)$. The results in Fig. 3.7(b) in the light of Eq. (3.11) suggest, that the droplet size distribution function is not independent of the supply rates and the system is not universal but rather depends on the initial conditions and the conditions of matter supply.

We perform the same analysis for the interface-kinetics limited case, for ($\beta \rightarrow 0$). Sugimoto in Ref. [68] predicted that narrowing of the droplet size distribution function in this regime is impossible. As we are increasing the supply J_c , we see that the standard deviation can at most be constant Fig. 3.8(a) (red dashed line). For the cases of higher supply, the ratio $\langle R(t;0) \rangle / R_c(t;0)$ in Fig. 3.8(b), does not converge to a fixed value anymore. However, we see a very clear convergence for lower supplies J_c to the same value as in Fig. 3.3 (orange dashed-dotted line $\langle R(t;0) \rangle / R_c(t;0) = 1.234$). This indicates, that there is a regime in which the system is described by a universal distribution function which is independent of the supply.

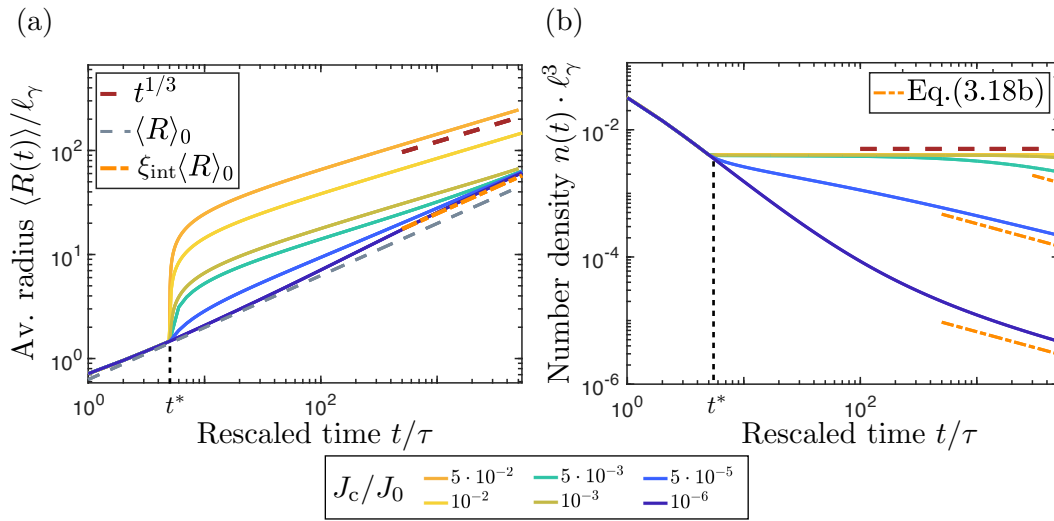


FIGURE 3.9: **Average radius and droplet number density in interface-kinetics limited regime:** (a) Average radius for lower supplies approaches the coarsening law derived in Eq. (3.12), with $\xi_{int} = 1.36$ (orange dashed-dotted line). For higher supplies the radius follows a $t^{1/3}$ law (red dashed line) indicating the crossover to the diffusion limited coarsening. (b) Droplet number density for lower supplies follows Eq. (3.18) (orange dashed-dotted lines) but for higher supplies becomes constant (red dashed line), which corresponds to the crossover to the diffusion limited regime, where the number density is constant. The time t and radius R are nondimensionalized according to Eq. (1.22), and $J_0 = c^0/\tau$.

Studying the effect of higher matter supply on the average radius and the droplet number density in the interface-kinetics limited regime, Fig. 3.9 reveals the regime of universality. For the supply corresponding to almost constant standard deviation (yellow and orange solid line), the average radius follows a $t^{1/3}$ power law (red dashed line in Fig. 3.9(a)). It indicates a transition to a diffusion limited growth law, and means that $\beta = kR/D \gg 0$. The supply J_c caused a transient increase in the average radius $\langle R(t; \infty) \rangle$, which although initialized in the interface-kinetics limited regime, has increased to values high enough that the interface-kinetics can not compete with the diffusion anymore. The droplet number density, Fig. 3.9(b), reaches in this case also a constant value, which is opposed to the predictions in Eq. (3.18) for the interface-kinetics limited regime. There, $n(t; 0) \propto t^{-1/2}$, which we see for lower supplies in Fig. 3.9(b). For these values of the supply J_c we have a broadening droplet size distribution function and the average radius follows the coarsening law described by Eq. (3.12) (orange dashed-dotted line). The observation is consistent with the results for the ratio of the critical and the average radius in Fig. 3.7(b). Next, we would like to look at the solutions of the droplet size distribution function, and discuss when the scaling ansatz we have used is valid.

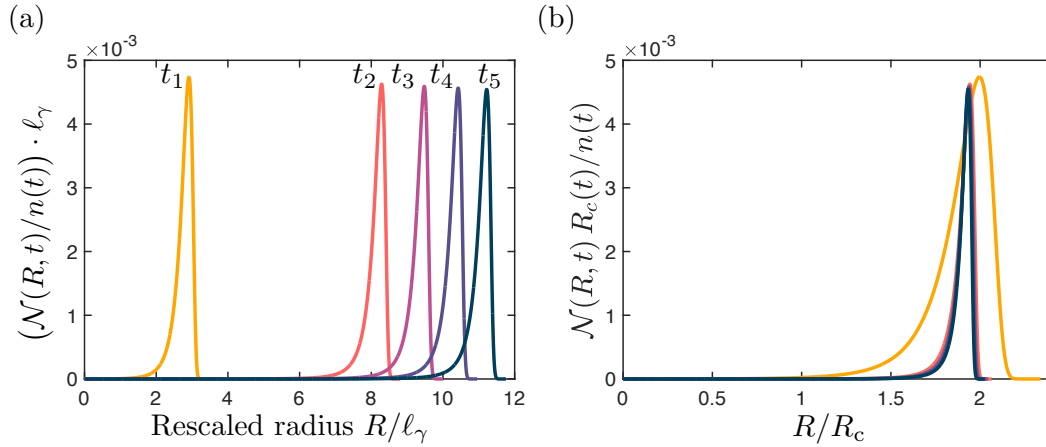


FIGURE 3.10: **Collapse of the droplet size distribution function in diffusion limited regime:** (a): At different time points we measure the distribution function for the choice of $J_c/J_0 = 1.25 \cdot 10^{-3}$, when the distribution function is broadening. The time point $t_1/\tau = 10^3$ is an early time point when the system did not reach the asymptotic coarsening kinetics yet. The later time points are equidistant from $t_2/\tau = 6 \cdot 10^3$ to $t_5/\tau = 2 \cdot 10^4$. (b): We find a separation ansatz for which the distribution function collapses on its self-similar shape. For nondimensionalization we use Eq. (1.22). The critical radius is a function of supersaturation $R_c = \ell_\gamma/\varepsilon(t)$.

3.1.3 Universal coarsening kinetics of emulsions with constant matter supply

In the following, we would like to study the evolution of the distribution function for systems with matter supply. In the previous subsection, Subsect. 3.1.2, we have learned when the distribution function narrows or broadens, and what scaling laws govern its evolution. We have also learned when the coarsening behavior is independent of matter supply J_c . We would like to study the behavior of the droplet size distribution function in these regimes and check the validity of the separation ansatz.

The collapse of the distribution function onto a self-similar, time-invariant shape was revisited and discussed for passive systems. If a collapse exists, we can successfully separate the distribution function $\mathcal{N}(R, t)$ into a time- and radial-dependent part. We start by looking at the distribution function for the diffusion limited case, with matter supply J_c below the threshold Eq. (3.19). Our choice of the supply is $J_c/J_0 = 1.25 \cdot 10^{-3}$, which corresponds to a broadening distribution function in Fig.3.7(a). We pick an early time point $t_1/\tau = 10^2$ when the system has not reached the coarsening kinetics of the power law in Eq. 3.16 yet (Fig. 3.6(a)), and then later time points from t_2

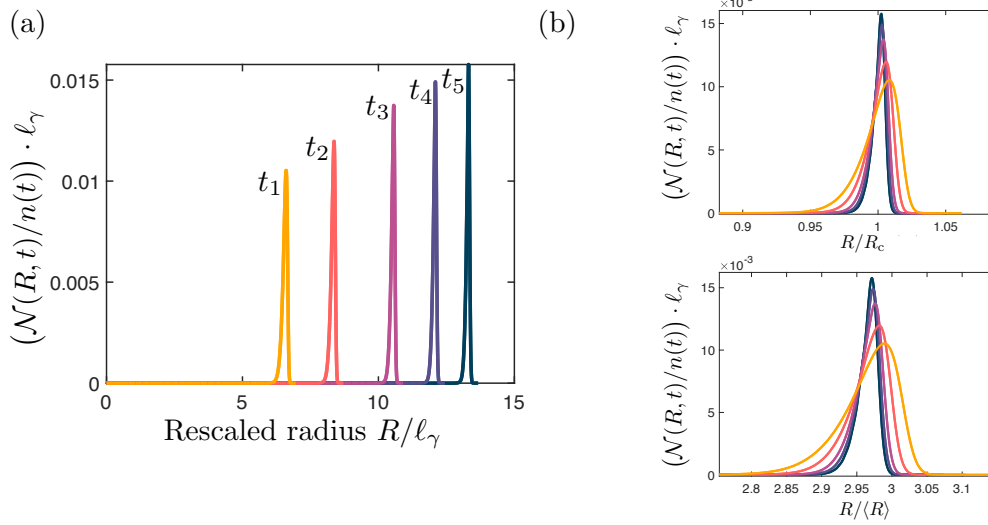


FIGURE 3.11: **No self-similarity droplet size distribution function in diffusion limited regime:** (a): At equidistant time points from $t_1/\tau = 10^5$ to $t_5/\tau = 8 \cdot 10^5$ we measure the distribution function for the choice of $J_c/J_0 = 3 \cdot 10^{-3}$ when the distribution function is narrowing. (b): It is not possible to find a separation ansatz to find a self-similar shape of the distribution function. We try rescaling the radius with the critical and the average radius respectively. For the nondimensionalization we use Eq. (1.22).

to t_5 (Fig. 3.10(a)), which are spread logarithmically from each other. It is essential to choose the time points to be distanced far enough from each other to talk about a possible collapse in time.

The choice of the nondimensional radius $\rho = R/R_c$, like for passive emulsions, works very well to separate the distribution function. In Fig. 3.10(b), we see a collapse of the distribution function for times from t_2 to t_5 onto a self-similar shape. The early time point t_1 , which does not fall on the collapsed shape, shows that there is still some non-trivial time dependence in the distribution function, which disappears at later times when the system enters the coarsening regime. The collapse highlights that in this regime, the distribution function belongs to the same universality class as the distribution function of Ostwald ripening and confirms the choices we have made for the analytical approximations in the previous subsection.

For a higher supply J_c , ($J_c/J_0 = 3 \cdot 10^{-3}$), for which the narrowing occurs, we are not able to find a collapse of the distribution function Fig. 3.11(b). There are several reason for this. As we have learned in Eq. (2.69), the rate of change of the number density implies the dependence of the droplet size distribution function $\mathcal{N}(R, t; \infty)$ on the radius R . Since the number density is constant here, we expect a different dependence on the radius R than in passive emulsions. It is non-trivial what kind of separation ansatz is suitable

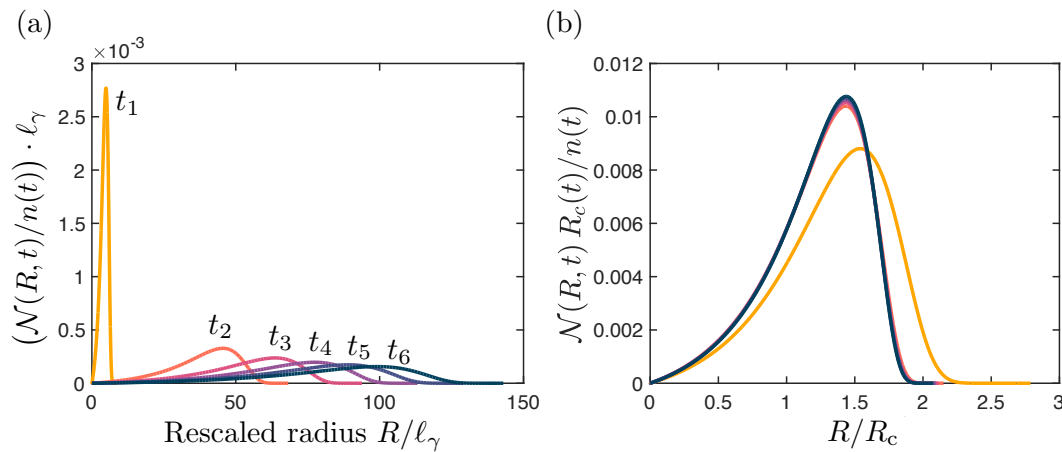


FIGURE 3.12: **Collapse of the droplet size distribution function in interface-kinetics limited regime:** (a): At different time points we measure the distribution function for the choice of $J_c/J_0 = 5 \cdot 10^{-5}$, when the distribution function is broadening. The time point $t_1/\tau = 10^2$ is an early time point when the system did not reach the asymptotic coarsening kinetics yet. The later time points are equidistant from $t_2/\tau = 6 \cdot 10^2$ to $t_6/\tau = 4 \cdot 10^3$. (b): We find a separation ansatz for which the distribution function collapses on its self-similar shape. For the nondimensionalization we use Eq. (1.22).

for the problem for the distribution function which in this regime of supply depends on its initial conditions as well as the conditions of the supply. The narrowing system reaches at late times a delta peak and corresponds to a monodispersed emulsion.

Analogously to the analysis of the evolution of the distribution function at low supply rates in the diffusion limited regime, we pick $J_c/J_0 = 5 \cdot 10^{-5}$ to analyze the distribution function and its temporal behaviour in the interface-kinetics limited case ($\beta \rightarrow 0$). We pick again an early time t_1 , and later time points from t_2 to t_5 , Fig. 3.12(a). Collapsing the distribution function onto its self-similar form is possible with a choice of a nondimensional radius $\rho = R/R_c$. As expected and discussed, the distribution function is universal even in the presence of the supply J_c . For a higher supply, which corresponds to a constant standard deviation ($J_c/J_0 = 1 \cdot 10^{-4}$), the distribution function has a constant width, and its peak moves with a velocity $d\langle R \rangle/dt$. By shifting each radius R by the average $\langle R \rangle$, the distribution function collapses at all times onto a self-similar shape.

We have explored the coarsening kinetics of emulsions with constant matter supply. We have found regimes that dictate a fixed acceleration of coarsening and correspond to a self-similar distribution function. We have also explored the behavior outside these regimes and the effect of high matter supply on

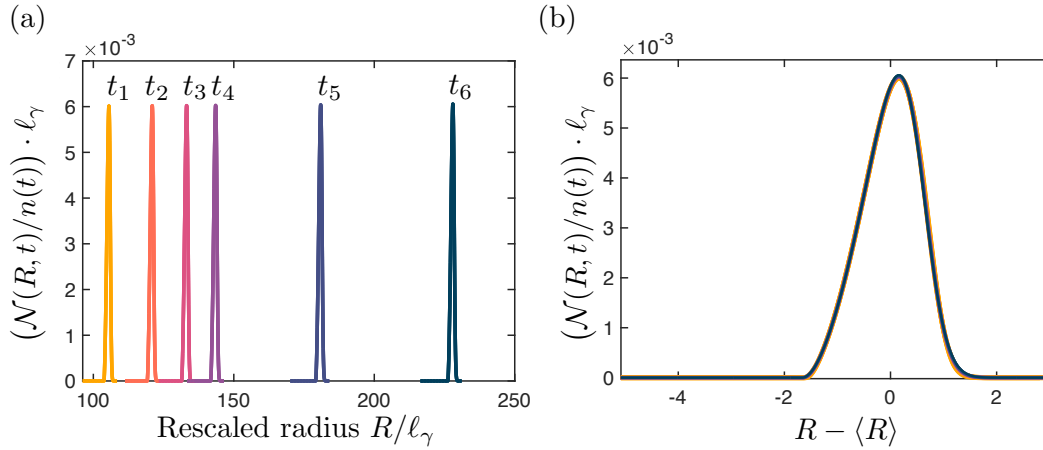


FIGURE 3.13: **Collapse of the droplet size distribution function in interface-kinetics limited regime:** (a): At different time points we measure the distribution function for the choice of $J_c/J_0 = 1 \cdot 10^{-4}$ when the distribution function is constant. The time points are equidistant and chosen from $t_1/\tau = 4 \cdot 10^2$ to $t_6/\tau = 4 \cdot 10^3$. (b): We find that a shift in the radial space by $(R - \langle R \rangle)$, collapses the distribution function on its self-similar shape. The distribution function has a constant width and moves for every radius R at the same speed. For the nondimensionalization we use Eq. (1.22).

the time evolution of emulsions. In the next section, we will choose the matter supply to be time-dependent, and see how we can tune it in accordance to the evolution of droplet sizes to find novel coarsening kinetics of emulsions with matter supply.

3.2 Emulsions with time-dependent matter supply maintaining constant supersaturation

Until now, we were introducing the droplet material with a constant supply J_c . It corresponded to a constant rate of change of the droplet phase volume fraction, $\dot{\Phi}(t) = \text{const}$, such that the droplet phase was growing linearly, $\Phi(t) \propto t$. Introducing a time dependence in $J_c(t)$, causes the droplet phase volume fraction, the supersaturation as well as the critical radius to have an additional time dependence. Analogously to the conservation law in Eq. (3.1), we can write for $J_c(t)$,

$$\frac{dc(t)}{dt} = -c_{\text{in}}^{(0)} \frac{d}{dt} \int_0^\infty \frac{4\pi}{3} R^3(t) \mathcal{N}(R, t) dR + J_c(t). \quad (3.20)$$

Using the droplet phase volume fraction $\Phi(t)$, Eq. (2.59),

$$\partial_t c(t) = -c_{\text{in}}^{(0)} \frac{d}{dt} \Phi(t) + J_c(t). \quad (3.21)$$

We can immediately see that an interesting choice for the matter supply is one such that $J_c = c_{\text{in}}^{(0)} \dot{\Phi}(t)$, in which matter supply balances the changes in the droplet phase volume fraction at each time t . This choice ensures $\dot{c}(t) = 0$, and the system is truly (quasi-)static. The supersaturation, being a measure of the excess concentration in the dilute phase, $\varepsilon = (c - c^{(0)})/c^{(0)}$, is constant and set by the initial condition. Thus, the constant concentration c , cannot now relax to its equilibrium value $c^{(0)}$. What is the effect of the constant supersaturation on the coarsening kinetics of droplets?

The droplet growth equation Eq. (2.29), can be rewritten using the constant supersaturation ε ,

$$\dot{R}(t) = \frac{k D}{D + k R(t)} \frac{c^{(0)}}{c_{\text{in}}^{(0)}} \left(\varepsilon - \frac{\ell_\gamma}{R(t)} \right). \quad (3.22)$$

Contrary to previous systems, the critical radius, $R_c = \ell_\gamma/\varepsilon$, is constant here. Two important consequences follow from this result. First of all, droplets are now decoupled from each other. The growth of every droplet is independent of the emulsion and of the information about the droplet size distribution function $\mathcal{N}(R, t)$. Furthermore, a constant critical radius R_c , means that after an initial phase, when the distribution function moves in its radial space past the radius R_c , such that $R > R_c$ for all radii R in $\mathcal{N}(R, t)$, droplets cannot dissolve anymore. The droplet number density $n(t)$ will be constant.

For emulsions with constant matter supply in the diffusion limited regime, the constant number density directly influenced the dependence of the droplet size distribution function $\mathcal{N}(R, t)$ on the radius R . We expect that the separation ansatz valid for passive emulsions will also not be possible here. Thus, we will try to analyze the moments and the coarsening kinetics of droplets in emulsions with constant supersaturation without specifying $\mathcal{N}(R, t)$ yet.

3.2.1 Moments of droplet size distribution function in emulsions with constant supersaturation

Since the droplets are decoupled from each other, every droplet follows a growth law from Eq. (3.22). We can replace $R(t)$ by the average radius $\langle R(t) \rangle$,

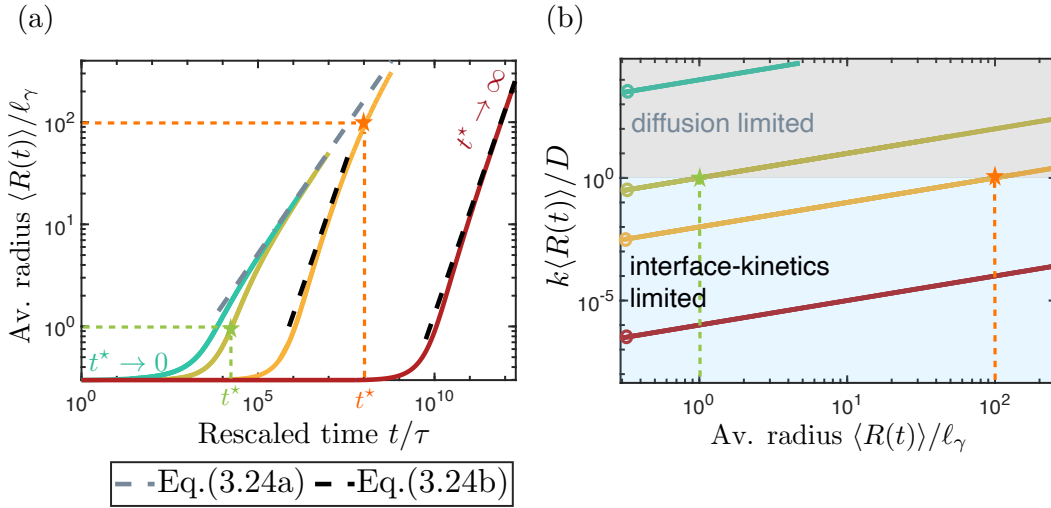


FIGURE 3.14: **Crossover in the scaling of the average radius for different initial conditions:** (a): Average radius for emulsions initialized with the initial ratio $k\langle R(0) \rangle / D$ depicted in (b) (circles at the y-axis, the different initial conditions are corresponding to the color code used). We see a crossover in the scaling laws of the average radius, from the interface-kinetics (black dashed line) to the diffusion limited regime (grey dashed line). The crossovers are indicated by a star and the times of the crossover are t^* . (b) The ratio $k\langle R(t) \rangle / D$ as a function of the average radius is depicted to document the initial conditions and to appreciate when, due to the increase in the average radius, the system crosses from the interface-kinetics (blue shaded region) to the diffusion limited regime (grey shaded region). The crossover is visualized by a star and corresponds to $\langle R(t^*) \rangle$. The system is nondimensionalized as in Eq. (1.22) with $\tau = \ell_\gamma^2 / D$.

such that

$$\frac{d\langle R(t) \rangle}{dt} = \frac{kD}{D + k\langle R(t) \rangle} \frac{c^{(0)}}{c_{\text{in}}^{(0)}} \left(\varepsilon - \frac{\ell_\gamma}{\langle R(t) \rangle} \right), \quad (3.23)$$

where the supersaturation $\varepsilon = (c - c^{(0)}) / c^{(0)}$. We expect that due to the evolution of $\langle R(t) \rangle$, an initial choice of $c = c^{(0)}$ is possible, such that at later times, $\varepsilon \gg \ell_\gamma / \langle R(t) \rangle$. Thus, we neglect the term $\ell_\gamma / \langle R(t) \rangle$ in Eq. (3.22). Note that the choice of $c^{(0)}$ should be such that the system is not in the overfeeding regime. We again identify two regimes through $\tilde{\beta} = k\langle R \rangle / D$, such that $\tilde{\beta} \rightarrow \infty$ and $\tilde{\beta} \rightarrow 0$, for the diffusion and interface-kinetic limited case respectively. The solution of the growth law in Eq. (3.23) is

$$\langle R(t; \infty) \rangle = \left(2 \frac{D(c - c^{(0)})}{c_{\text{in}}^{(0)}} t \right)^{1/2}, \quad (3.24a)$$

$$\langle R(t; 0) \rangle = \frac{k(c - c^{(0)})}{c_{\text{in}}^{(0)}} t. \quad (3.24b)$$

The average radius follows a $t^{1/2}$ or a linear growth law in the diffusion and interface-kinetics limited case, respectively. Fig. 3.14(a) shows these scaling laws for a few cases that differ in the initialization through the choice of $\tilde{\beta}$ at $t = 0$. The measure of the competition between the processes of diffusion to interface-kinetics is the value $\tilde{\beta}$, which is a measure that changes with the growth of the emulsion. By tracing the value of $\tilde{\beta}$, Fig. 3.14(b), during the evolution of the emulsion we can see how the system is able to cross between the two asymptotic regimes, Eq. (3.24). We refer to the time point of the crossover by t^* , which corresponds to the average radius $\langle R(t^*) \rangle$.

For emulsions that are initialized in the diffusion limited regime, $k\langle R(0) \rangle/D \gg 1$ (cyan), the crossover happens at $t^* \rightarrow 0$. For emulsions that are initialized in a strong interface-kinetics limited regime, $k\langle R(0) \rangle/D \simeq 0$, we need to wait for very long times to see the crossover, $t^* \rightarrow \infty$ (for the red line). But for intermediate choices of $k\langle R(0) \rangle/D \simeq 1$ a crossover at a measurable time t^* is possible. In Fig. 3.14(a) we see a crossover in the scaling of the average radius at time t^* from the linear scaling law to a $t^{1/2}$ scaling for the choice of $k\langle R(0) \rangle/D = 3 \cdot 10^{-3}$ (orange solid line). We learn that systems which are initialized in the interface-kinetics limited growth regime, will eventually follow the diffusion limited coarsening kinetics.

In a similar way, we can estimate the standard deviation $\sigma(t)$, and the variance $\sigma^2(t)$. The temporal change of the variance, $\sigma^2(t) = \langle R^2(t) \rangle - \langle R(t) \rangle^2$ is

$$\frac{d}{dt}\sigma^2(t) = \frac{d}{dt}\langle R^2(t) \rangle - 2\langle R(t) \rangle \frac{d}{dt}\langle R(t) \rangle. \quad (3.25)$$

We modify the definition of the k -th moment, Eq. (2.58), by the constant number density n , such that

$$\langle R^k(t) \rangle = \frac{1}{n} \int_0^\infty dR R^k \mathcal{N}(R, t). \quad (3.26)$$

We substitute the definition of moments into Eq. (3.25) and use the continuity equation (Eq. (2.53)) for the temporal derivatives of $\mathcal{N}(R, t)$. We perform partial integration, for which we use vanishing boundary terms (due to $\mathcal{N}(R, t) = 0$ for $R = 0$ and $R = \infty$), and obtain

$$\frac{d}{dt}\sigma^2(t) = \frac{2}{n} \left[\left(\int_0^\infty dR \frac{DkR}{D+kR} \mathcal{N}(R, t) \right) - \langle R \rangle \int_0^\infty dR \frac{Dk}{D+kR} \mathcal{N}(R, t) \right]. \quad (3.27)$$

In the growth law, Eq. (3.22), we have used the condition $\varepsilon \gg \ell_\gamma/R$.

For the expressions in the integrals, Eq. (3.27), we identify two regimes which

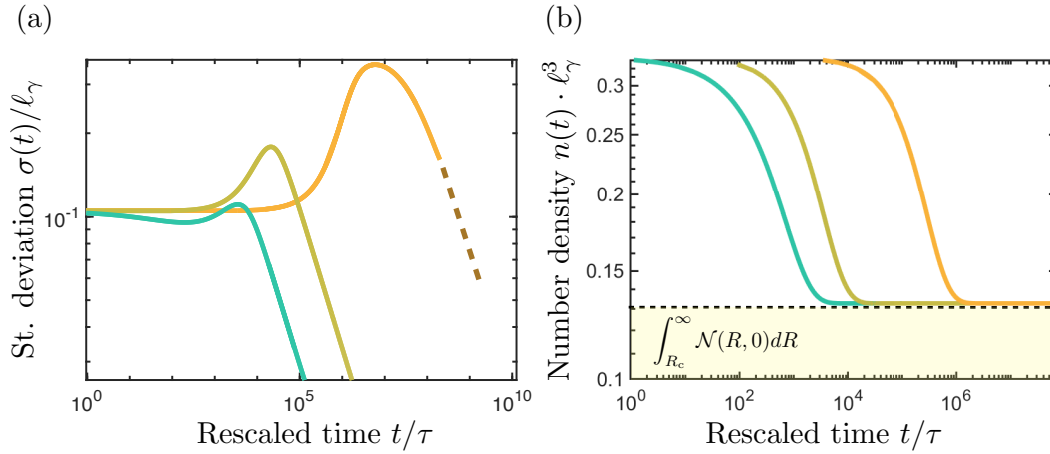


FIGURE 3.15: **Narrowing distribution function as the emulsion reaches fixed droplet number density:** (a): Standard deviation as a function of time for emulsions initialized according to a choice in Fig. 3.14(b). Since the numerical calculations to maintain proper resolution are very slow, by the dashed orange line we visualize the prediction of the evolution for the one case (orange solid line). (b) Droplet number density for all cases reaches the same value. The drop in the number density from the initial value corresponds to the amount of droplets between $R = 0$ and $R = R_c$ that will dissolve. Due to the critical radius being constant, the emulsion can only lose this fixed amount of droplets.

are distinguished for every droplet by $\beta = kR/D$, such that $\sigma^2(t; \beta)$. In the diffusion limited regime, for $\beta \rightarrow \infty$, we obtain,

$$\frac{d}{dt} \sigma^2(t; \infty) = 2D \frac{c - c^{(0)}}{c_{\text{in}}^{(0)}} \left(1 - \langle R \rangle \left\langle \frac{1}{R} \right\rangle \right). \quad (3.28)$$

Since $1/R$ is a convex function, we can use Jansen's inequality [85], which implies, $\langle R \rangle \langle 1/R \rangle \geq 1$. The droplet size distribution function in the diffusion limited regime for emulsions with constant supersaturation will always narrow,

$$\frac{d}{dt} \sigma^2(t; \infty) \leq 0. \quad (3.29)$$

Evaluating the integrals in Eq. (3.27) for $\beta \rightarrow 0$, which corresponds to the interface-kinetics limited regime, gives us

$$\frac{d}{dt} \sigma^2(t; 0) = 0. \quad (3.30)$$

The standard deviation is constant, and the droplet size distribution function has a constant width over time. As we have learned, the cases initialized in the interface-kinetics limited regime, will crossover to the diffusion limited regime and eventually evolve with a narrowing distribution function. The

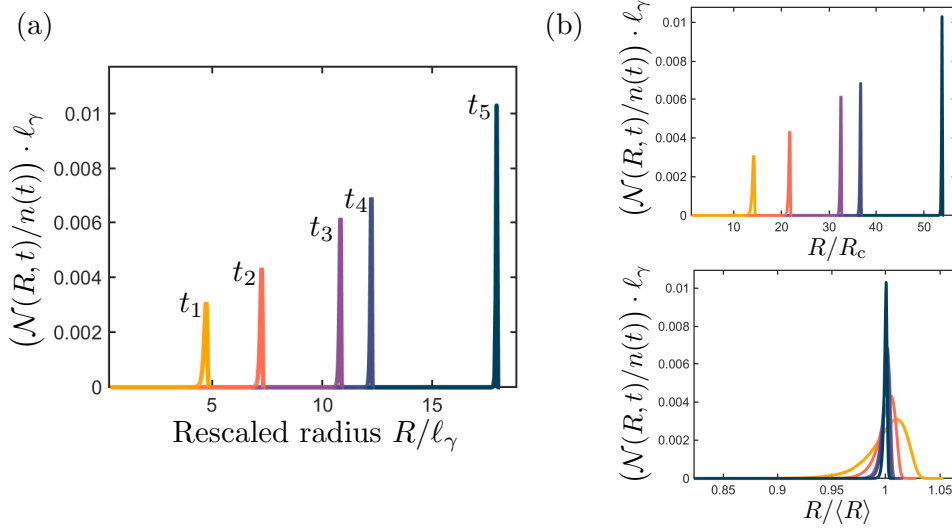


FIGURE 3.16: **No self-similar droplet size distribution function in diffusion limited regime:** (a): At equidistant time points from $t_1/\tau = 5 \cdot 10^4$ to $t_5/\tau = 5 \cdot 10^6$, we measure the distribution function for the system with initial conditions $k\langle R(0)\rangle/D = 3 \cdot 10^3$, corresponding to the diffusion limited regime. (b): It is not possible to find a separation ansatz to find a self-similar solution of the droplet size distribution function. For the nondimensionalization we use Eq. (1.22).

results of the narrowing distribution function for systems from Fig. 3.14 are depicted in Fig. 3.15(a).

Furthermore, Fig. 3.15(b) shows an agreement with our assumption about the constant number density n . The system is initialized for different choices of $k\langle R(t)\rangle/D$ with the same droplet size distribution function $\mathcal{N}(R, 0)$ and the constant supersaturation ε . During the evolution, we loose some droplets and settle at a constant droplet number density n . The amount of droplets lost corresponds to the amount of droplets between $R = 0$ and $R = R_c$ at $t = 0$, a range which due to constant supersaturation is constant in time and for all cases. The asymptotic number density n is set by the initial conditions that determined the critical radius,

$$n = \int_{R_c}^{\infty} \mathcal{N}(R, 0) dR, \quad (3.31)$$

and stays constant, Fig. 3.15(b).

3.2.2 Universal coarsening kinetics of emulsions with constant supersaturation

In the last part of this chapter, we study the time evolution of the distribution function in the two asymptotic regimes $\beta \rightarrow \infty$ and $\beta \rightarrow 0$. For emulsions

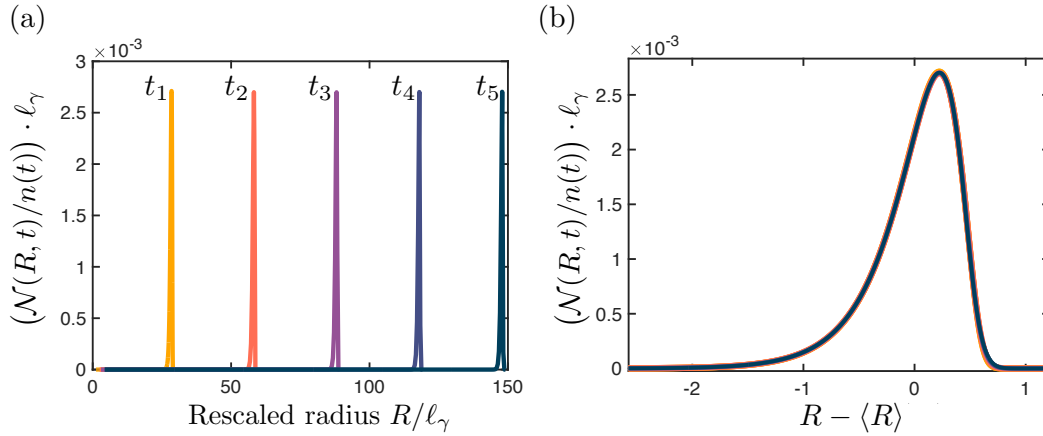


FIGURE 3.17: **Collapse of the droplet size distribution function in interface-kinetics limited regime:** (a): At equidistant time points from $t_1/\tau = 10^{11}$ to $t_5/\tau = 8 \cdot 10^{11}$ we measure the distribution function for the system with initial conditions $k\langle R(0)\rangle/D = 3 \cdot 10^{-7}$, corresponding to the interface-kinetics limited regime. (b): The shift in the radial space by $(R - \langle R \rangle)$, collapses the distribution function on its self-similar shape. The distribution function has a constant width and moves for every radius R at the same speed. For the nondimensionalization we use Eq. (1.22).

initialized in the diffusion limited regime, ($k\langle R(0)\rangle/D = 3 \cdot 10^3$), we again do not see a possibility of finding a length scale that would allow for a successful separation of the distribution function into the time- and radial dependent scaling function, Fig. 3.16(b). This is due to the same reasons discussed in Subsect. 3.1.3 for emulsions with constant matter supply in the narrowing regime. The narrowing distribution function and the constant droplet number density require a different ansatz for the droplet size distribution function than the ansatz used for passive emulsions.

For emulsions initialized in the interface-kinetics limited regime ($k\langle R(0)\rangle/D = 3 \cdot 10^{-7}$), the constant standard deviation implies that for all radii the distribution function moves at the same speed. This speed is defined by the movement of the average radius, $dt\langle R(t)\rangle/dt$. A shift $(R - \langle R \rangle)$ immobilizes the distribution function, and we see a collapse at all times, Fig. 3.17(b). As we have learned, this is temporary, and the system at asymptotic times will crossover to the diffusion limited regime, which evolves with a narrowing droplet size distribution function and thus lose the self-similarity.

3.3 Summary

In this chapter, we have learned about coarsening kinetics in emulsions with matter supply. For a constant supply, we found regimes in which emulsions

grow with a new scaling law independent of the supply. We derived the prefactors presented in Tab. 1.1. In both regimes the average radius evolves with the same time exponent as passive emulsions but with a higher prefactor. We found that in the interface-kinetics limited regime the average radius is shifted compared to passive emulsions, but the shift is independent of the supply values. Beyond the threshold of the supply discussed in [83], the droplet size distribution function in the diffusion limited regime narrows, and the coarsening kinetics is not universal anymore but depends on the supply and the initial conditions. At the same time, narrowing cannot be reached in the interface-kinetics limited regime even for very high supply rates. Narrowing poses a challenge in deriving a self-similar form of the droplet size distribution function. A distribution function that evolves into a delta-peak corresponds to a monodispersed emulsion which is interesting from the perspective of size control. In the later part of the chapter, we choose the matter supply in such a way as to keep the supersaturation constant. Droplets are decoupled from each other and grow independently of the whole emulsion. Even if we initialize the system in the interface-kinetics limited regime, the crossover to the diffusion limited regime will always happen for a large enough system, and the droplet size distribution function will always narrow.

Chapter 4

Coarsening kinetics of chemically-active emulsions

In Chapt. 3, droplet material was directly added to the system from a material reservoir. We now want to address a more general case of matter supply relevant to chemistry and biology, which consists of a chemical reaction of multiple components like precursor molecules and fuel that lead to droplet material supply. Through a fuel-driven chemical reaction, we control the concentration and production of the droplet material. Since we keep the system away from relaxing to its thermodynamic equilibrium due to matter supplied in a chemical reaction manner, we call such emulsions chemically-active.

We have discussed in Chapt. 1 that droplets present in cells are often subject to chemical cues that actively control the droplets' formation and evolution. These chemical cues often involve a chemical reaction cycle fueled by the hydrolysis of ATP and organelles in cells are often actively regulated by ATP-dependent chemical reaction cycles [86, 19, 87, 88]. To incorporate multiple components in the emulsion and a fuel-driven reaction cycle, we need to introduce a minimal model and discuss when we can write the mass action law kinetics. We will discuss a possible chemical realization of the model which fulfills these conditions. The experimental findings of droplet coarsening kinetics in emulsion with fuel-driven chemical reaction cycle are result of the collaboration with the Boekhoven laboratory. We will analyse these results together with the model of chemically-active emulsions to understand the effect of matter supply on the coarsening kinetics of chemically-active emulsions.

4.1 Model for emulsions with fuel-driven chemical reactions in dilute phase

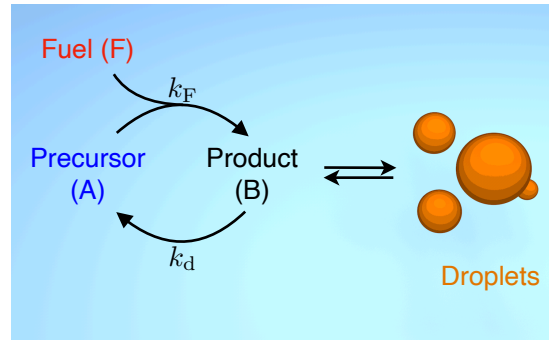


FIGURE 4.1: **Schematic representation of fuel-driven droplet formation:** A chemical reaction cycle in the dilute phase drives the activation of precursor (A) through fuel consumption of to the droplet forming product (B). The product (B) is unstable, and in reaction with solvent, i.e., hydrolysis reaction for a water solvent, it is deactivated to the precursor. The reaction rate constants at each arrow, correspond to these reactions respectively. Modified from [89].

Until now, we were discussing a binary mixture, made of a component that phase separates in the solvent into a dense and dilute phase. To discuss a more complicated system, like the one represented in Fig. 4.1, we need to introduce more components and discuss the chemical reaction cycle. Until now, our phase separating component corresponded to the **product (B)** molecules, which was phase separating into droplets. We extend now the model by **precursor (A)** and **fuel (F)**, which do not phase separate and are not present in droplets but are present in the dilute phase. The reaction cycle happens only in the dilute phase and consists of activation through fuel consumption (forward reaction): $A \rightarrow B$, and the deactivation through the reaction with solvent (backward reaction): $B \rightarrow A$.

In the following, we introduce the necessary assumptions and simplifications the model must fulfill for further discussion. The concentrations $c^{A,B,FS}(t)$ correspond to the concentrations in the dilute phase of the precursor, product, fuel and solvent respectively. For the inside phase $c_{in}^{A,B,FS}$ accordingly.

Model simplifications and assumptions

1. **Strong phase separation:** If the solvent (S) is water, we can describe the strength of the interactions between the molecules and solvent through

their hydrophobicity. Here we assume that the product (B) is highly hydrophobic, thus it phase separates strongly and forms droplets in which the presence of the solvent (and other components such as fuel or precursor) can be neglected. The other components precursor (A), fuel (F) are highly hydrophilic, which means they do not phase separate. The precursor (A) and fuel (F) molecules are as often present inside the droplets as the solvent is. Thus, we can neglect their concentration inside the droplets, such that $c_{\text{in}}^{\text{A,F}} \simeq 0$. The conditions inside the droplet, with no space for molecules other than the product, correspond to a high packing fraction of the order of 0.8. The concentration inside corresponds to the inverse of the molecular volume of the product ν , $c_{\text{in}} \simeq 1/\nu$. Furthermore, the concentration of the product in the dilute phase is much lower than in the dense phase, $c^{\text{B}}(t) \ll c_{\text{in}}^{(0)}$. The case of strong phase separation is also reflected in the constant concentration inside $c_{\text{in}}^{\text{B}} = c_{\text{in}}^{(0)}$, which is the case we have derived and discussed in Chapt. 2.

2. **Exchange of droplet material:** As a consequence of the condition 1, droplets exchange between each other only the droplet building material (B). No fuel, product, or solvent is exchanged during droplet growth kinetics. The growth law and the discussion of emulsion kinetics in Chapt. 2 hold in this limit.
3. **Reactions solely in the dilute phase:** The reactive components of the reaction cycle are only present at quantitative relevant levels in the dilute phase. Thus, the reaction happens outside the droplets only. The deactivation reaction can occur at the interface of the droplet. But we will assume that its effect on the total reaction outcome is negligible.
4. **Broken detailed balance condition:** The product (B) is activated by fuel and the thermal pathway of creating B from the precursor (A) can be neglected. As a result, stationary states are non-equilibrium steady states, and the system cannot relax to thermodynamic equilibrium. Thus, we call the system a chemically-active emulsion.
5. **Fast diffusion:** The diffusion of precursor, fuel, and the solvent is very fast compared to droplet growth, so there are no spatial inhomogeneities in the concentration profiles. Since droplets can grow in the diffusion limited regime, the diffusion of the product is relevant for the exchange of material between the droplets. We can, however, assume that the product concentration in the dilute phase is very low, and this

accounts for weak spatial inhomogenities. We assume the concentration of product in the dilute phase to be quasi-static.

6. **Composition independent reaction rate constants:** Since there are no reactions inside the droplets, the reaction rate constants $k_{F,d}(c^A, c^B, c^F, c^S)$ correspond to the dilute phase only and can be in general composition dependent. During nucleation, when the concentration of the building block in the dilute phase is high, the reaction rate constants could change. However, since we do not consider this regime in our discussion and are interested at times when the components in the phase outside the droplets are dilute, we can treat the reaction rate constants $k_{F,d}$ as constant and thus composition independent. This condition must be tested in the experimental realization.

In this model, the concentrations of the precursor (A) and fuel (F) change only due to the activation and deactivation reactions in the dilute phase, and we can write:

$$\frac{dc^A(t)}{dt} = -k_F c^F(t)c^A(t) + k_d c(t), \quad (4.1a)$$

$$\frac{dc^F(t)}{dt} = -k_F c^F(t)c^A(t). \quad (4.1b)$$

The concentration of the building block in the dilute phase, changes according to the conservation law discussed in Eq. (3.20), where we take into account how the droplet phase volume fraction $\Phi(t)$ changes due to emulsion growth. Furthermore, the activation and deactivation reactions influence the conservation law, such that the concentration of the building blocks in the dilute phase $c^B(t)$ changes according to

$$\frac{dc^B(t)}{dt} = -c_{in}^{(0)} \frac{d}{dt} \Phi(t) + k_F c^F(t)c^A(t) - k_d c^B(t), \quad (4.2)$$

where we have used the condition of small droplet phase volume compared to the total system volume, $V_{in} \ll V$. The droplet phase volume fraction $\Phi(t)$ is defined as

$$\Phi(t) = \int_0^\infty \frac{4\pi}{3} R^3(t) \mathcal{N}(R, t) dR, \quad (4.3)$$

with a time evolution given by

$$\frac{d}{dt} \Phi(t) = \int_0^\infty 4\pi R^2(t) \dot{R}(t) \mathcal{N}(R, t) dR. \quad (4.4)$$

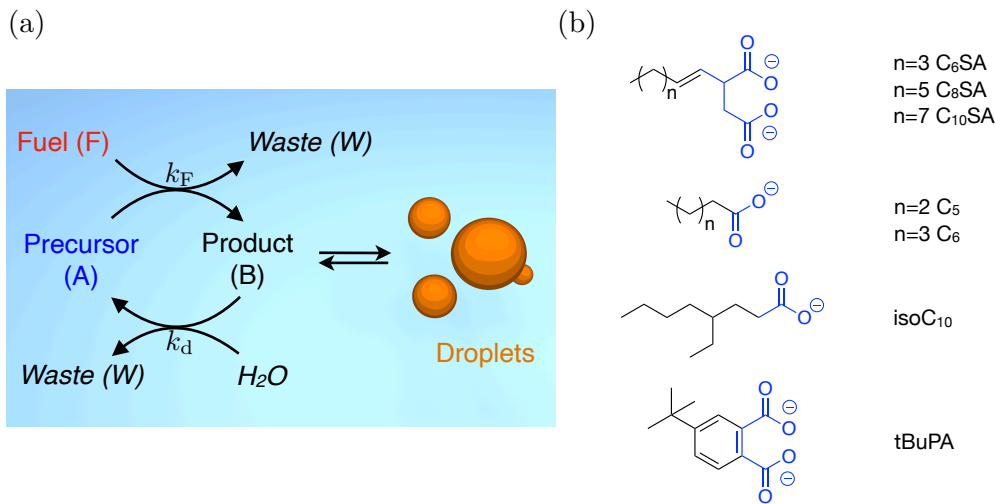


FIGURE 4.2: **Schematic representation of fuel-driven droplet formation in the chemical realization:** (a): A chemical reaction cycle from Fig. 4.1 has been extended by waste and water according to the experimental realization. (b): List and chemical structure of precursors used in the experiments. Modified from [89].

This time evolution of the droplet phase volume fraction is only valid in the regime in which we do not consider nucleation of droplets. This means that for droplet radii smaller than the critical radius $R < R_c(t)$ droplets will shrink. In this regime the droplet size distribution function $\mathcal{N}(R, t)$ evolves according to the continuity equation in Eq. (2.53) and for the droplet growth $\dot{R}(t)$ we use Eq. (2.65). Compared to Eq. (3.20), we can see that the term which corresponded to matter supply, $J_c(t)$, is here given by a time dependent expression

$$J_c(t) = k_F c^F(t) c^A(t) - k_d c^B(t), \quad (4.5)$$

which is coupled to the time evolution of the other components in the reaction cycle.

Furthermore, the total concentration of the building block (B) is not a constant anymore, but depends on the concentration of the precursor (A), such that:

$$c_{\text{tot}} = c^A(t) + c^B(t) + c_{\text{in}}^{(0)} \Phi(t), \quad (4.6)$$

where $c_{\text{tot}} = c^A(t = 0)$ before the start of the reaction cycle.

4.1.1 Experimental realization of emulsions with fuel-driven chemical reactions in the dilute phase

The field of fuel-driven self-assembly has recently gained interest. In the experiment, the self-assembly of molecules is regulated by a chemical reaction cycle that comprises two reactions: a building block activation and deactivation reaction. In the activation, a precursor molecule is activated for self-assembly by the irreversible consumption of a chemical fuel. In the deactivation, the product is reverted to the precursor [86].

The following discussion is based on our work with the Boekhoven group [89]. Here, we study water-soluble precursor molecules Fig. 4.2(b) in a water solvent. The reaction cycle Fig. 4.2(a) is driven by hydrolysis of 1-Ethyl-3-(3-dimethylaminopropyl)carbo-diimide (EDC) as a carbodiimide-based fuel. The carboxylate-based precursor (A) is activated by a reaction with fuel (F, EDC). The activation reaction is a two step process involving intramolecular carboxylate to form the product. The deactivation happens via hydrolysis of the product [89]. The concentration of the product, fuel and precursor is measured by HPLC method.

To be able to analyze the results of the experiment and write a correct model, we need to check how the experimental realization corresponds to the assumptions in 1-6. Starting from this section, we will, for simplicity, drop the index B in the concentration of the building blocks (product).

Conditions of the experimental realization

1. **Oil droplets:** The product, during the activation reaction, loses the negatively charged carboxylate group of the precursor, which decreases the solubility of the product compared to the precursor, and the nucleation of droplets. The chemical structure of the product is hydrophobic, as opposed to the hydrophilic structure of the precursor and fuel (EDC). The packing fraction within the droplets is very high compared to the dilute conditions outside. The equilibrium concentration of the droplet building blocks of the dense phase, $c_{\text{in}}^{(0)}$, is estimated through the molecular volume $c_{\text{in}}^{(0)} \simeq 1/\nu$ for each product and is in agreement with the measurements. The estimated solubility of the droplet building blocks, $c^{(0)}$, is for all products in the order of 1mM, whereas $c_{\text{in}}^{(0)} \simeq 1\text{M}$. The concentration of the other compounds in the dilute phase, $c^{\text{A,F}}(t) \simeq 10\text{mM}$, is dilute compared to the conditions inside the droplets. The droplets in the experimental conditions are oil droplets.

As a result of fulfilled condition 1, the conditions 2 and 3 follow directly. Droplets only exchange the product material with each other, and the reaction between the precursor and fuel, as well as product and water, happens only in the dilute phase. The estimate of the total number of product molecules (B) at the droplet interface N_{int} , compared to the total amount of molecules in the dilute phase N_{out} in the experiments is, $N_{\text{out}} \simeq 10^5 \cdot N_{\text{int}}$. The difference amounts for five orders of magnitude, and we can neglect the effect of hydrolysis at the droplet interface to the hydrolysis in the dilute phase.

4. **Broken detailed balance condition:** Without the fuel, the backward reaction (deactivation) has a very low chemical equilibrium constant, $K^{\text{eq}} = c(t)/c_A(t) \simeq 10^{-3}$ [89]. As soon as there is fuel and we activate a lot of B, we can neglect the pathway of $A \rightarrow B$ compared to the reaction with fuel.
5. **Fast diffusion:** The diffusion of all reactants is $D = 500 \mu\text{m}^2/\text{s}$. Furthermore, the distance between the droplets is $\ell_{\text{int}} \simeq 30 \mu\text{m}$. For the deactivation reaction, $\ell_{\text{deact}} = \sqrt{D/k_d} \simeq 300 \mu\text{m}$, such that $\ell_{\text{deact}} \gg \ell_{\text{int}}$ is well fulfilled, and the diffusion between the droplets is fast compared to chemical reactions.
6. **Composition independent reaction rate constants:** The reaction rate constants $k_{\text{F,d}}$ have been estimated through experimental measurements and do not show a dependence on the composition [90]. Even in the regimes where the concentration profile of the components changes strongly, the experimental data can be well described using $k_{\text{F,d}} = \text{const}$. Thus, the dependence on the composition must be very weak in the regimes we are discussing, and we chose to approximate them as constants.

There are two additional conditions the experimental realization satisfies. In the chemical reaction cycle, there are typically waste and intermediate products, depicted in Fig. 4.2. However, for the following reasons, we can neglect their impact on the reaction cycle.

- **Waste:** The hydrolysis of fuel, during which waste (EDU) is produced, occurs at the lowest reaction rate compared to all other reactions. The half-life of fuel is in the order of a day, and experiments are conducted within a few hours. Thus, in the regime we are looking at, the hydrolysis of fuel into the waste can be neglected. Furthermore, for some products, the hydrolysis into precursor produces waste. The time-frame of

the experiments has been adjusted such that these effects can be neglected and do not cause any problems in the measurements. However, the production of waste limits the possible observational time in the experiments, especially for the continuously-fuelled experiments, which we will discuss in more detail.

- **Short-lived intermediate product:** The reaction between precursor and fuel involves an intermediate step of an intermediate product that is short-lived and reacts quickly to the precursor and product. The intermediate product is quasi-static, and in the approximation, it is incorporated into a yield factor λ , such that



the precursor is activated by fuel, and the product is deactivated by hydrolysis. The yield factor λ is estimated from the reaction rate constants of the intermediate reaction and for all cases is in the order of $\lambda \simeq 0.8$ [89].

Given these conditions, the experimental realization can be described by the model in Eq. (4.2) and Eq. (4.1) with the modification of Eq. (4.7).

4.2 Experimentally observed acceleration of coarsening in chemically-active emulsions

In experiments, fuel was supplied in two ways: In single-fuelled emulsions, fuel was supplied only once to the mixture of solvent and precursor molecules Fig. 4.3(a). The publication in Ref. [89] refers to this set-up as one-batch mode. In the second method, called continuously-fuelled emulsions, fuel was supplied after the initial batch of fuel at equal time intervals, in such a way as to maintain the fuel concentration constant, Fig. 4.4(a). We distinguish between two set-ups, single- and continuously-fuelled emulsions.

The difference between these two set-ups is visible in the results of the total product concentration (B) that accounts for the product in the dilute phase and the droplet phase, Fig. 4.3(b) and Fig. 4.4(b). In single-fuelled experiments, the total concentration of product increases while the fuel is depleted. Once the fuel has been completely used, the product reaches its maximum concentration. Now, the forward reaction cannot happen anymore, and the

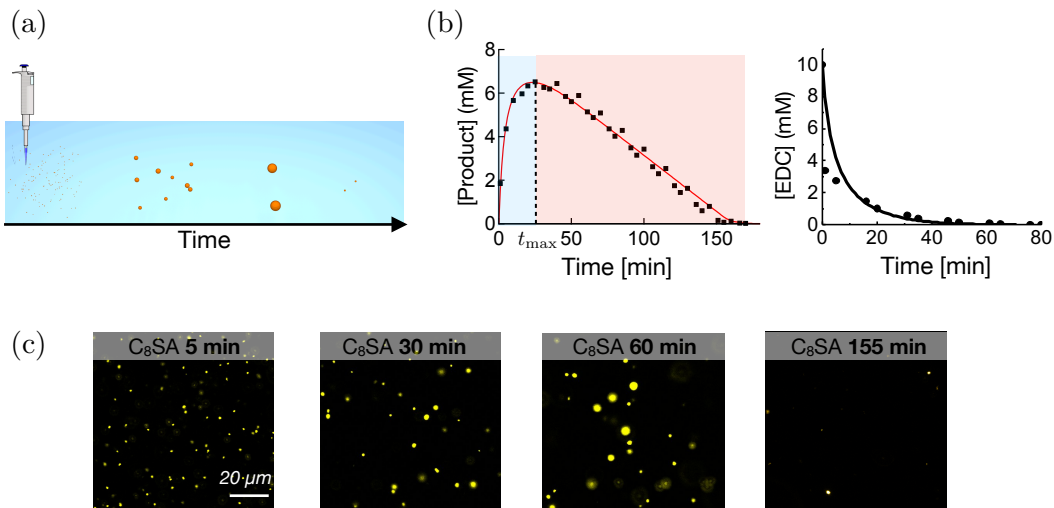


FIGURE 4.3: **Schematic of the set-up and results in single-fuelled experiments:** (a): Schematic of the single-fuelled set-up. The pipette corresponds to the fuel supply at the beginning of the experiment. Droplets emerge, grow, and, after a coarsening phase, dissolve, when the total concentration of product has been fully depleted. (b): Total concentration of product and fuel measured by HPLC method. The product initially increases (light blue region) and after reaching maximum concentration decreases linearly (red region). The concentration of fuel (EDC) decreases from its initial value until it is completely used. Markers correspond to experimental data and the solid lines to the theoretical model. (c): Micrographs at several time points in the cycle described in (b). The results (b), (c) are for the precursor C₈SA. Modified from [89].

product can be only deactivated. Its concentration decreases until the emulsion fully dissolves. For continuously-fuelled experiments, due to supply of fuel at constant time intervals, it is possible to maintain a semi-fixed concentration of fuel and of the product. We will now try to approximate the average droplet volume and compare it to classical Ostwald ripening, which for a diffusion limited growth valid in these experiments, is a good reference case.

4.2.1 Estimation of the average volume

In order to understand the coarsening kinetics of emulsions in the experimental realization, we make a theoretical estimate of the average volume for both set-ups.

For both cases, the time evolution of the droplet phase volume fraction $\Phi(t)$, Eq. (4.3), in the quasi-static regime discussed in the earlier sections, $\dot{c}(t) \simeq 0$, for the droplet material (B) in the dilute phase, simplifies to Eq. (2.63), which

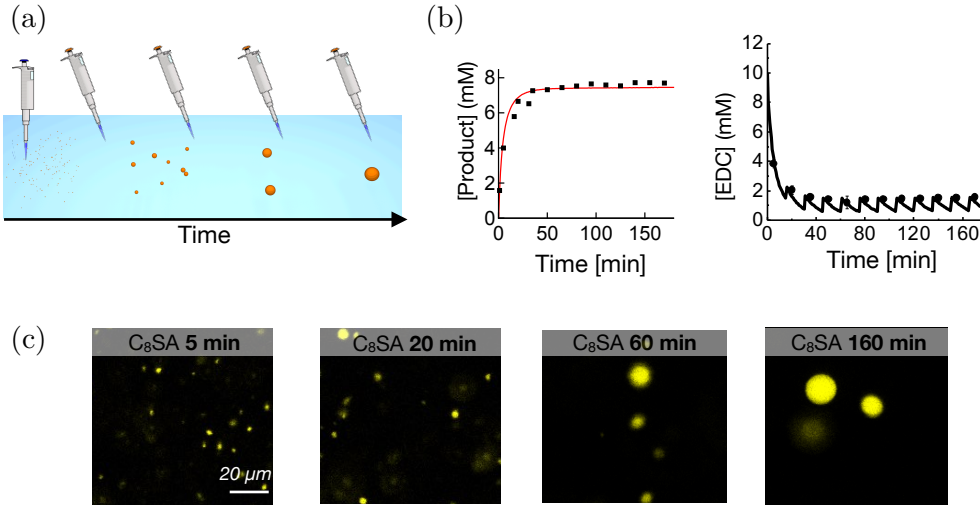


FIGURE 4.4: **Schematic of the set-up and results in continuously-fuelled experiments:** (a): Schematic of the continuously-fuelled set-up. The pipette corresponds to the fuel supply at the beginning of the experiment and later at equal time intervals. Droplets emerge, grow, and continuously coarsen. (b): Total concentration of product and fuel measured by HPLC method. The product increases and after reaching a maximum maintains constant concentration. The concentration of fuel (EDC) decreases from its initial value and through the continuous supply maintains a constant concentration. Markers correspond to experimental data and the solid line to the theoretical model. (c): Micrographs at several time points in the cycle described in (b). The results (b), (c) are for the precursor C_8SA . Modified from [89].

states

$$\frac{d\Phi(t)}{dt} = \frac{J_c(t)}{c_{in}^{(0)}}. \quad (4.8)$$

For the single-fuelled experiments, we can focus on the regime when fuel has been completely depleted, which corresponds to $t = t_{max}$ in Fig. 4.3(b). For $c^F(t) = 0$, the matter supply $J_c(t)$ from Eq. (4.5) has only the contribution from the degradation reaction. In the quasi-static approximation, the concentration of the droplet material in the dilute phase in the presence of droplets can be approximated by its equilibrium value, $c(t) \simeq c^{(0)}$, such that,

$$J_c = -k_d c^{(0)}. \quad (4.9)$$

In this regime, when fuel has been depleted, for $t \geq t_{max}$ the droplet phase volume fraction,

$$\Phi(t) = \frac{1}{c_{in}^{(0)}} \left(\lambda c^F(0) - c^{(0)} - k_d c^{(0)} (t - t_{max}) \right), \quad (4.10)$$

where the term $(\lambda c^F(0) - c^{(0)})$ estimates the amount of product (B) that has been produced by the initial amount of fuel $c^F(0)$, given the yield factor λ . We subtracted the minimal droplet material needed for phase separation, which is the solubility $c^{(0)}$. We can write the average volume as,

$$\langle V(t) \rangle = \frac{\Phi(t) V}{N(t)}, \quad (4.11)$$

with the total number of droplets $N(t)$, which must be still estimated. In experiments, the total system volume was estimated to $V = 6 \cdot 10^5 \mu\text{m}^3$. In experiments, the droplet size distribution function in both set-ups was broadening (which we will discuss in detail in the next section), and the total number of droplets decreased linearly [89]. As we have learned from Eq. (2.69) the number of droplets changes due to dissolution events, and by estimating the timescale of droplet dissolution τ_d we can approximate

$$N(t) = \eta \frac{\tau_d}{t}, \quad (4.12)$$

where η contains the numerical factor from the integration over the droplet size distribution function and all other constants. For passive emulsions in the diffusion-limited regime,

$$N_0(t) = V \frac{3\Phi}{4\pi R_c(t)^3} \frac{\int_0^\infty h(\rho) d\rho}{\int_0^\infty \rho^3 h(\rho) d\rho}, \quad (4.13)$$

where the subscript 0 corresponds to passive emulsions. We have used the definition of the droplet number density in Eq. (2.55), the separation ansatz valid in the diffusion limited regime, together with the result in Eq. (2.71). The critical radius for passive emulsions is $R_c(t)^3 = (4/9)D\ell_\gamma c^{(0)}t/c_{\text{in}}^{(0)}$, and the droplet phase volume fraction is approximately constant, $\Phi \simeq \text{const}$. For passive emulsions we can choose to write

$$\frac{\tau_{d,0}}{t} = 3V \frac{\Phi}{4\pi R_c(t)^3}, \quad (4.14)$$

such that $\eta^0 = \int_0^\infty h(\rho) d\rho / \int_0^\infty \rho^3 h(\rho) d\rho$. Using the solution of the droplet size distribution function for passive emulsion $\eta^0 = 0.885$. For the single-fuelled set-up, we estimated η for all experiments through a fit to data and found $\eta = 12.5$ [89], which can be expected to correspond to $\eta \approx 4\pi$.

To approximate τ_d , consider an emulsion of one droplet only. The droplet phase volume fraction for a single droplet $\Phi_s(t)$, changes according to Eq. (4.8)

with $J_c(t)$ given by Eq. (4.9), such that

$$\frac{d\Phi_s(t)}{dt} = -k_d \frac{c^{(0)}}{c_{\text{in}}^{(0)}}. \quad (4.15)$$

It follows, that the time scale of droplet dissolution is

$$\tau_d \simeq \frac{\Phi_s c_{\text{in}}^{(0)}}{k_d c^{(0)}}. \quad (4.16)$$

In experiments, we approximate Φ_s by considering the early stage of droplet kinetics and measuring an average-sized droplet captured in a box whose size corresponds to the interdroplet distance ℓ_{int} . There, $\Phi_s \simeq 2 \cdot 10^{-3}$ [89]. Alternatively, taking into account the physicochemical properties of the reactants and the initial conditions of the experiments, Φ_s can be estimated using the conservation law Eq. 4.6 and assuming that most of the precursor has turned over to products. Under the condition $c(t) \simeq c^{(0)}$ and $c^{(0)} \ll c_{\text{in}}^{(0)}$, follows $\Phi_s = c_{\text{tot}}/c_{\text{in}}^{(0)}$. We crosscheck and validate this estimation with the approximation of $\Phi_s \simeq 2 \cdot 10^{-3}$, which is valid for all reactants.

The estimate of the average volume $\langle V(t) \rangle$ from Eq. (4.11), using Eq. (4.16) and Eq. (4.10), is [89]

$$\langle V(t) \rangle = \langle V(t_{\text{max}}) \rangle + \frac{V}{\eta} \frac{k_d c^{(0)} (t - t_{\text{max}})}{c_{\text{in}}^{(0)}} \left(1 - \frac{k_d c^{(0)} (t - t_{\text{max}})}{\lambda c^{\text{F}}(0) - c^{(0)}} \right), \quad (4.17)$$

where for Φ_s we have used $c_{\text{tot}} = (\lambda c^{\text{F}}(0) - c^{(0)})$, valid for $t \geq t_{\text{max}}$. This result is in agreement with the experimental results and reflects the parabolic shape of the average volume Fig. 4.5(a) (red line: Eq. (4.17), dots: experiments). The estimation has been applied to the measurements of the average volume for all precursors used in the single-fuelled experiment. In total, there were seven different precursors used, for which the estimate was in a very good quantitative agreement [89].

For the continuously-fuelled experiments, we estimate the average volume analogously. The main difference is that the droplet phase volume fraction $\Phi(t)$ is directly estimated from the conservation law of the total material Eq. (4.6). For the condition $c(t) \simeq c^{(0)}$, we can solve Eq. (4.6) for $\Phi(t)$,

$$\Phi(t) = \frac{1}{c_{\text{in}}^{(0)}} \left(c_{\text{tot}} - c^{(0)} \left(\frac{c^{\text{A}}(t)}{c^{(0)}} - 1 \right) \right). \quad (4.18)$$

For continuously-fuelled set-ups, the quasi-static concentration of fuel Fig. 4.4(b)

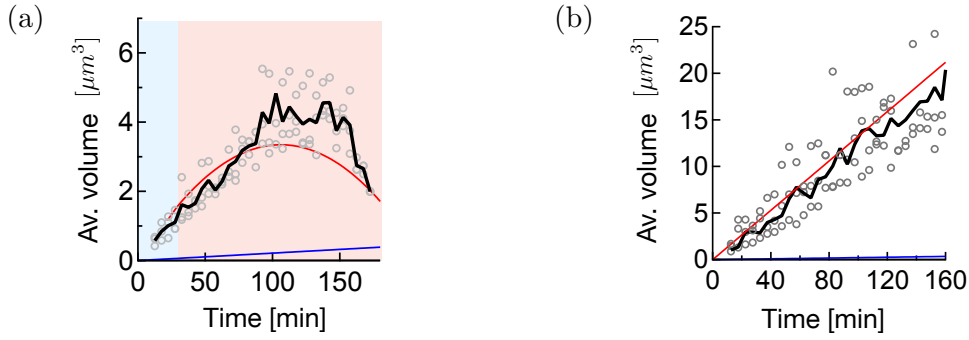


FIGURE 4.5: **Agreement of theoretical approximation of the average droplet volume with experiments:** The average droplet volume against time for C₈SA. The markers represent the data measured by image analysis software in three repeated experiments. The black line represents the average of the repeated experiments. The blue line corresponds to Ostwald ripening. (a): Single-fuelled experiment. The theoretically estimated average droplet volume from Eq. (4.17) is depicted by red solid line. The region where fuel has been depleted is depicted by the red shaded area, in contrary to the blue shaded region, which corresponds to $t < t_{\max}$. (b): Continuously-fuelled experiment. The theoretically estimated average droplet volume from Eq. (4.21) is depicted by red solid line. Modified from [89].

implies that there is a stationary fuel concentration $c^{F,0}$.

For $c(t) \simeq c^{(0)}$, Eq. (4.1a) results thus in a stationary concentration of the precursor $c^{A,0}$, which is given by

$$c^{A,0} = \frac{k_d c^{(0)}}{\lambda k_F c^{F,0}}, \quad (4.19)$$

where the constant concentration of $c^{F,0}$ is estimated from the concentration profiles. Note, that under these conditions, the matter supply in Eq. (4.5), $J_c(t) \simeq k_F c^{F,0} c^{A,0} - k_d c^{(0)}$. The stationary conditions of the concentration profiles of fuel and precursor, correspond to vanishing matter supply, $J_c(t) = 0$. The droplet phase volume fraction $\Phi(t)$ from Eq. (4.18), using the quasi-stationary concentration profile of the precursor Eq. (4.19) [89],

$$\Phi(t) = \frac{1}{c_{\text{in}}^{(0)}} \left(c_{\text{tot}} - c^{(0)} \left(\frac{k_d}{\lambda k_F c^{F,0}} - 1 \right) \right). \quad (4.20)$$

For the total droplet number $N(t)$ we can use the same arguments as before, with $N(t) = \eta \tau_d / (bt)$. The factor $\eta = 12.5$ as before, obtained from the fit to data. We expect the dissolution timescale to be shorter than in the single-fuelled experiments, and $b > 1$ accounts for this difference. This is

due to additional activation events to the product, which were absent in the single-fuelled experiments. The parameter b is estimated as the relative increase of the slope of the average volume in the continuously-fuelled compared to single-fuelled experiments. In the experiments we find: (C₆SA) $b = 3.84$, (C₈SA) $b = 2.89$, (C₁₀SA) $b = 4.29$. For the estimate of the dissolution timescale τ_d in Eq. (4.16) we calculate the droplet phase volume fraction Φ_s from Eq. (4.20).

For the average volume $\langle V(t) \rangle$ from Eq. (4.11), by plugging in the results for the droplet phase volume fraction and the droplet number, the estimate simplifies to [89],

$$\langle V(t) \rangle = \frac{b V k_d c^{(0)}}{\eta c_{\text{in}}^{(0)}} t, \quad (4.21)$$

where the linear growth is consistent with the experimental results, Fig. 4.5(b) (red line: Eq. (4.21), dots: experiment).

4.2.2 Collapse of the acceleration of coarsening

For the comparison of the experimental data to the theoretical estimates Eq. (4.11) and Eq. (4.21) in the two regimes, respectively, we have additionally depicted the average volume for Ostwald ripening, calculated using the physicochemical properties of the product (blue line in in Fig. 4.5(a),(c)). The average volume for Ostwald ripening can be approximated $\langle V(t) \rangle_0 = (4\pi/3) \langle R(t) \rangle_0^3$, where the average radius corresponds to the result in Eq. (1.17a), such that

$$\langle V(t) \rangle_0 = \frac{4\pi}{3} \left(\frac{4 D c^{(0)} \ell_\gamma}{9 c_{\text{in}}^{(0)}} \right) t, \quad (4.22)$$

where the diffusion constant D , and the equilibrium concentrations are known for each experiment. The capillary length ℓ_γ , discussed in Eq. (1.9),

$$\ell_\gamma = \frac{2\gamma}{k_B T c_{\text{in}}^{(0)}}, \quad (4.23)$$

is calculated for each product after measuring its surface tension γ . The results in Fig. 4.5(a),(b) show that the coarsening kinetics of emulsions in experiments, in the regime when the growth is linear exceeds the prediction of Ostwald ripening (blue line).

We want to estimate the acceleration of coarsening between the coarsening of active and passive emulsions. We assume that the average volume $\langle V(t) \rangle$ in the chemically-active emulsions has both a contribution from coarsening

coming from Ostwald ripening, $\langle V(t) \rangle_0$ as well as from the active growth $\langle V(t) \rangle_a$, from Eq. (4.11) and Eq. (4.21). We can thus write $\langle V(t) \rangle = \langle V(t) \rangle_0 + \langle V(t) \rangle_a$, and the acceleration of coarsening m is defined as,

$$m = \frac{\langle V(t) \rangle}{\langle V(t) \rangle_0} = 1 + \frac{\langle V(t) \rangle_a}{\langle V(t) \rangle_0}. \quad (4.24)$$

For the comparison of the active and passive growth, we are only interested in the regime where the average droplet volume grows linearly. We use the results in Eq. (4.11) for the linear growth and Eq. (4.21) as well as Eq. (4.22) accordingly and write,

$$m = 1 + \frac{9}{8} \frac{V k_B T}{(4\pi/3)\eta} \frac{k_d c_{\text{in}}^{(0)} \gamma}{c^{(0)}} \left\{ \begin{array}{l} 1 \\ b \end{array} \right. , \quad (4.25)$$

where V , $k_B T$ and η are the same in all experiments. Since the different precursors and products vary in their physicochemical properties reflected in k_d , $c_{\text{in}}^{(0)}$, γ and $c^{(0)}$, we want to write the expression for m in terms of a rescaled variable, which holds all active parameters of the reactants. We define a reference surface tension, γ_{ref} , which corresponds in value to the surface tension of C₈SA. We can then define a rescaled deactivation rate r_{eff} ,

$$r_{\text{eff}} = k_d \frac{c_{\text{in}}^{(0)}}{c^{(0)}} \frac{\gamma}{\gamma_{\text{ref}}}, \quad (4.26)$$

such that the acceleration of coarsening m in Eq. (4.25) becomes, [89]

$$m = 1 + \frac{9}{8} \frac{V k_B T \gamma_{\text{ref}}}{(4\pi/3)\eta} r_{\text{eff}} \left\{ \begin{array}{l} 1 \\ b \end{array} \right. , \quad (4.27)$$

In Fig. 4.6, we show a plot of the result in Eq. (4.27) for $b = 1$ (single-fuelled experiments, light red line) and a choice of $b = 2.95$ (continuously-fuelled, dark red line). For Ostwald ripening, $m = 1$ and is depicted as a reference (blue line). In the same figure, we show the experimentally measured values of m by directly reading off the linear growth rate of the average volume for every experiment and comparing it to the prefactor of the average volume in Ostwald ripening.

The experimental results and the theoretical estimate match each other very well. There is an excellent quantitative agreement; additionally, products from the same physicochemical family of similar properties are found to cluster into groups in the vicinity of a common parameter regime. Through the

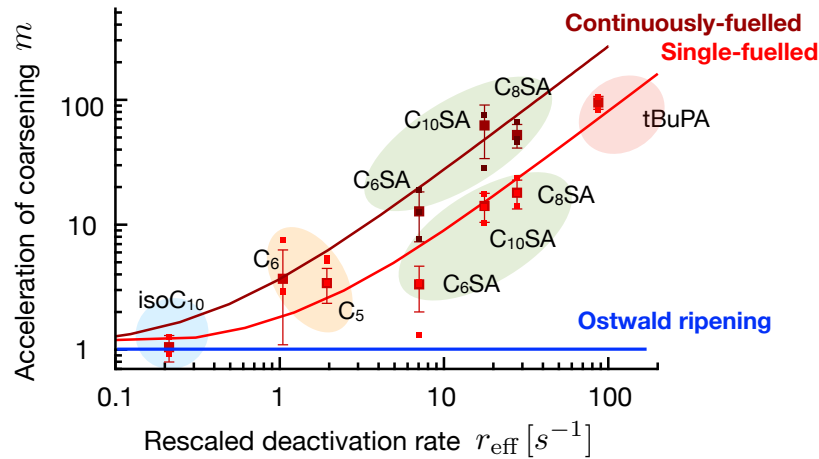


FIGURE 4.6: **Collapse of the acceleration of coarsening as a function of rescaled deactivation rate:** Acceleration of coarsening against the rescaled deactivation rate when products are subjected to single-fuel (red) or continuous-fuel (dark red). The products are grouped into families by common physicochemical properties (blue, yellow, green, red). The markers corresponds to the experimental measurements, with the error bars corresponding to the standard deviation from the average of the experiments. The solid lines correspond to Eq. (4.27), the blue solid line is the acceleration of coarsening for Ostwald ripening. Modified from [89].

estimations, we were able to understand that the active chemical reaction cycle regulates the increase in the average droplet volume. The deactivation reaction determines the time scale of droplet dissolution, and its possible to collapse the acceleration of coarsening using the physicochemical properties of the product material and the deactivation rate constant. We will now use the numerical calculations of the evolution of the droplet size distribution function, to better understand how the experimentally observed acceleration of coarsening is reflected in the theory of emulsions with matter supply.

4.3 Transient acceleration of coarsening in chemically-active emulsions

To understand the mechanism of accelerated coarsening in chemically-active emulsions, we solve numerically the continuity equation for the droplet size distribution function $\mathcal{N}(R, t)$ as discussed in Chapt. 1, Eq. (1.21). We extend the model by adding the evolution of fuel and precursor, which follow Eq.(4.1), and for the droplet material, we extend the conservation law by the chemical reaction cycle in Eq. (4.2). As before for the time and radial components we use the nondimensional form, $t \rightarrow t/(\ell_\gamma^2/D)$ and $R \rightarrow R/\ell_\gamma$, such

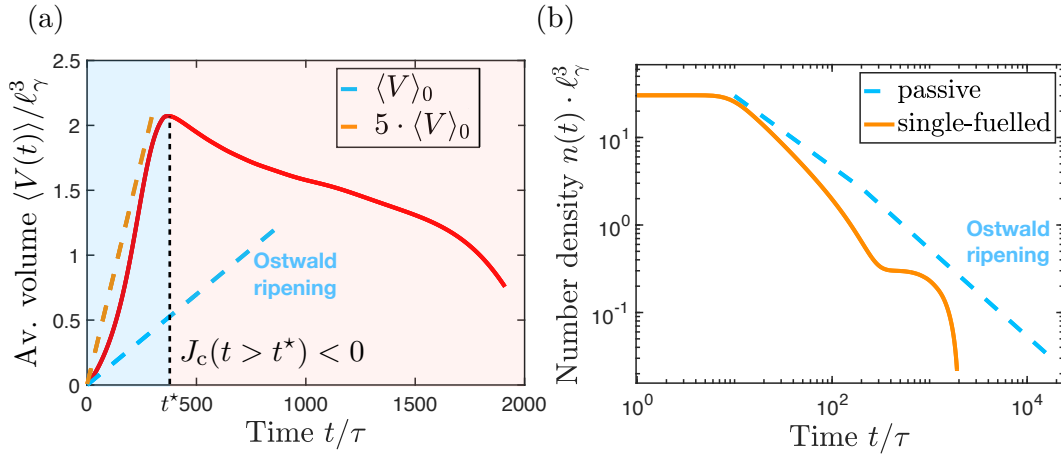


FIGURE 4.7: **Acceleration of the average volume in the single-fuelled set-up:** (a): In the single-fuelled conditions, we find the acceleration of the average volume five-fold compared to Ostwald ripening. The solution of the model (red solid line) is depicted together with the average volume for Ostwald ripening (light blue dashed line). The light blue dashed area corresponds to the regime where fuel is still present, which is depleted at $t = t^*$. In the red shaded area the matter supply due to lack of fuel is negative. (b): The number density in the single-fuelled set-up (orange solid line) decreases faster as in passive systems (Ostwald ripening, light blue dashed line). The time is t rescaled by $\tau = \ell_\gamma^2/D$, and the length by ℓ_γ .

that the nondimensional growth law Eq. (1.15) is

$$\frac{d}{dt}R(t) = \frac{k}{1 + k R(t)} \frac{c_{\text{out}}^{(0)}}{c_{\text{in}}^{(0)}} \left(\varepsilon(t) - \frac{1}{R(t)} \right), \quad (4.28)$$

where the supersaturation, $\varepsilon(t)c^{(0)} = (c(t) - c^{(0)})$. For the numerical calculations we chose: $\ell_\gamma = 0.001\mu\text{m}$, $D = 5 \cdot 10^2 \mu\text{m}^2/\text{s}$, which correspond the experimental conditions. For the diffusion limited case the choice of $k = 10^{20} \mu\text{m}/\text{s}$, fulfills the condition $D\ell_\gamma \ll k$. The choice of the equilibrium concentration in the dense and dilute phase corresponds to the experimental values of $C_8\text{SA}$, $c_{\text{in}}^{(0)} = 5000\text{mM}$, $c_{\text{out}}^{(0)} = 0.15\text{mM}$. The choice of the reaction rate constants is in the regime of the experimental values.

We initialize the system with an initial amount of precursor and fuel, first without droplets, and calculate how much fuel and precursor are used to produce enough product to phase separate. The threshold is chosen $c(t) = 3 \cdot c^{(0)}$. When this condition is reached, the emulsion is initialized with a droplet size distribution function which corresponds to the LSW-theory solution for the diffusion limited case (Ostwald ripening). Since with our method we cannot study the regime of nucleation, the solution of the distribution function for

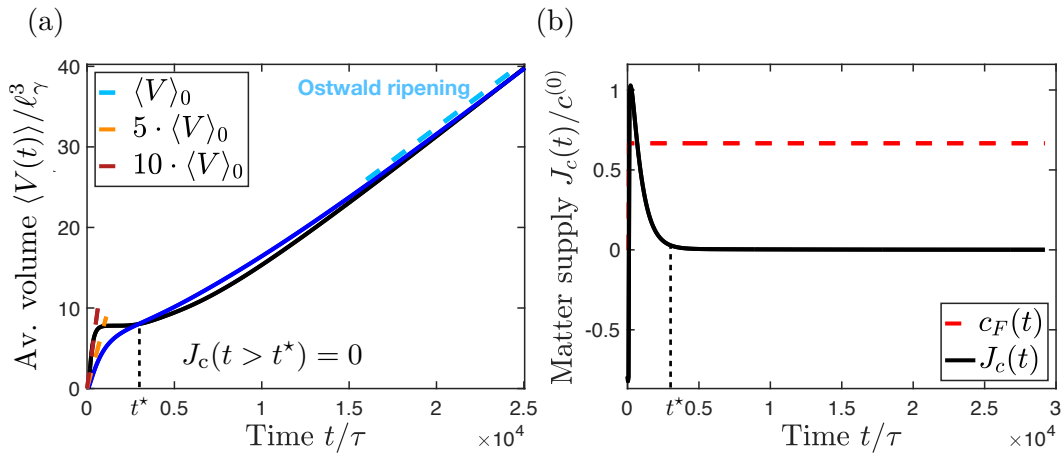


FIGURE 4.8: **Acceleration of the average volume in the continuously-fuelled set-up:** (a): In the continuously-fuelled conditions, we find the acceleration of the average volume five-fold and ten-fold compared to Ostwald ripening. The solution of the model (blue and black solid line) is depicted together with the average volume for Ostwald ripening (light blue dashed line). The blue line corresponds to a lower choice of the degradation rate constant $k_{d,\text{black}} = 1.14k_{d,\text{blue}}$ and the time t^* refers to this system. The observation is consistent with the prediction that a higher deactivation rate constant leads to higher acceleration of coarsening. (b): The matter supply in continuously-fuelled set-up (black solid line) decreases to $J_c(t) = 0$ at $t = t^*$. The concentration of fuel (red dashed line) is maintained constant. The data correspond to the system depicted by blue solid line in (a). The time is t rescaled by $\tau = \ell_\gamma^2/D$, the length by ℓ_γ and the concentration by $c^{(0)}$.

Ostwald ripening seems a natural choice. We initialize the emulsions with $c_F(0) = 45\text{mM}$ and $c_P(0) = 724.5\text{mM}$. This condition is higher than in the experiments, but due to the nature of the system we solve and the lack of the nucleation regime, we need to add much more material for the already existing droplets to notice the matter supply and the chemical reactions.

Given these conditions, we study the evolution of single- and continuously-fuelled emulsions. The results for the single-fuelled set-up are depicted in Fig. 4.7. We find the acceleration of the average volume, which can be five-fold of the Ostwald ripening. The power law of the average volume does not change, and the acceleration comes through the higher prefactor only, as predicted in Subsect. 4.2.1. The red shaded region in Fig. 4.7(a) corresponds to a regime when fuel has been depleted. The time $t = t^*$ corresponds to the time when $c_F(t \geq t^*) = 0$. In experiments we referred to this time as t_{max} , since it was measured when the total product concentration reached its maximum value. Beyond this time, the degradation of the product dominates the matter supply, which is now negative $J_c(t \geq t^*) < 0$. The shape of the

average volume has similarities to the parabolic shape from Fig. 4.18(a). The presence of the deactivation reaction, as expected through the estimate of the time scale of droplet dissolution τ_d in Eq. 4.16, causes droplets to dissolve faster than in Ostwald ripening Fig. 4.7(b). Since matter supply is negative, the single-fuelled emulsion evolves further until its complete dissolution.

For the continuously-fuelled emulsion, we fix the fuel concentration to a constant before the fuel has been completely depleted. The fuel concentration is chosen in such a way as to correspond to the quasi-static concentration of fuel in experiments, $c^{F,0} = 1.5\text{mM}$. The results of the average volume in Fig. 4.8(a) show that, as expected, the emulsion will not dissolve in contrary to single-fuelled set-up. We find in the initial regime, for $t < t^*$, a ten-fold acceleration in coarsening compared to Ostwald ripening (black solid line in Fig. 4.8(a)). At the time $t = t^*$, although the concentration of fuel is maintained constant, the matter supply becomes zero, $J_c(t > t^*) = 0$, Fig. 4.8(b). This is consistent with the discussion of the quasi-static concentration profiles of fuel and precursor, which will lead to matter supply reaching $J_c(t) = 0$. As we can expect, under this condition, the system will not dissolve, since for the dissolution matter supply must be negative. However it will relax from the accelerated coarsening towards the passive system. At late times, we find that the average volume approaches Ostwald ripening Fig. 4.8(a) (light blue dashed line).

Consistent with the experimental results, we find that in the continuously-fuelled emulsions, the acceleration of coarsening can be higher than in the single-fuelled experiments. In both cases, the average volume evolves with the same power law as in passive systems. Furthermore, in the continuously-fuelled case, the emulsion will not dissolve, contrary to single-fuelled experiments. We have learned that at very long times, which are not accessible to the experiments, emulsions in the continuously-fuelled experiments will always relax to the passive emulsions described in the diffusion limited case by Ostwald ripening. The increase in the dilute concentration of the droplet material $c(t)$ due to a constant matter supply through the forward reaction, and the growth of droplets, balance out the effect of the forward reaction in the matter supply term, such that $J_c(t) = k_F c^{F,0} c^{A,0} - k_d c(t)$, becomes zero.

As the last comparison to experiments, we look at the evolution of the droplet size distribution function $\mathcal{N}(R, t)$ for the experiments Fig. 4.9 and the model Fig. 4.10, in the single-fuelled and continuously-fuelled set-ups, (a) and (b) respectively. In experiments, it was possible to measure the number of droplets

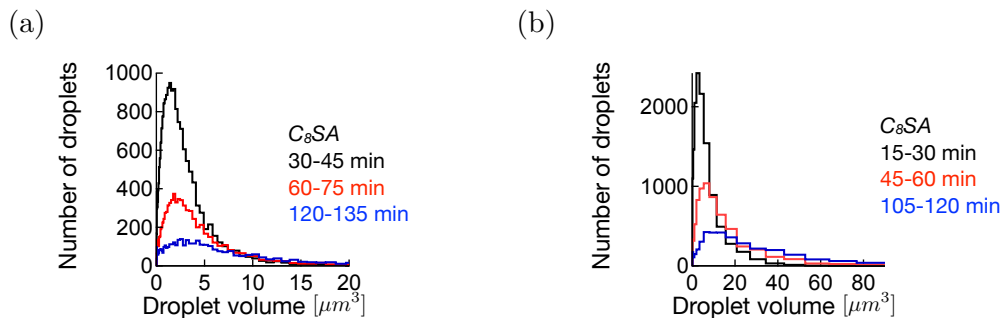


FIGURE 4.9: **Size distribution histograms for single- and continuously fuelled experiments:** The distribution of droplet volumes at different times measured for C₈SA. The colors of the lines correspond to the times of the measurement. (a): Single-fuelled experiment. (b): Continuously-fuelled experiment. Taken from [89].

having a particular droplet volume and represent the data in a form of a histogram. It is not the same measure as the droplet size distribution function, but it tells about the qualitative feature of the distribution of droplet sizes. In Fig. 4.9 we see that in both set-ups the amplitude of the number of droplets is decreasing, indicating that droplets dissolve, and the tail of the function is moving towards right. This indicates a broadening in the droplet size distribution function. For the model, we see analogous results for both set-ups. We choose time points, $(t_1 - t_4)$, that in both cases are equally spread around t^* , not too close to the initial stage nor too far in the dissolution regime for the single-fuelled set-up. We plot the droplet size distribution function as a function of the droplet volume, to be consistent with the experiments. We find that the droplet size distribution function is broadening, droplets are dissolving and the number is decreasing. As we have learned in Chapt. 3, for the distribution function to narrow, the matter supply must exceed a fixed threshold. Here, matter supply is high only in the initial regime, and later decreases to negative values or 0. Thus, the distribution function here is not expected to narrow.

4.4 Summary

In this chapter we discussed the effect of a chemical reaction cycle on matter supply and on the coarsening kinetics of emulsions. We discussed how the reaction cycle changes the conservation law and the droplet kinetics. Through an experimental realization it was possible to find acceleration in the coarsening kinetics for chemically-active emulsions. The prefactor of the scaling law of the average volume increased compared to passive emulsions.

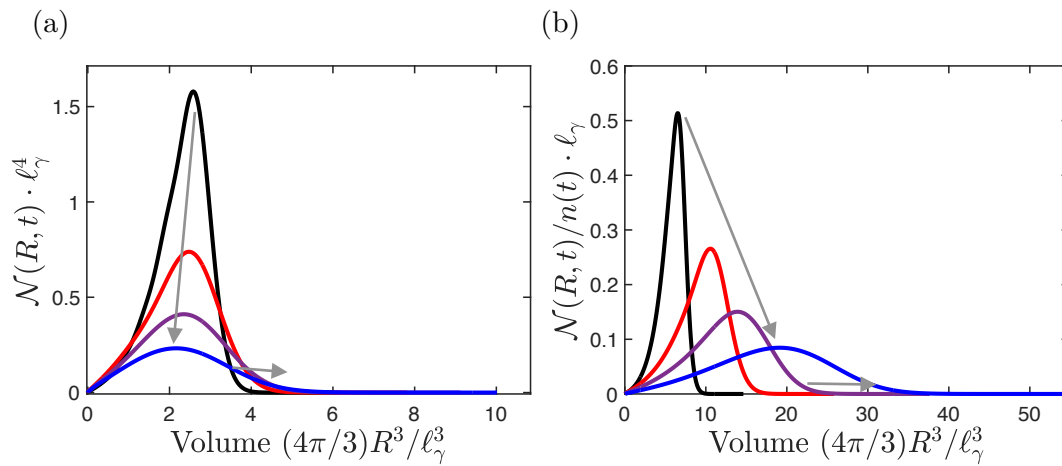


FIGURE 4.10: **Droplet size distribution function in single- and continuously-fuelled set-ups:** For the model fulfilling the conditions of the single- and continuously-fuelled conditions, we measure the droplet size distribution function at times $t_1/\tau = 0.2 \cdot 10^4$ (black solid line), $t_2/\tau = 0.4 \cdot 10^4$ (red), $t_3/\tau = 0.6 \cdot 10^4$ (purple) and $t_4/\tau = 0.8 \cdot 10^4$ (blue), where $\tau = \ell_\gamma^2/D$. The arrows indicate how the amplitude is decreasing over time, due to decreasing droplet number and that the distribution function is broadening. (a): Single-fuelled set up. (b): Continuously-fuelled set up.

On the other hand, the power law in time for the average volume is the same as in passive systems. We understood how the chemical reaction, especially the deactivation reaction and the physicochemical conditions of the experimental realization influence the acceleration of coarsening. Furthermore, by solving the model numerically, we found that the acceleration of coarsening is only transient. Droplets either dissolve after the acceleration regime in the single-fuelled set-ups or relax towards passive systems at very late times in the continuously-fuelled cases. The observed acceleration is relevant only at short time scales. In the experimental realization of the continuously-fuelled set-ups, these late times cannot be reached.

Chapter 5

Summary and future outlook

This thesis is dedicated to the coarsening of emulsions under conditions of matter supply. In the first part, in Chapt. 1, we defined an emulsion and its different stages of evolution. After exploring the physics of liquid-liquid phase separation, we have learned about the coarsening kinetics in passive emulsions, what is the scaling law of the average droplet radius in the two asymptotic regimes of the droplet growth law: the diffusion limited and the interface-kinetics limited growth. Furthermore, we have learned about the solution of the droplet size distribution function and its self-similarity in passive emulsions. Emulsions are present in cells, which are active systems, and because active systems are often subject to matter and energy supply, we decided to explore the effect of matter supply on emulsion coarsening kinetics.

The next chapter, Chapt. 2, was dedicated to the theory of single droplet growth kinetics, which was later used to construct the theory of emulsion coarsening kinetics with broken conservation law. We derived a complete theoretical framework that describes the growth of a single droplet considering the scenarios of the diffusion or the interface-kinetics limited growth. We focused on a special case of constant conditions inside the droplet. After deriving the full picture of single droplet growth kinetics, we derived the theory of emulsion kinetics, where we look at an ensemble of droplets sharing the same concentration field in the dilute phase. The concentration shared by the droplets changes additionally to the growth of the emulsion due to a general matter supply term. We have derived how a single droplet grows in such emulsion given the conditions of matter supply. The discussion is only valid for homogeneous matter supply in the dilute phase. We found that even with matter supply it is possible to find the solution of the critical radius, and how it evolves in time. The solution is the same as in passive emulsions as long as the critical radius is not constant and the distribution

Supply / Growth process	Diffusion limited	Interface-kinetics limited
Passive <i>no supply</i>	$\langle R(t) \rangle = \left(D \frac{4}{9} \frac{\ell_\gamma c_{\text{out}}^{(0)}}{c_{\text{in}}^{(0)}} t \right)^{1/3}$ $n(t) \propto t^{-1}$ broadening	$\langle R(t) \rangle = \frac{8}{9} \left(k \frac{\ell_\gamma c_{\text{out}}^{(0)}}{2c_{\text{in}}^{(0)}} t \right)^{1/2}$ $n(t) \propto t^{-3/2}$ broadening
Time-dependent <i>constant supersaturation</i>	$\langle R(t) \rangle = \left(2 \frac{D\varepsilon c_{\text{out}}^{(0)}}{c_{\text{in}}^{(0)}} t \right)^{1/2}$ $n(t) \propto \text{const}$ narrowing	$\langle R(t) \rangle = \left(\frac{k\varepsilon c_{\text{out}}^{(0)}}{c_{\text{in}}^{(0)}} t \right)$ $n(t) \propto \text{const}$ constant width
Constant supply	$\langle R(t) \rangle = \xi_{\text{diff}} \left(D \frac{4}{9} \frac{\ell_\gamma c_{\text{out}}^{(0)}}{c_{\text{in}}^{(0)}} t \right)^{1/3}$ $n(t) \propto \text{const}$ broadening - narrowing	$\langle R(t) \rangle = \xi_{\text{int}} \frac{8}{9} \left(k \frac{\ell_\gamma c_{\text{out}}^{(0)}}{2c_{\text{in}}^{(0)}} t \right)^{1/2}$ $n(t) \propto t^{-1/2}$ broadening

TABLE 5.1: **Summary of coarsening kinetics in emulsions with different matter supply:** Table summarising asymptotic scaling laws for the average radius $\langle R(t) \rangle$ and the droplet number density $n(t)$, and whether the distribution function is narrowing or broadening in emulsions under different constraints. We differentiate between the two processes that define the growth law, diffusion limited and interface-kinetics limited regime. The table has been introduced in Chapt. 1 and we have now added the information about the droplet number density $n(t)$. Through the numerical calculations, we were able to determine the value of $\xi_{\text{int}} \approx 1.39$, which is fixed and independent of the supply. However, ξ_{diff} remains undetermined and has a more pronounced dependence on the supply.

function is broadening. The solution of the critical radius is very robust, and the perturbations which can occur due to matter supply, have only transient effect. The solution of the critical radius determines the power law of the average radius. Thus, even with matter supply it is very difficult to change the scaling exponent in the power law of the average radius compared to passive emulsions. Due to the broken conservation law of the total droplet material and an increasing droplet phase volume fraction it is not possible to solve analytically for the whole scaling function of the droplet size distribution function, which determines the scaling prefactor of the average radius, and can, in general, depend on the matter supply conditions.

In Chapt. 3, we decided to look at specific classes of matter supply and solve the system numerically. We chose first to look at a constant matter supply. We found that in the interface-kinetics limited regime, the scaling function of the droplet size distribution function is independent of the supply rates. We estimated the scaling law for the average radius, for which the prefactor of the scaling law differs by a constant shift independent of the supply, compared to passive emulsions. For high enough supplies, there was a crossover

to the diffusion limited regime due to the rapid but transient acceleration in the average radius. The number density of droplets is described by a different power law behaviour than in passive emulsions.

For the diffusion limited regime, the results imply that the distribution function depends on matter supply, and so does the prefactor of the scaling law for the average radius. The droplet number density in this regime with a constant matter supply becomes constant. We found that in the regime of low supply rates, as long as the distribution function broadens, we can find a separation ansatz that leads to a universal and self-similar droplet size distribution function in both diffusion and interface-kinetics limited regime. However, for increasing supply rates in the diffusion limited regime, we observed a transition to a narrowing distribution function, proposed and discussed in the literature. There, it was impossible to find a collapse of the distribution function onto a self-similar shape.

Another class of matter supply we studied maintains the supersaturation constant. We derived new scaling laws for the average radius that differ from passive emulsions in the scaling exponent and in the scaling prefactor. Furthermore, the droplet size distribution function for emulsions with constant supersaturation is narrowing and the droplet number density is constant. Initializing the emulsion in the interface-kinetics limited regime introduces a transient regime, when the system evolves and grows with a constant standard derivation. However, at later times, when the emulsion becomes large enough, there will always be a crossover to the diffusion limited regime and the narrowing will eventually occur there as well. In the narrowing regime we again find that a self-similar solution of the distribution function is not found. These observations are summarized in Tab. 5.1.

In the last part, Chapt. 4, we discussed chemically-active emulsions, for which matter supply is controlled through a chemical reaction cycle in the dilute phase. After understanding the minimal model from the theoretical perspective, we discussed an experimental realization of the system. In the experimental realization, it was found that due to the chemical reaction cycle, there is an acceleration in the coarsening kinetics compared to passive emulsions. The acceleration of coarsening was not affecting the scaling exponent in time but only the scaling prefactor of the average droplet volume. In the single-fuelled experiments after the initial acceleration of coarsening, due to the depletion of fuel and the ongoing degradation of the droplet material, the emulsion has dissolved. In the continuously-fuelled experiments, the dissolution was not observed and the acceleration of coarsening was believed in

experiments to persist. By combining the theory and experiments, we could understand better what happens at times beyond the observation times of the experiments. In the continuously-fuelled set-up, after the initial acceleration, the emulsion relaxed to the passive evolution through Ostwald ripening due to vanishing matter supply. In our discussion we have only considered chemical reactions in the dilute phase. It would be interesting to extend the chemical reaction cycle also to the inside of the droplets. It is known that chemical reactions inside the droplets can arrest Ostwald ripening [91], and thus this mechanism could offer an additional control of the relaxation kinetics towards Ostwald ripening.

If the supersaturation is maintained constant, or during overfeeding and nucleation, the scaling in time of the average radius will be different than in passive emulsions. Otherwise, it is very difficult to observe a new power law behavior in the coarsening kinetics of emulsions compared to passive systems, even in the presence of matter supply in the dilute phase. However, matter supply highly affects and changes the power law behaviour of the droplet number density or the standard deviation. Studying the power law behaviour of other observables than the average droplet radius or the average droplet volume, could tell us much more about the active processes that might regulate the emulsion kinetics compared to passive systems. By studying the average droplet radius or volume only, in some experimental set-ups, it might be not possible to differentiate between the passive and non-passive coarsening kinetics. For cells, the division of cells and the cell cycle limit the possible time window for the droplets to evolve. Matter supplied and controlled through a chemical reaction cycle offers rapid acceleration and an increase in the average droplet volume at very short time scales. This mechanism might have a functional relevance for cells. Collecting more experimental results for the emulsion kinetics in cells as well as for droplets *in vitro*, and comparing them to our theoretical prediction, would be relevant to understanding the interplay between active processes like matter supply and the evolution of emulsions.

List of Figures

1.1	Schematic of stages during the evolution of an emulsion	2
1.2	Classification of membraneless organelles in cells	4
1.3	Biophysical properties of condensates	6
1.4	A schematic of protocell cycle and active kinetics	8
1.5	Schematic free energy and phase diagram for a binary mixture	11
1.6	Schematic concentration profile and phase diagram for finite interface effects	13
1.7	Schematic for droplet growth in a rate limiting process	16
1.8	Temporal evolution of the average radius and standard deviation in passive emulsions	20
1.9	Temporal evolution of the number of droplets and supersaturation in passive emulsions	21
1.10	Temporal evolution of the droplet size distribution function in passive emulsions	22
1.11	Collapse of the distribution function	23
2.1	Schematic of the concentration profile for the inside and outside phase across the interface	30
2.2	Schematics of the chemical potential profile across the phases	32
2.3	Schematic of emulsion	37
2.4	Schematic of the coordinate system	38
2.5	Schematics of the droplet size distribution function	42
2.6	Narrowing and broadening zones in the growth rate of the average radius	52
3.1	Constant rate of change of the droplet phase volume fraction .	56
3.2	Convergence of the critical radius in emulsions with matter supply to the passive solution	57
3.3	Universality of the droplet size distribution function	59
3.4	Temporal evolution of the average radius for emulsions with constant matter supply	60

3.5	New scaling laws of the droplet number density for emulsions with constant matter supply	62
3.6	Average radius and droplet number density in diffusion limited regime	63
3.7	Broadening and narrowing zones of the distribution function in diffusion limited regime	64
3.8	Broadening distribution function in interface-kinetics limited regime	65
3.9	Average radius and droplet number density in interface-kinetics limited regime	66
3.10	Collapse of the droplet size distribution function in diffusion limited regime	67
3.11	No self-similarity droplet size distribution function in diffusion limited regime	68
3.12	Collapse of the droplet size distribution function in interface-kinetics limited regime	69
3.13	Collapse of the droplet size distribution function in interface-kinetics limited regime	70
3.14	Crossover in the scaling of the average radius for different initial conditions	72
3.15	Narrowing distribution function as the emulsion reaches fixed droplet number density	74
3.16	No self-similar droplet size distribution function in diffusion limited regime	75
3.17	Collapse of the droplet size distribution function in interface-kinetics limited regime	76
4.1	Schematic representation of fuel-driven droplet formation	79
4.2	Schematic representation of fuel-driven droplet formation in the chemical realization	82
4.3	Schematic of the set-up and results in single-fuelled experiments	86
4.4	Schematic of the set-up and results in continuously-fuelled experiments	87
4.5	Agreement of theoretical approximation of the average droplet volume with experiments	90
4.6	Collapse of the acceleration of coarsening as a function of rescaled deactivation rate	93
4.7	Acceleration of the average volume in single-fuelled set-up	94

4.8	Acceleration of the average volume in continuously-fuelled set-up	95
4.9	Size distribution histograms for single- and continuously fuelled experiments	97
4.10	Droplet size distribution function in single- and continuously-fuelled set-ups	98

List of Tables

1.1	Summary of coarsening kinetics in emulsions with different matter supply	26
5.1	Summary of coarsening kinetics in emulsions with different matter supply	100

Bibliography

- [1] J. A. Marqusee and John Ross. Kinetics of phase transitions: Theory of Ostwald ripening. *The Journal of Chemical Physics*, 79(1):373–378, July 1983.
- [2] Peter W. Voorhees. The theory of Ostwald ripening. *Journal of Statistical Physics*, 38(1):231–252, January 1985.
- [3] Eric D. Siggia. Late stages of spinodal decomposition in binary mixtures. *Physical Review A*, 20(2):595–605, August 1979.
- [4] Michael Cates. Complex fluids: The physics of emulsions. In *Soft Interfaces: Lecture Notes of the Les Houches Summer School*, pages 317–358. Oxford Academic, November 2017.
- [5] Wilhelm Ostwald. *Lehrbuch der Allgemeinen Chemie*. W. Engelmann, Leipzig, 2 edition, 1896.
- [6] Wilhelm Ostwald. Studien über die Bildung und Umwandlung fester Körper. 1. abhandlung: Übersättigung und Überkaltung. *Zeitschrift für Physikalische Chemie*, 22(1):289–330, 1897.
- [7] I. M. Lifshitz and V.V. Slyozov. The kinetics of precipitation from supersaturated solid solutions. *Journal of Physics and Chemistry of Solids*, 19(1):35–50, April 1961.
- [8] Carl Wagner. Theorie der Alterung von Niederschlägen durch Umlösen (Ostwald-Reifung). *Zeitschrift für Elektrochemie, Berichte der Bunsengesellschaft für physikalische Chemie*, 65(7-8):581–591, September 1961.
- [9] Lorenz Ratke and Peter W. Voorhees. *Growth and Coarsening: Ostwald Ripening in Materials Processing*. Springer-Verlag, 2002.
- [10] J. A. Marqusee and John Ross. Theory of Ostwald ripening: Competitive growth and its dependence on volume fraction. *The Journal of Chemical Physics*, 80(1):536–543, January 1984.

- [11] Barbara Niethammer and Robert L. Pego. Non-Self-Similar Behavior in the LSW Theory of Ostwald Ripening. *Journal of Statistical Physics*, 95(5):867–902, June 1999.
- [12] Barbara Niethammer. Effective Theories for Ostwald Ripening. In *Analysis and Stochastics of Growth Processes and Interface Models*, pages 223–243. Oxford University Press, July 2008.
- [13] Barbara Niethammer and Robert L. Pego. The LSW Model for Domain Coarsening: Asymptotic Behavior for Conserved Total Mass. *Journal of Statistical Physics*, 104(5):1113–1144, September 2001.
- [14] Barbara Niethammer and Robert L. Pego. On the Initial-Value Problem in the Lifshitz–Slyozov–Wagner Theory of Ostwald Ripening. *SIAM Journal on Mathematical Analysis*, 31(3):467–485, January 2000.
- [15] Salman F. Banani, Hyun O. Lee, Anthony A. Hyman, and Michael K. Rosen. Biomolecular condensates: organizers of cellular biochemistry. *Nature Reviews Molecular Cell Biology*, 18(5):285–298, May 2017.
- [16] J. Ross Buchan, Denise Muhrad, and Roy Parker. P bodies promote stress granule assembly in *Saccharomyces cerevisiae*. *Journal of Cell Biology*, 183(3):441–455, November 2008.
- [17] Ji-Long Liu, Christine Murphy, Michael Buszczak, Sarah Clatterbuck, Robyn Goodman, and Joseph G. Gall. The *Drosophila melanogaster* Cajal body. *Journal of Cell Biology*, 172(6):875–884, March 2006.
- [18] Marina Feric, Nilesh Vaidya, Tyler S. Harmon, Diana M. Mitrea, Lian Zhu, Tiffany M. Richardson, Richard W. Kriwacki, Rohit V. Pappu, and Clifford P. Brangwynne. Coexisting Liquid Phases Underlie Nucleolar Subcompartments. *Cell*, 165(7):1686–1697, June 2016.
- [19] Clifford P. Brangwynne, Christian R. Eckmann, David S. Courson, Agata Rybarska, Carsten Hoege, Jöbin Gharakhani, Frank Jülicher, and Anthony A. Hyman. Germline P Granules Are Liquid Droplets That Localize by Controlled Dissolution/Condensation. *Science*, 324(5935):1729–1732, June 2009.
- [20] Christoph A. Weber, Lars Hubatsch, and Frank Jülicher. Die Physik Dynamischer Tropfen. *Physik-Journal*, 19(12):42–47, 2020.

- [21] Bruce Alberts, Dennis Bray, Karen Hopkin, Alexander D. Johnson, Julian Lewis, Martin Raff, Keith Roberts, and Peter Walter. *Essential Cell Biology*. CRC Press, 2015.
- [22] Anthony A. Hyman, Christoph A. Weber, and Frank Jülicher. Liquid-Liquid Phase Separation in Biology. *Annual Review of Cell and Developmental Biology*, 30(1):39–58, October 2014.
- [23] Mathias L Heltberg, Judith Miné-Hattab, Angela Taddei, Aleksandra M Walczak, and Thierry Mora. Physical observables to determine the nature of membrane-less cellular sub-compartments. *eLife*, 10:e69181, October 2021.
- [24] Christoph A. Weber and Christoph Zechner. Drops in cells. *Physics Today*, 74(6):38–43, June 2021. Publisher: American Institute of Physics.
- [25] Adam Klosin, Florian Oltsch, Tyler Harmon, Alf Honigmann, Frank Jülicher, Anthony A. Hyman, and Christoph Zechner. Phase separation provides a mechanism to reduce noise in cells. *Science*, 367(6476):464–468, January 2020.
- [26] Yongdae Shin and Clifford P. Brangwynne. Liquid phase condensation in cell physiology and disease. *Science*, 357(6357):eaaf4382, September 2017.
- [27] Joel Berry, Clifford P. Brangwynne, and Mikko Haataja. Physical principles of intracellular organization via active and passive phase transitions. *Reports on Progress in Physics*, 81(4):046601, feb 2018.
- [28] Joel Berry, Stephanie C. Weber, Nilesh Vaidya, Mikko Haataja, and Clifford P. Brangwynne. Rna transcription modulates phase transition-driven nuclear body assembly. *Proceedings of the National Academy of Sciences of the United States of America*, 112(38):E5237–E5245, 2015.
- [29] Daniel S.W. Lee, Ned S. Wingreen, and Clifford P. Brangwynne. Chromatin mechanics dictates subdiffusion and coarsening dynamics of embedded condensates. *Nature Physics*, 17(6560):531–538, 2021.
- [30] Andrew W. Folkmann, Andrea Putnam, Chiu Fan Lee, and Geraldine Seydoux. Regulation of biomolecular condensates by interfacial protein clusters. *Science*, 373(6560):1218–1224, 2021.
- [31] Fabio Pessina, Fabio Giavazzi, Yandong Yin, Ubaldo Gioia, Valerio Vitelli, Alessandro Galbiati, Sara Barozzi, Massimiliano Garre, Amanda

- Oldani, Andrew Flaus, Roberto Cerbino, Dario Parazzoli, Eli Rothenberg, and Fabrizio d'Adda di Fagagna. Functional transcription promoters at DNA double-strand breaks mediate RNA-driven phase separation of damage-response factors. *Nature Cell Biology*, 21(10):1286–1299, October 2019.
- [32] A.J. Bray. Theory of phase-ordering kinetics. *Advances in Physics*, 43(3):357–459, June 1994.
- [33] Pavel L. Krapivsky, Sidney Redner, and Eli Ben-Naim. *A Kinetic View of Statistical Physics*. Cambridge University Press, 2010.
- [34] N. Amy Yewdall, Alain A. M. André, Tiemei Lu, and Evan Spruijt. Coacervates as models of membraneless organelles. *Current Opinion in Colloid & Interface Science*, 52:101416, April 2021.
- [35] Shogo Koga, David S. Williams, Adam W. Perriman, and Stephen Mann. Peptide–nucleotide microdroplets as a step towards a membrane-free protocell model. *Nature Chemistry*, 3(9):720–724, September 2011.
- [36] T-Y. Dora Tang, C. Rohaida Che Hak, Alexander J. Thompson, Marina K. Kuimova, D. S. Williams, Adam W. Perriman, and Stephen Mann. Fatty acid membrane assembly on coacervate microdroplets as a step towards a hybrid protocell model. *Nature Chemistry*, 6(6):527–533, June 2014.
- [37] Björn Drobot, Juan M. Iglesias-Artola, Kristian Le Vay, Viktoria Mayr, Mrityunjay Kar, Moritz Kreysing, Hannes Mutschler, and T-Y Dora Tang. Compartmentalised RNA catalysis in membrane-free coacervate protocells. *Nature Communications*, 9(1):3643, September 2018.
- [38] John Crosby, Tom Treadwell, Michelle Hammerton, Konstantinos Vasilakis, Matthew P. Crump, David S. Williams, and Stephen Mann. Stabilization and enhanced reactivity of actinorhodin polyketide synthase minimal complex in polymer–nucleotide coacervate droplets. *Chemical Communications*, 48(97):11832–11834, 2012.
- [39] T.-Y. Dora. Tang, Dirk van Swaay, Andrew deMello, J. L. Ross Anderson, and Stephen Mann. In vitro gene expression within membrane-free coacervate protocells. *Chemical Communications*, 51(57):11429–11432, 2015.
- [40] Andrew S. Lyon, William B. Peeples, and Michael K. Rosen. A framework for understanding the functions of biomolecular condensates

- across scales. *Nature Reviews Molecular Cell Biology*, 22(3):215–235, March 2021.
- [41] Jasper van der Gucht, Evan Spruijt, Marc Lemmers, and Martien A. Cohen Stuart. Polyelectrolyte complexes: Bulk phases and colloidal systems. *Journal of Colloid and Interface Science*, 361(2):407–422, September 2011.
- [42] Jingcheng Fu and Joseph B. Schlenoff. Driving Forces for Oppositely Charged Polyion Association in Aqueous Solutions: Enthalpic, Entropic, but Not Electrostatic. *Journal of the American Chemical Society*, 138(3):980–990, January 2016.
- [43] Benjamin Harrow. The Origin of Life: The Origin of Life. By A. I. Oparin. Translated by Sergius Morgulis. Macmillan, 1938. *Science*, 88(2272):58–58, July 1938.
- [44] Annemiek D. Slootbeek, Merlijn H. I. van Haren, Iris B. A. Smokers, and Evan Spruijt. Growth, replication and division enable evolution of coacervate protocells. *Chemical Communications*, 58(80):11183–11200, 2022.
- [45] Leroy Cronin and Sara Imari Walker. Beyond prebiotic chemistry. *Science*, 352(6290):1174–1175, June 2016.
- [46] N. Amy Yewdall, Alexander F. Mason, and Jan C. M. van Hest. The hallmarks of living systems: towards creating artificial cells. *Interface Focus*, 8(5):20180023, August 2018.
- [47] David Zwicker, Rabea Seyboldt, Christoph A. Weber, Anthony A. Hyman, and Frank Jülicher. Growth and division of active droplets provides a model for protocells. *Nature Physics*, 13(4):408–413, April 2017.
- [48] Jan Kirschbaum and David Zwicker. Controlling biomolecular condensates via chemical reactions. *Journal of The Royal Society Interface*, 18(179):20210255, June 2021.
- [49] Christoph A Weber, David Zwicker, Frank Jülicher, and Chiu Fan Lee. Physics of active emulsions. *Reports on Progress in Physics*, 82(6):064601, April 2019.
- [50] Samuel Safran. *Statistical thermodynamics of surfaces, interfaces, and membranes*. CRC Press, 2018.

- [51] Herbert B. Callen. Thermodynamics Wiley, New York, 1963. *Thermodynamics and an Introduction to Thermostatistics*, 1985.
- [52] Simon Alberti, Amy Gladfelter, and Tanja Mittag. Considerations and Challenges in Studying Liquid-Liquid Phase Separation and Biomolecular Condensates. *Cell*, 176(3):419–434, January 2019.
- [53] Michael Rubinstein and Ralph H Colby. *Polymer physics*, volume 23. Oxford university press New York, 2003.
- [54] Paul J. Flory. Thermodynamics of High Polymer Solutions. *The Journal of Chemical Physics*, 10(1):51–61, December 2004.
- [55] Maurice L. Huggins. Some Properties of Solutions of Long-chain Compounds. *The Journal of Physical Chemistry*, 46(1):151–158, January 1942.
- [56] S. W. Ip and J. M. Toguri. The equivalency of surface tension, surface energy and surface free energy. *Journal of Materials Science*, 29(3):688–692, February 1994.
- [57] Richard C. Tolman. The Effect of Droplet Size on Surface Tension. *The Journal of Chemical Physics*, 17(3):333–337, December 2004.
- [58] Edgar M. Blokhuis and Joris Kuipers. Thermodynamic expressions for the Tolman length. *The Journal of Chemical Physics*, 124(7):074701, February 2006.
- [59] Marta Tena-Solsona, Caren Wanzke, Benedikt Riess, Andreas R. Bausch, and Job Boekhoven. Self-selection of dissipative assemblies driven by primitive chemical reaction networks. *Nature Communications*, 9(1):2044, May 2018.
- [60] Marta Tena-Solsona, Benedikt Rieß, Raphael K. Grötsch, Franziska C. Löhner, Caren Wanzke, Benjamin Käs Dorf, Andreas R. Bausch, Peter Müller-Buschbaum, Oliver Lieleg, and Job Boekhoven. Non-equilibrium dissipative supramolecular materials with a tunable lifetime. *Nature Communications*, 8(1):15895, July 2017.
- [61] Marian von Smoluchowski. Drei vorträge über diffusion, brownsche molekularbewegung und koagulation von kolloidteilchen. *Physikalische Zeitschrift*, 17:557–571, 1916.
- [62] E. J. Scott, L. H. Tung, and H. G. Drickamer. Diffusion through an Interface. *The Journal of Chemical Physics*, 19(9):1075–1078, December 1951.

- [63] L. H. Tung and H. G. Drickamer. Diffusion through an Interface—Binary System. *The Journal of Chemical Physics*, 20(1):6–9, December 1952.
- [64] J. T. Davies. The The Mechanism of Diffusion of Ions across a Phase Boundary and through Cell Walls. *The Journal of Physical and Colloid Chemistry*, 54(2):185–204, February 1950.
- [65] P. L. Auer and E. W. Murbach. Diffusion across an Interface. *The Journal of Chemical Physics*, 22(6):1054–1059, December 1954.
- [66] James S. Langer and Robert F. Sekerka. Theory of departure from local equilibrium at the interface of a two-phase diffusion couple. *Acta Metallurgica*, 23(10):1225–1237, October 1975.
- [67] Piscounova Lialikov and Cerdycev Chipilov. IX Congrès International de Photographie Scientifique et Appliquée. 1935.
- [68] Tadao Sugimoto. Preparation of monodispersed colloidal particles. *Advances in Colloid and Interface Science*, 28:65–108, January 1987.
- [69] Tadao Sugimoto. Appendix. In *Monodispersed Particles (Second Edition)*, pages 737–766. Elsevier, Amsterdam, January 2019.
- [70] James S. Langer. Metastable states. *Physica*, 73(1):61–72, April 1974.
- [71] Claude Godrèche. *Solids Far from Equilibrium*. Aléa-Saclay. Cambridge University Press, 1992.
- [72] Peter W. Atkins, Loretta Jones, and Leroy Laverman. *Chemical Principles: The Quest for Insight*. W.H. Freeman, 2013.
- [73] Robert A Alberty. *Thermodynamics of biochemical reactions*. John Wiley & Sons, 2005.
- [74] Jean-Louis Burgot. *The Notion of Activity in Chemistry*. Springer International Publishing, 2016.
- [75] Gerold Adam, Peter Läger, and Günther Stark. *Physikalische Chemie und Biophysik*. Springer-Lehrbuch. Springer Berlin Heidelberg, 2009.
- [76] Jonathan Bauermann, Sudarshana Laha, Patrick M. McCall, Frank Jülicher, and Christoph A. Weber. Chemical Kinetics and Mass Action in Coexisting Phases. *Journal of the American Chemical Society*, 144(42):19294–19304, October 2022.

- [77] K. R. Elder, Martin Grant, Nikolas Provatas, and J. M. Kosterlitz. Sharp interface limits of phase-field models. *Physical Review E*, 64(2):021604, July 2001.
- [78] Sybren Ruurds de Groot and Peter Mazur. *Non-equilibrium Thermodynamics*. Dover Books on Physics. Dover Publications, 1984.
- [79] Frank Jülicher, Armand Ajdari, and Jacques Prost. Modeling molecular motors. *Reviews of Modern Physics*, 69(4):1269–1282, October 1997.
- [80] Martin Grant. *Dirty tricks for statistical mechanics: time dependent things. Lecture Notes for Advanced Statistical Physics*. Version 0.8 edition, August 2005.
- [81] David Jeffrey Griffiths. *Introduction to Electrodynamics*. Pearson Education, 2014.
- [82] Janine J. Weins and John W. Cahn. The effect of size and distribution of second phase particles and voids on sintering. In G. C. Kuczynski, editor, *Sintering and Related Phenomena*, pages 151–163. Springer US, 1973.
- [83] Michael D. Clark, Sanat K. Kumar, Jonathan S. Owen, and Emory M. Chan. Focusing Nanocrystal Size Distributions via Production Control. *Nano Letters*, 11(5):1976–1980, May 2011.
- [84] Jürgen Vollmer, Ariane Papke, and Martin Rohloff. Ripening and focusing of aggregate size distributions with overall volume growth. *Frontiers in Physics*, 2, 2014.
- [85] Johan Ludwig William Valdemar Jensen. Sur les fonctions convexes et les inégalités entre les valeurs moyennes. *Acta Mathematica*, 30(none):175–193, January 1906.
- [86] Carsten Donau, Fabian Späth, Marilyne Sosson, Brigitte A. K. Kriebisch, Fabian Schnitter, Marta Tena-Solsona, Hyun-Seo Kang, Elia Salibi, Michael Sattler, Hannes Mutschler, and Job Boekhoven. Active coacervate droplets as a model for membraneless organelles and protocells. *Nature Communications*, 11(1):5167, October 2020.
- [87] Vladimir N. Uversky, Irina M. Kuznetsova, Konstantin K. Turoverov, and Boris Zaslavsky. Intrinsically disordered proteins as crucial constituents of cellular aqueous two phase systems and coacervates. *FEBS Letters*, 589(1):15–22, January 2015.

-
- [88] Arpan Kumar Rai, Jia-Xuan Chen, Matthias Selbach, and Lucas Pelkmans. Kinase-controlled phase transition of membraneless organelles in mitosis. *Nature*, 559(7713):211–216, July 2018.
- [89] Marta Tena-Solsona, Jacqueline Janssen, Caren Wanzke, Fabian Schnitter, Hansol Park, Benedikt Rieß, Julianne M. Gibbs, Christoph A. Weber, and Job Boekhoven. Accelerated Ripening in Chemically Fueled Emulsions. *ChemSystemsChem*, 3(2):e2000034, March 2021.
- [90] Job Boekhoven, Wouter E. Hendriksen, Ger J. M. Koper, Rienk Eelkema, and Jan H. van Esch. Transient assembly of active materials fueled by a chemical reaction. *Science*, 349(6252):1075–1079, 2015.
- [91] David Zwicker, Anthony A. Hyman, and Frank Jülicher. Suppression of Ostwald ripening in active emulsions. *Physical Review E*, 92(1):012317, July 2015.

Selbständigkeitserklärung

Hiermit versichere ich, dass ich die vorliegende Arbeit ohne unzulässige Hilfe Dritter und ohne Benutzung anderer als der angegebenen Hilfsmittel angefertigt habe; die aus fremden Quellen direkt oder indirekt übernommenen Gedanken sind als solche kenntlich gemacht. Die Arbeit wurde bisher weder im Inland noch im Ausland in gleicher oder ähnlicher Form einer anderen Prüfungsbehörde vorgelegt. Die Arbeit wurde in Dresden am Max-Planck-Institut für Physik komplexer Systeme unter der Betreuung von Prof. Dr. Frank Jülicher angefertigt.

Jacqueline Anna Janssen

Dresden, Juni 2023